DIRECT SYNTHESIS OF DIMETHYL ETHER (DME) FROM SYNTHESIS GAS USING NOVEL CATALYSTS

A THESIS SUBMITTED TO
THE GRADUATE SCHOOL OF NATURAL AND APPLIED SCIENCES
OF
MIDDLE EAST TECHNICAL UNIVERSITY

BY

AYÇA ARINAN

IN PARTIAL FULFILLMENT OF THE REQUIREMENTS
FOR
THE DEGREE OF MASTER OF SCIENCE
IN
CHEMICAL ENGINEERING

JANUARY 2010

Approval of the thesis:

DIRECT SYNTHESIS OF DIMETHYL ETHER (DME) FROM SYNTHESIS GAS USING NOVEL CATALYSTS

submitted by **AYÇA ARINAN** in partial fullfillment of the requirements for the degree of Master of Science in **Chemical Engineering Department, Middle East Technical University** by,

Prof. Dr. Canan Özgen _____
Dean, Graduate School of **Natural and Applied Sciences**

Prof. Dr. Gürkan Karakaş _____
Head of Department, **Chemical Engineering**

Prof. Dr. Timur Doğu _____
Supervisor, **Chemical Engineering Dept., METU**

Assist. Prof. Dr. Dilek Varışlı _____
Co-Supervisor, **Advanced Technologies, Gazi University**

Examining Committee Members:

Prof. Dr. H. Önder Özbelge
Chemical Engineering Dept., METU _____

Prof. Dr. Timur Doğu
Chemical Engineering Dept., METU _____

Prof. Dr. Serpil Takaç
Chemical Engineering Dept., Ankara University _____

Assoc. Prof. Dr. Naime A. Sezgi
Chemical Engineering Dept., METU _____

Assoc. Prof. Dr. Sena Yaşyerli
Chemical Engineering Dept., Gazi University _____

Date: **19.01.2010**

I hereby declare that all information in this document has been obtained and presented in accordance with academic rules and ethical conduct. I also declare that, as required by these rules and conduct, I have fully cited and referenced all material and results that are not original to this work.

Name, Last name: Ayça ARINAN

Signature :

ABSTRACT

DIRECT SYNTHESIS OF DIMETHYL ETHER (DME) FROM SYNTHESIS GAS USING NOVEL CATALYSTS

Arınan, Ayça
M.Sc., Department of Chemical Engineering
Supervisor: Prof. Dr. Timur Doğu
Co-Supervisor: Assist. Prof. Dr. Dilek Varışlı

January 2010, 156 pages

Increasing prices of crude oil derived transportation fuels ascended the researches on seeking alternative fuels, in last decades. Moreover, the increasing rate of global warming, because of high greenhouse gas emissions initiated new research for environment-friendly clean alternative fuels. Due to its low NO_x emission, good burning characteristics and high cetane number, dimethyl ether (DME) attracted major attention as a transportation fuel alternative. Two possible pathways have been proposed for DME production. One of these pathways is DME synthesis through conventional methanol dehydration. More recently, direct DME synthesis in a single step has attracted significant attention of researchers and fuel producers. Catalysts having two active sites are required for direct DME synthesis from synthesis gas.

The aim of this work was to synthesize novel bifunctional direct DME synthesis catalysts and test their activity in a high pressure fixed bed flow reactor. Bifunctional mesoporous catalysts were synthesized by using one-pot hydrothermal synthesis, impregnation and physical mixing methods. These materials were

characterized by XRD, EDS, SEM, N_2 physisorption and diffuse reflectance FT-IR (DRIFTS) techniques.

Characterization results of the catalysts synthesized by one-pot hydrothermal synthesis procedures in basic and acidic routes showed that pH value of the synthesis solution was highly effective on the final physical structure and chemical nature of the catalysts. Increase in the pH value promoted the incorporation of Cu, Zn and Al into the mesoporous MCM-41 structure. Also, effects of Na_2CO_3 addition on the catalyst structure during the hydrothermal synthesis procedure were investigated. The characterization results showed that metals were incorporated into the catalyst structure successfully. However, surface area results showed that loaded metals blocked the pores of MCM-41 and decreased the surface area of the catalysts. Effects of zirconium (Zr) metal with different weight ratios were also investigated. Results showed that Zr loading increased the surface area of the catalyst.

A high pressure fixed bed flow reactor was built and the catalyst testing experiments were performed between the temperature range of 200-400°C, at 50 bars. The activity results of the catalyst synthesized by impregnation method showed that no DME was formed over this catalyst; however it showed promising results for production of methanol and ethanol. Selectivity values of these alcohols were between 0.35 and 0.2. Formation of methane and CO_2 indicated the occurrence of reverse dry reforming reaction. Incorporation of Zr into the catalyst structure at neutral synthesis condition caused significant activity enhancement, giving CO conversion values of about 40% at 400°C. Product distribution obtained with this catalyst indicated the formation of DME, ethanol, methanol as well as CH_4 and CO_2. Highest DME selectivity (60%) was observed with the catalyst prepared by physical mixing of commercial methanol reforming catalyst with silicotungstic acid incorporated methanol dehydration catalyst having W/Si ratio of 0.4.

Keywords: Bifunctional Catalyst, DME, Synthesis Gas, Direct Synthesis, Zirconium

ÖZ

YENİ KATALİZÖRLER KULLANARAK DOĞRUDAN SENTEZ GAZINDAN DİMETİL ETER (DME) ÜRETİMİ

Arınan, Ayça
Yüksek Lisans, Kimya Mühendisliği
Tez Yöneticisi: Prof. Dr. Timur Doğu
Ortak Tez Yöneticisi: Yrd. Doç. Dr. Dilek Varışlı

Ocak 2010, 156 sayfa

İşlenmemiş petrolden üretilen ulaşım yakıtlarının fiyatlarında görülen artış, son on yıllarda alternatif yakıt bulma çalışmalarına büyük ivme kazandırmıştır. Bununla beraber, yüksek sera gazı salınımından dolayı hızla artan küresel ısınma problemi, araştırmaların çevre dostu alternatif yakıtlar bulma yönünde ilerlemesini gerektirmiştir. Düşük NO_x salınım değerleri, iyi yanma özellikleri ve yüksek setan sayısından dolayı, dimetil eter (DME) özellikle ulaşım yakıt alternatifi olarak büyük dikkat çekmektedir. DME iki farklı sentez yöntemi ile üretilebilmektedir. Bunlardan biri geleneksel metanol dehidrasyon reaksiyonu ile DME üretimidir. Günümüzde, doğrudan sentez gazından DME üretimi, araştırmacıların ve yakıt üreticilerinin büyük ilgisini çekmektedir. Doğrudan sentez gazından DME üretimi için iki aktif merkeze sahip katalizörlere gerek duyulmaktadır.

Bu çalışmanın amacı, doğrudan sentez gazından DME üretimi için iki aktif merkezli katalizörlerin sentezlenmesi ve sentezlenen bu katalizörlerin aktivite testlerinin yüksek basınçlı, sabit yataklı reaktör sisteminde yürütülmesidir. İki fonksiyonlu mezogözenekli katalizörler, doğrudan hidrotermal sentez, emdirme ve fiziksel karıştırma yöntemleri ile sentezlenmiştir. Sentezlenen bu malzemeler, XRD,

EDS, SEM, azot adsorplanması ve DRIFTS teknikleri kullanılarak karakterize edilmiştir.

Doğrudan sentez yöntemi ile asidik ve bazik koşullarda sentezlenen katalizörlerin karakterizasyon sonuçları, sentez çözeltisinin son pH değerinin, katalizörün fiziksel ve kimyasal yapısı üzerinde önemli etkisi olduğunu göstermektedir. Sentez çözeltisinin pH değerindeki artışın, bakır, çinko ve alüminyumun, mezogözenekli MCM-41 yapısına tutunumunu arttırdığı gözlemlenmiştir. Ayrıca, doğrudan sentez yöntemi sırasında yapıya eklenen sodyum karbonatın (Na_2CO_3) katalizör yapısı üzerindeki etkileri incelenmiştir. Karakterizasyon sonuçları, metallerin bu yöntemle yapıya başarılı bir şekilde girdiklerini ancak yüzey alanı değerlerindeki düşme yapıya giren metallerin MCM-41 yapısının gözeneklerini tıkamış olduğunu göstermektedir. Zirkonyumun (Zr) katalizör yapısına etkisi, yapıya farklı oranlarda Zr metali eklenerek incelenmiştir. Sonuçlar yapıya eklenen Zr metalinin katalizör yüzey alanını arttırdığını göstermektedir.

Kurulan yüksek basınçlı sabit yataklı reaktör sisteminde, katalizör aktivite deneyleri 200-400°C sıcaklıkları arasında ve 50 bar basınçta gerçekleştirilmiştir. Emdirme yöntemi ile hazırlanan katalizörün aktivite sonuçlarında, DME oluşumu gözlemlenmemiştir. Ancak, elde edilen sonuçlar metanol ve etanol üretimi açısından ümit vericidir. Bu alkollerin seçicilik değerleri 0.35 ile 0.2 arasındadır. Metan ve karbondioksit oluşumu, ters yönde kuru reformlama reaksiyonunun gerçekleştirdiğini göstermektedir. Nötr sentez koşullarında yapıya eklenen Zr metali, aktivite değerlerini önemli bir şekilde yükseltmiştir ve karbon monoksit dönüşümü 400°C'de %40 olarak bulunmuştur. Bu katalizör ile elde edilen ürün dağılımı, gerçekleşen reaksiyonlar sonucunda; DME, etanol, metanol ve ayrıca metan ve karbon dioksitin oluştuğunu göstermektedir. En yüksek DME seçiciliği (60%), ticari metanol reformlama katalizörü ile Silikotungstik asit (STA) (W/Si ratio=0.4) aktif merkezli metanol dehidrasyon katalizörünün fiziksel karıştırılması ile hazırlanmış olan katalizörün aktivite testleri sonucunda elde edilmiştir.

Keywords: İki fonksiyonlu katalizör, DME, Sentez Gazı, Doğrudan Sentez, Zirkonyum

To my beloved family

ACKNOWLEDGEMENTS

I wish to express my deepest gratitude to my supervisor Prof. Dr. Timur Doğu for his guidance, endless support and encouragement throughout this research. He guided and helped me with his deepest knowledge at all points of this study. I also want to thank him for his understanding and kindly attitude in every aspect and for giving me chance to work under his supervision.

I would like to thank my co-supervisor Assist. Prof. Dr. Dilek Varışlı for her endless support and guidance throughout this thesis. Her understanding and friendly attitude are invaluable for me.

I would like to thank Assoc. Prof. Dr. Naime A. Sezgi for her encourangment and support in this study. I also want to thank for her positive guidance not only for my thesis but also for my future carrier.

I would like to offer my sincere thanks to Prof. Dr. Gülşen Doğu and her Gazi University Chemical Engineering Department research group for their positive manner and support for this study.

I would like to thank METU Chemical Engineering department technical staff; Nevzat Bekçi, Turgut Aksakal, İsa Çağlar, Yavuz Güngör, Gülten Orakçı, Mihrican Açıkgöz, Selahattin Battal and Süleyman Nazif Kuşhan, Kemal Yıldırım for their endless support and positive attitude. I would also like to thank METU Central Laboratory and Metallurgical and Materials Engineering technical staff for the characterization analyses.

Thanks are not enough to my friends Zeynep Obalı, Canan Martı, Kenan Cem Tokay, Ayşegül Çiftçi, Sultan Orman, Seval Gündüz and Caner Hocaoğlu in Kinetic Laboratory. I would like to offer my special thanks to Zeynep Obalı for her friendship, support and help through the progress of this study. I would also like to thank Canan Martı and Kenan Cem Tokay for their valuable help and friendship. I am grateful to Sultan Orman for her valuable friendship and support. I would like to

thank Ayşegül Çiftçi for her nice friendship since primary school. Her assistance through the course of this thesis and also my life is invaluable.

I would like to thank my friends Serra Caner, Elif İspir Gürbüz, Korhan Sezgiker, Başar Çağlar, Canan Yeniova, Eda Açık and İrem Vural for their friendship and for all the nice memories that we have shared in this department.

I would also like to thank my friends Burcu Kasım, Ayşen Yargan, Emin Kaya, Murat Tolga Ertürk, Evrim Sönmez, Asım Özkan and Burçak Bulut for their endless support and friendship for thirteen years. I would also like to thank Kerem Altun, İlker Ünsal, Semra Yalçın, Saygın Ozan and Çağrı Zeybek for the nice times shared together. I would like to express my special thanks to Servet Güney for his encouragement, support, valuable friendship and also for every moment that he made me smile. I want to thank all my friends who are standing by me throughout my life.

I owe my special thanks to Onur Koşar who has been my biggest support through my master studies. The words are not enough to thank him for his motivation, endless support, nights he waited for me in the laboratory and lovely friendship.

Finally, I owe my deepest gratitude to my lovely family; Muazzez Arınan, Eşref Arınan, Alev Bedirkurum, Tanay Bedirkurum and –my little love- Demir Bedirkurum who are always standing by me in all stages of my life. I cannot thank them enough for all their support, encouragement and endless love. I dedicate my thesis to them.

The support received from TÜBİTAK through 108M571 project is gratefully acknowledged.

TABLE OF CONTENTS

ABSTRACT iv

ÖZ vi

ACKNOWLEDGEMENTS ix

TABLE OF CONTENTS xi

LIST OF TABLES xv

LIST OF FIGURES xvii

NOMENCLATURE xx

CHAPTER

1. INTRODUCTION 1

2. DIESEL ALTERNATIVE CLEAN FUELS AND DIMETHYL ETHER (DME) .. 3

2.1. Properties of Dimethyl Ether (DME) and Its Fuel Use 4

2.1.1. Physical Properties of DME 4

2.1.2. Fuel Properties of DME and Other Alternative Fuels 5

2.2. Usage Areas of DME 7

3. SYNTHESIS METHODS OF DIMETHYL ETHER (DME) 9

3.1. Routes of Dimethyl Ether (DME) Synthesis 9

3.1.1. Methanol Synthesis 9

3.1.2. Indirect Synthesis of Dimethyl Ether (DME) (Methanol Dehydration) ... 11

3.1.3. Direct Synthesis of Dimethyl Ether (DME) from Synthesis gases 12

4. CATALYTIC FORMATION OF DIMETHYL ETHER (DME) 18

4.1. Catalytic Formation of Methanol 18

4.2. Catalytic Dehydration of Methanol to Dimethyl Ether (DME) 20

4.3. Catalytic Formation of DME from Synthesis Gases 24
5. M41S MOLECULAR SIEVE MATERIALS 31
5.1. Classification of Porous Solids 32
5.2. Properties and Formation Mechanism of MCM-41 33
5.2.1. MCM-48 35
5.2.2. MCM-50 36
5.3. Characterization Methods for MCM-41 Mesoporous Materials 37
5.3.1. X-Ray Diffraction (XRD) 37
5.3.2. Transmission Electron Microscopy (TEM) 38
5.3.3. Nitrogen Physisorption 38
5.4. Modification of M41S Molecular Sieves Materials for Catalytic Applications 40
6. PREPARATION METHODS OF CATALYTIC MATERIALS 42
6.1. Hydrothermal Synthesis 43
6.1.1. Washing Process 44
6.1.2. Drying & Calcination Processes 44
6.2. Impregnation 45
6.3. Precipitating Agent 46
7. THERMODYNAMIC ANALYSIS OF DIRECT DME SYTNHESIS REACTIONS 48
7.1. Equilibrium Constant Calculations for the Reaction 50
8. EXPERIMENTAL STUDIES 55
8.1. Synthesis of Catalysts 55
8.1.1. Synthesis of CuO-ZnO-Al_2O_3-MCM-41 Type Mesoporous Catalysts by One-pot Hydrothermal Synthesis Method (HS1 & HS5) 56
8.1.1.1. Synthesis Procedure 56

8.1.2. Synthesis of CuO-ZnO-(Al_2O_3/SiO_2) Type Mesoporous Catalyst by Impregnation Method (IMP1) 59
8.1.2.1. Synthesis Procedure 59
8.1.3. Synthesis of CuO-ZnO-Al_2O_3-MCM-41 Type Mesoporous Catalysts by Na_2CO_3 Modified One-pot Hydrothermal Synthesis Method (HS3 & HS4) 62
8.1.3.1. Synthesis Procedure 62
8.1.4. Synthesis of ZrO_2 modified CuO-ZnO-Al_2O_3-MCM-41 Type Mesoporous Catalysts by One-pot Hydrothermal Synthesis Method (Zr-1, Zr-2 & Zr-3) 66
8.1.4.1. Synthesis Procedure 67
8.1.5. Synthesis of Methanol Dehydration Catalysts to be Physically Mixed with Commercial Methanol Reforming Catalyst (HiFUEL-R120) 70
8.1.5.1. Synthesis Procedures of Dehydration Catalysts 70
8.2. Material Characterizaton Techniques 73
8.2.1. X-Ray Diffraction (XRD) 73
8.2.2. N_2 Physisorption 74
8.2.3. Scanning Electron Microscopy (SEM) 74
8.2.4. Energy Dispersive Spectroscopy (EDS) 74
8.2.5. Diffuse Reflectance Infrared Fourier Transform Spectroscopy (DRIFTS) of Pyridine Adsorption 74
8.3. Experimental Set-up of Direct DME Synthesis Reaction System 75
9. RESULTS AND DISCUSSION 78
9.1. Characterization Results of the Catalysts 78
9.1.1. Characterization Results of CuO-ZnO-Al_2O_3-MCM-41 Type Mesoporous Catalysts Synthesized by One-pot Hydrothermal Synthesis and Impregnation Methods 78
9.1.1.1. X-Ray Diffraction 78
9.1.1.2. Energy Dispersive Spectroscopy (EDS) 82
9.1.1.3. Scanning Electron Microscopy (SEM) 82

9.1.1.4. Nitrogen Physisorption 84
9.1.1.5. DRIFT Spectra of Pyridine Adsorption 87
9.1.2. Characterization Results of CuO-ZnO-Al_2O_3-MCM-41 Type Mesoporous Catalysts Synthesized by Na_2CO_3 Modified One-pot Hydrothermal Synthesis Method 88
9.1.2.1. X-Ray Diffraction 88
9.1.2.2. Energy Dispersive Spectroscopy (EDS) 91
9.1.1.3. Scanning Electron Microscopy (SEM) 91
9.1.2.4. Nitrogen Physisorption 92
9.1.2.5. DRIFT Spectra of Pyridine Adsorption 95
9.1.3. Characterization Results of ZrO_2 modified CuO-ZnO-Al_2O_3-MCM-41 Type Mesoporous Catalysts by One-pot Hydrothermal Synthesis Method 96
9.1.3.1. X-Ray Diffraction 96
9.1.3.2. Energy Dispersive Spectroscopy (EDS) 97
9.1.3.3. Scanning Electron Microscopy (SEM) 98
9.1.3.4. Nitrogen Physisorption 98
9.1.3.5. DRIFT Spectra of Pyridine Adsorption 100
9.1.4. Characterization Results of the Catalysts Prepared by Physical Mixing Method 103
9.1.4.1. X-Ray Diffraction 103
9.1.4.2. Energy Dispersive Spectroscopy (EDS) 104
9.1.4.3. Scanning Electron Microscopy (SEM) 105
9.1.4.4. Nitrogen Physisorption 105
9.2. Activity Results of the Synthesized Catalysts 108
9.2.1. Activity tests of IMP1 catalyst 108
9.2.2 Activity Tests of Zr-1, Zr-2 and Zr-3 Catalysts 110
9.2.3. Activity tests of HS4 catalyst 114

9.2.4. Activity tests of TRC75(L)-C catalyst 115
10. CONCLUSIONS AND RECOMMENDATIONS 122
REFERENCES 125
APPENDICES
A. THERMODYNAMIC CALCULATIONS 133
A.1. Fugacity Coefficients of the Species 133
A.1.1. Fugacity Coefficient of DME by Peng-Robinson Equation of State 133
A.1.2. Fugacity Coefficient of H_2O by Peng-Robinson Equation of State 134
A.1.3. Fugacity Coefficient of CO by Peng-Robinson Equation of State 135
A.1.4. Fugacity Coefficient of CO_2 by Peng-Robinson Equation of State 136
A.1.5. Fugacity Coefficient of H_2 by Peng-Robinson Equation of State 137
A.2. Equilibrium Conversions 141
A.2.1. Equilibrium conversion calculation for feed ratio (H_2/CO) of 1 [considering reaction (9): $3CO+3H_2 \rightarrow CH_3OCH_3 + CO_2$] 142
A.2.2. Equilibrium conversion calculation for feed ratio (H_2/CO) of 1 [considering reaction (10): $2CO+4H_2 \rightarrow CH_3OCH_3 + H_2O$] 143
B. CALIBRATION OF GAS CHROMATOGRAPH 146
B.1. Calibration Factors for Carbondioxide, Methane and DME 146
B.2. Calibration Factors for Methanol and Ethanol 147
B.3. Calibration Factor for Formic Acid 150
B.4. Conversion of Carbon Monoxide and Selectivities of Products 151
C. CRYSTALLITE THICKNESS CALCULATIONS 153
C.1. Crystalline thickness calculations of HS1 catalyst 154
C.2. Crystalline thickness calculations of IMP1 catalyst 155
C.3. Crystalline thickness calculations of HS3 catalyst 155
C.4. Crystalline thickness calculations of HS4 catalyst 156

LIST OF TABLES

TABLES

Table 1. Comparison of Dimethyl Ether and Other Alternative Fuels' Physical Properties (Adapted from [5]) 6
Table 2. Reaction conditions of direct DME synthesis [18] 15
Table 3. Molar Heat Capacity Coefficients [85] 49
Table 4. Standard Enthalpies and Gibbs Energies of Formation at 298.15 K for One Mole of Each Substance [86] 50
Table 5. Equations of $K_{f/P}$ and K_P for reactions (9) and (10) 51
Table 6. Critical temperature and critical pressure values for each species [86] 52
Table 7. Flow rates and molar compositions of the species at equilibrium 52
Table 8. Experimental conditions of the catalysts synthesized by one-pot hydrothermal synthesis and impregnation methods 62
Table 9. Experimental conditions of the catalysts synthesized by Na_2CO_3 modified one-pot hydrothermal synthesis 66
Table 10. Experimental conditions of the catalysts synthesized by ZrO_2 modified one-pot hydrothermal synthesis 69
Table 11. Comparison of catalysts prepared by physical mixing method 73
Table 12. The programme information of Gas Chromatograph 76
Table 13. Crystallites Thickness of HS1 and IMP1 catalysts 80
Table 14. Comparison of XRD pattern data of HS1 and IMP1 catalysts with literature data [89] 81
Table 15. EDS results of HS1, HS5 and IMP1 catalysts 82
Table 16. Physical properties of synthesized catalysts 85
Table 17. Crystallites Thickness of HS3 and HS4 catalysts 89
Table 18. Comparison of XRD pattern data of HS3 and HS4 catalysts with literature data [89] 90
Table 19. EDS results of HS3 and HS4 catalysts 91

Table 20. Physical properties of the synthesized catalysts 93
Table 21. EDS results of Zr-1, Zr-2 and Zr-3 catalysts 97
Table 22. Physical properties of the synthesized catalysts 99
Table 23. Summary of the catalysts prepared by one-pot hydrothermal synthesis method 102
Table 24. EDS results of the catalysts 105
Table 25. Physical properties of the synthesized catalysts 106
Table 26. Fugacity coefficients of the species at 1 bar 138
Table 27. Fugacity coefficients of the species at 10 bar 139
Table 28. Fugacity coefficients of the species at 30 bar 139
Table 29. Fugacity coefficients of the species at 50 bar 140
Table 30. Fugacity coefficients of the species at 80 bar 141
Table 31. Equilibrium conversion values for reaction (9) at different temperature and pressure values [feed ratio (H_2/CO) = 1] 144
Table 32. Equilibrium conversion values for reaction (10) at different temperature and pressure values [feed ratio (H_2/CO) = 1] 145
Table 33. Calibration Results 151

LIST OF FIGURES

FIGURES

Figure 1. A schematic representation of Dimethyl ether as an energy carrier for a sustainable development (Adapted from [9]) 7
Figure 2. Manufacturing processes of dimethyl ether (Adapted from [10]) 10
Figure 3. Equilibrium conversion of synthesis gas (260°C, 5MPa) [21] 14
Figure 4. Conceptual diagram of a liquid phase slurry bed reactor for direct DME synthesis [23] 16
Figure 5. Classification of porous materials according to their pore diameters (Adapted from [67]) 33
Figure 6. Liquid Crystal Templating (LCT) Mechanism proposed by Beck et al. [61] representing two possible formation routes of MCM-41: (1) liquid-crystal- initiated and (2) silicate-initiated 35
Figure 7. The schematic representation of proposed model of MCM-48 [74] 36
Figure 8. The schematic representation of proposed model of MCM-50 [66] 36
Figure 9. XRD pattern of calcined MCM-41 (Adapted from [72]) 38
Figure 10. Nitrogen Adsorption Isotherm for pure MCM-41 [72] 39
Figure 11. The equilibrium curve for direct DME synthesis with feed ratio (H_2/CO) of 1 [considering reaction (9): $3CO + 3H_2 \rightarrow CH_3OCH_3 + CO_2$] 53
Figure 12. The equilibrium curve for direct DME synthesis with feed ratio (H_2/CO) of 1 [considering reaction (10): $2CO + 4H_2 \rightarrow CH_3OCH_3 + H_2O$] 54
Figure 13. Synthesis procedures of HS1 and HS5 catalysts 58
Figure 14. Synthesis procedure of IMP1 type mesoporous catalyst 61
Figure 15. Synthesis procedure of HS3 type mesoporous catalyst 64
Figure 16. Synthesis procedure of HS4 type mesoporous catalyst 65
Figure 17. Synthesis procedures of Zr-1, Zr-2 and Zr-3 mesoporous catalysts 68
Figure 18. Synthesis procedures of Al-MC-1 and TRC75(L)-C catalysts 72
Figure 19. Schematic representation of experimental set-up 77

Figure 20. XRD Patterns of HS1, HS5 and IMP1 catalysts 79
Figure 21. SEM image of HS1 (magnified 100 times) 83
Figure 22. SEM image of HS1 83
Figure 23. SEM image of HS5 (magnified 100 times) 83
Figure 24. SEM image of HS5 83
Figure 25. SEM image of IMP1 (magnified 100 times) 84
Figure 26. SEM image of IMP1 84
Figure 27. Nitrogen adsorption-desorption isotherms of HS1, HS5 and IMP1 catalysts 86
Figure 28. Pore size distributions of HS1, HS5 and IMP1 type catalysts 86
Figure 29. DRIFTS spectra of HS1, HS5 and IMP1 catalysts 87
Figure 30. XRD Patterns of HS3 and HS4 catalysts 89
Figure 31. SEM image of HS3 (magnified 1000 times) 92
Figure 32. SEM image of HS3 (magnified 5000 times) 92
Figure 33. SEM image of HS4 (magnified 100 times) 92
Figure 34. SEM image of HS4 (magnified 5000 times) 92
Figure 35. Nitrogen adsorption-desorption isotherms of HS3 and HS4 catalysts 94
Figure 36. Pore size distributions of HS3 and HS4 catalysts 94
Figure 37. DRIFTS spectra of HS3 and HS4 catalysts 95
Figure 38. XRD Patterns of Zr-1 and Zr-2 catalysts 96
Figure 39. XRD Pattern of Zr-3 catalysts 97
Figure 40. SEM image of Zr-1 (magnified 500 times) 98
Figure 41. SEM image of Zr-3 (magnified 1000 times) 98
Figure 42. Nitrogen adsorption-desorption isotherms of Zr-1, Zr-2 and Zr-3 catalysts 99
Figure 43. Pore size distributions of Zr-1, Zr-2 and Zr-3 catalysts 100
Figure 44. DRIFTS spectra of Zr-1, Zr-2 and Zr-3 catalysts 101
Figure 45. XRD Patterns of Al-MCM-41 and TRC75(L) catalysts 103
Figure 46. XRD Pattern of commercial methanol reforming catalyst 104
Figure 47. SEM image of Commercial Methanol Reforming Catalyst 105
Figure 48. SEM image of TRC75(L) [87] 105
Figure 49. Nitrogen adsorption-desorption isotherms of Al-MCM-41, TRC75(L) and commercial methanol reforming catalysts 107

Figure 50. Pore size distributions of of Al-MCM-41, TRC75(L) and commercial methanol reforming catalysts 107
Figure 51. The variation in carbon monoxide conversion with 0.2 g of IMP1 catalyst (Feed stream molar ratio (H_2/CO=1) 109
Figure 52. The variation of selectivities of products with 0.2 g of IMP1 catalyst (Feed stream molar ratio (H_2/CO=1) 109
Figure 53. The variations in CO conversions with 0.2 g of Zr-2 and Zr-3 catalysts (Feed stream molar ratio (H_2/CO=1) 112
Figure 54. The variation of selectivities of products with 0.2 g of Zr-2 catalyst (Feed stream molar ratio (H_2/CO=1)..... 113
Figure 55. The variation of selectivities of products with 0.2 g of Zr-3 catalyst (Feed stream molar ratio (H_2/CO=1)..... 113
Figure 56. The variation in carbon monoxide conversion with 0.2 g of HS4 catalyst (Feed stream molar ratio (H_2/CO=1) 114
Figure 57. The variation of selectivities of products with 0.2 g of HS4 catalyst (Feed stream molar ratio (H_2/CO=1)..... 115
Figure 58. The variation in carbon monoxide conversion with 0.2 g of commercial methanol reforming and TRC75(L)-C catalyst (Feed stream molar ratio (H_2/CO=1) 116
Figure 59. The variation of selectivities of products with 0.2 g of TRC75(L)-C catalyst (Feed stream molar ratio (H_2/CO=1) 117
Figure 60. The variation of selectivities of products with 0.2 g of commercial catalyst (Feed stream molar ratio (H_2/CO=1) 117
Figure 61. DME selectivities of TRC75(L)-C and commercial methanol reforming catalysts (Feed stream molar ratio (H_2/CO=1)..... 118
Figure 62. Formic acid selectivities of TRC75(L)-C and commercial methanol reforming catalysts (Feed stream molar ratio (H_2/CO=1)..... 119
Figure 63. XRD Pattern of HS1 catalyst (2θ= 38-40°) 154

NOMENCLATURE

Cp: Heat Capacity (J/mol.K)

DME: Dimethyl Ether

DRIFTS: Diffuse Reflectance Infrared Fourier Transform Spectroscopy

EDS: Energy Dispersive Spectroscopy

f: Fugacity (bar)

F: Molar flow rate (mol/hr)

G: Gibbs Free Energy (kJ/mol)

H: Enthalpy (kJ/mol)

IUPAC: International Union of Pure and Applied Chemistry

K: Equilibrium Constant

MW: Molecular weight (g/mol)

MCM: Mobil Composition of Matter

MeOH: Methanol

n: Mole

P: Pressure (bar)

P_c : Pressure at Critical Point (bar)

R: Gas constant (8.314×10^{-5} m^3.bar /mol.K)

S: Selectivity

SEM: Scanning Electron Microscopy

T: Temperature (°C)

T_c : Absolute Temperature at Critical point (K)

T_r : Reduced Temperature

X: Conversion

XRD: X-Ray Diffraction

Z : Compressibility Factor

ω: Acentric factor

y: Molar composition

ρ: Density (g/cm^3)

CHAPTER 1

INTRODUCTION

Researches on alternative fuels are mainly started due to ecological and economical considerations. Increasing trend in oil prices and fast decrease of oil reserves have initiated new researches. Also the increasing rate of global warming caused new studies on the development of alternative fuels with less greenhouse gas emissions.

Among the alternative fuels, dimethyl ether (DME), which is recently discovered as a new clean fuel, can be synthesized from different primary sources. In Chapter 2 of this thesis, physical and fuel properties of DME are summarized and also these properties are compared with the other alternative fuels, such as methanol, ethanol, methane, hydrogen, gasoline and diesel fuel.

DME can be synthesized from natural gas, coal, heavy oil and also from biomass. Up to now, two DME synthesis procedures from synthesis gases have been claimed; one of them is traditional methanol synthesis followed by methanol dehydration and the second one is direct conversion of synthesis gas to DME in a single step. Details of these methods are discussed in Chapter 3.

Methanol synthesis can be carried out over copper-based catalysts and addition of metals such as zinc and zirconium in the catalyst structure increases its activity. Methanol dehydration reaction occurs over solid acid catalysts such as γ-alumina, zeolites and aluminum silicates. For direct synthesis of DME from syngas, catalysts having two active sites, one for methanol formation and one for methanol dehydration, are needed. In Chapter 4, a literature survey on catalytic formation of DME is presented.

Especially in the catalytic applications of petrochemical industry, silicate structured mesoporous M41S family materials are getting more and more attention because of their long range pore order and high surface area. In Chapter 5, properties and formation mechanisms and also modifications of M41S mesoporous molecular sieve materials and their catalytic applications are presented.

Direct DME synthesis from synthesis gas requires catalysts having two active sites. In this study, different preparation methods were used for the synthesis of catalysts. The properties of these synthesis methods are described in Chapter 6, in detail.

Thermodynamic analyses of direct DME synthesis reactions are discussed in Chapter 7. The equilibrium curves of DME formation reactions are given as a function of temperature at different pressure values.

In Chapter 8, experimental studies performed for the synthesis of the new mesoporous catalytic materials are presented. In addition to these, the material characterization techniques used for the synthesized materials and the instruments used in this thesis work are explained. Finally, the experimental set-up built in the Chemical Reaction Engineering Laboratory for direct DME synthesis is described.

Results of the applied characterization tests to the synthesized materials and their comparison are given in Chapter 9. Moreover, the catalyst testing results of the synthesized catalysts are presented in this chapter. In the activity test results, effects of temperature on carbondioxide conversion and product selectivities are investigated. Finally, conclusions and recommendations on the work performed in this thesis are given in Chapter 10.

CHAPTER 2

DIESEL ALTERNATIVE CLEAN FUELS AND DIMETHYL ETHER (DME)

Increasing consumption of oil reserves because of their excessive use for energy requirements is one of the major problems of the next century. Due to limited capacities of oil resources and other economical factors causing unsystematic changes in oil prices, processes for production of alternative motor fuels from different available raw materials are getting more and more attention in last decades [1-2].

Natural gas and petroleum are important raw materials for industry and their consumption rate has increased more than 200 times in the last century. Among them, petroleum is the one having the fastest depletion rate because of its excessive usage for transportation. Its overuse for transportation (about 57% of total oil consumption) causes problems in the petrochemical industry, in which petroleum is the major raw material [3-4]. According to the predicted lifetimes of precious raw materials, it is expected that there will be significant fuel shortage problems in the future because of their fast depletion.

Excessive use of oil reserves for transportation also causes drastic increase in the concentration of carbondioxide (CO_2) in the atmosphere, which is reported as one of the main reasons of the global warming. For this reason, production of hydrocarbons, alcohols and ethers starting from CO_2 over catalytic reactions is reported as a promising solution both for global warming and depletion of oil reserves [3].

Among the alternative fuels, dimethyl ether (DME) is considered as one of the cleanest diesel fuel alternative due to its benign properties, which will be discussed in the following sections of this chapter, in detail.

2.1. Properties of Dimethyl Ether (DME) and Its Fuel Use

2.1.1. Physical Properties of DME

Dimethyl ether is a promising alternative clean and economical transportation fuel of the next century. Its chemical formula is CH_3OCH_3 and it is the smallest ether compound. At standard temperature and pressure, it is a colorless gas and it may be liquefied at about 6 atmospheres at 25°C, which allows its storage and transportation just like LPG, with small changes in the current LPG storage and distribution technologies, such as changing the sealing materials. Its liquid viscosity is between 0.12-0.15 kg/ms, which is as low as that of propane or butane. Flame of DME is visible blue and it forms no peroxide in pure or in aerosol form [5].

According to toxicity results of its use as propellant, to replace fluorocarbons, its toxicity is extremely low, as LPG, and much lower than methanol. In addition to this property, DME is decomposed in troposphere for several ten hours, so that it has no greenhouse effect and it does not cause ozone layer depletion. Song et al. [4] worked on a model that exhibited the effect of DME on global warming and the results showed that DME lifetime in troposphere is 5.1 days.

Volatile organic compounds are environmentally unfriendly gases and their industrial emissions have been limited with Clean Air Act amendments, in 1990. DME is also a volatile organic compound. However, it is non-carcinogenic, non-teratogenic, non-mutagenic, and non-toxic [6].

High oxygen content (35 %) of DME causes no black diesel exhaust smoke (particulate matter) and low NO_x formation. Also, it does not contain sulfur in its content so that there is no SO_x emission at the end of DME combustion process [5]. In addition, it is not corrosive to any metals and not harmful to human body.

Calorific value of DME is 28.9 x10^6 J/kg as a liquid and 59.44×10^6 J/Nm^3 as a gas, which means that it is 1.37 times greater than methanol in liquid phase and 1.65 times higher than methane in gas phase. Finally when we look at the liquid densities, DME has a liquid density 1.37 times higher than propane which means than 85% energy of propane can be obtained from a equal size DME storage tank [5,7].

2.1.2. Fuel Properties of DME and Other Alternative Fuels

The high cetane number of DME, which indicates the combustion quality of a diesel fuel, is higher than diesel oil and other alternative fuels. This property makes DME so attractive for compression ignition engines. DME easily vaporizes during injection because of its low boiling point which allows relatively low fuel injection pressures. The required fuel injection pressure is only 220 atm at full loading which is very low when compared to diesel engines that requires injection pressure higher than 1200 atm [5].

Existing diesel engines can be converted to DME usage by some modifications that are needed to maintain stable fuel injection into engine. Similar to other alternative fuels, DME has low energy density per unit volume than conventional diesel fuel and gasoline, which means that some modifications not for engines but also for storage tanks are needed. In order to travel same distance larger storage tank volumes (about 1.7 times larger fuel volume) are required [5, 8]. In Table 1, physical and fuel properties of dimethyl ether and other alternative fuels are listed.

Table 1. Comparison of Dimethyl Ether and Other Alternative Fuels' Physical Properties (Adapted from [5])

Properties	**DME**	**Methanol**	**Methane**	**Ethanol**	**Hydrogen**	**Gasoline**	**Diesel Fuel**
Chemical Structure	**CH_3OCH_3**	CH_3OH	CH_4	C_2H_5OH	H_2	-	-
Molecular Weight (g/mol)	**46.07**	32.04	16.04	46.07	2.02	-	-
Liquid density (g/cm^3 @20°C)	**0.667**	0.7866	0.415	0.7893	0.071	0.73-0.76	0.84
Liquid viscosity (cP @20°C)	**0.15**	0.539	0.02(191K)	1.057	-	-	-
Vapor pressure (MPa @25°C)	**0.53**	0.0129	0.0053	0.006	-	-	-
Explosion limit (vol %)	**3.4 -18.6**	6.7-36	5-15	3.3-19	4-75	1.4-7.6	0.6-6.5
Cetane number	**55-60**	5	-	40,50	-	5-20	40-55
Liquid Molar Heat Capacity (J/molK)	**56.57 (100K)**	43.56	54.81(100K)	46.97(100K)	-	-	-
Gas Molar Heat Capacity (J/molK)	**60.71 (298K)**	43.89	35.79(25K)	73.60(25K)	2.9014	-	41.86
Sulfur content (ppm)	**0**	0	7-25	0	-	~200	~250
Specific gravity of gas (vs.Air)	**1.591**	1.106	0.554	1.591	0.07	-	-
Ignition Temperature (K)	**350**	385	540	365	400	228	-
Heat of Vaporization (kJ/mol)	**21.51**	35.2	8.18	38.9	0.9	-	-

2.2. Usage Areas of DME

Dimethyl ether (DME) can be synthesized from different primary energy sources and it can be used for various important commercial applications (Figure 1). As it is previously mentioned, DME can be used as an ideal diesel fuel alternate for transportation where low NO_x and SO_x emissions, high engine efficiency and quieter engines are needed.

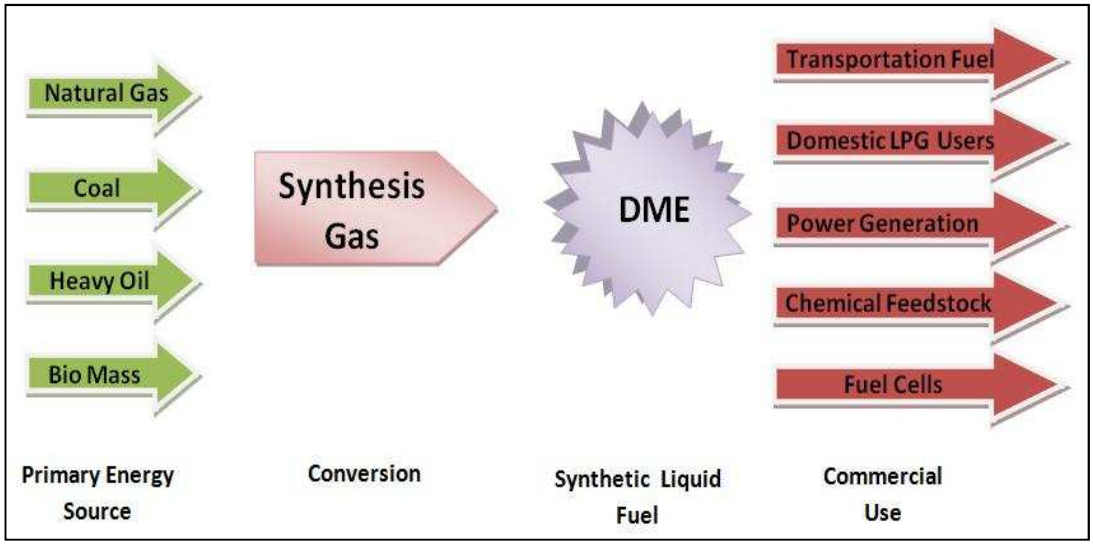

Figure 1. A schematic representation of Dimethyl ether as an energy carrier for a sustainable development (Adapted from [9])

DME has similar properties with natural gas, such as its Wobe index and thermal efficiency. Wobe index shows the ratio of calorific value to flow resistance of gaseous fuel and this value is 52 to 54 for DME, which is almost the same value as the natural gas [5]. For this reason DME can be used for cooking and heating

purposes without making any modifications in the equipments designed for using natural gas.

Actually, DME has been used as an aerosol propellant of spray can in order to replace chlorofluorocarbons (CFC's) which have undesired effects on ozone layer. Moreover, DME can change its phase easily from liquid to gas, so that it can be used as a refrigerant [7].

DME is an excellent feedstock in the production of several important chemicals such as olefins. In addition to production of olefins, DME can be used as a raw material for the chemical products which are recently produced from methanol. Moreover, enthalpy value of DME is lower than methanol, so that for the production of same chemical, the heat of reaction will be lower when DME is used as raw material instead of methanol [5].

CHAPTER 3

SYNTHESIS METHODS OF DIMETHYL ETHER (DME)

3.1. Routes of Dimethyl Ether (DME) Synthesis

Dimethyl ether can be synthesized from several primary energy resources such as; natural gas, coal, biomass, municipal solid waste and also from agricultural residues. Two processes have been claimed so far for the production of DME (Figure 2). The first one uses traditional two-step process consisting of methanol formation from synthesis gas followed by a methanol dehydration step. This process is known as dimethyl ether synthesis by dehydration of methanol which is 'indirect synthesis'. The second way is dimethyl ether synthesis directly from synthesis gases (CO, CO_2 and H_2) which is also named as 'direct synthesis'. Direct synthesis of DME is getting more and more attention because of its favorable thermodynamical and economical properties.

In this chapter, a brief literature survey on methanol synthesis, methanol dehydration and direct DME synthesis reactions is given.

3.1.1. Methanol Synthesis

Methanol is a very versatile fuel and it can be produced from various feed stocks, including natural gas, coal, and various biomass sources. Recently, the vast majority of worldwide methanol production is based on the steam reforming of natural gas and coal-based methanol synthesis [11].

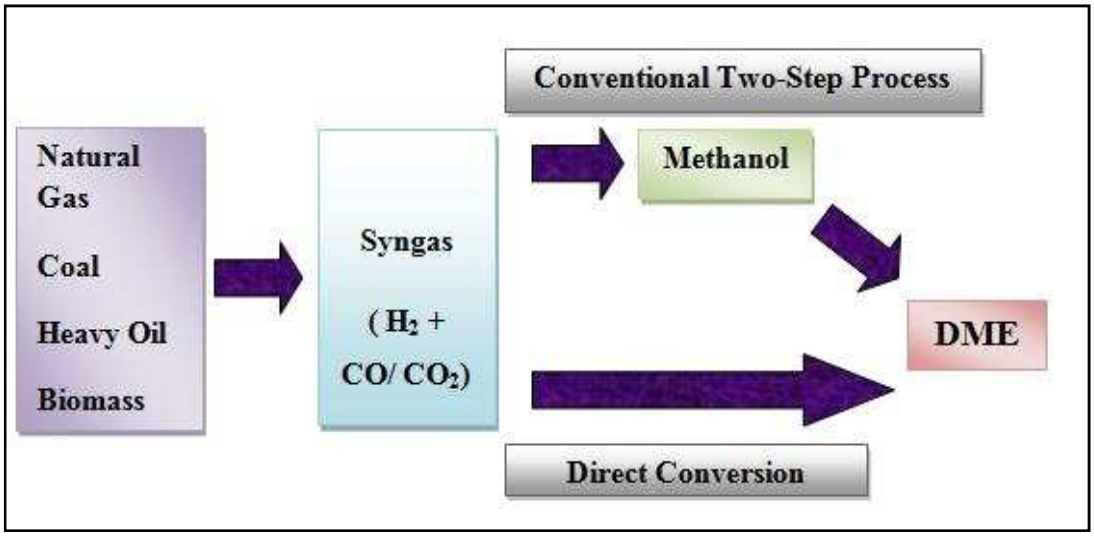

Figure 2. Manufacturing processes of dimethyl ether (Adapted from [10])

Commercial methanol synthesis was first carried out in 1923 by BASF chemists in Leuna, Germany and developed via new improvements. However, the 'high pressure' process (operating pressure between 250-300 bar and operating temperature between 320-450°C) developed by BASF was the single process for over 50 years until Imperical Chemical Industries (ICI) developed a new 'low pressure' process (operating pressure between 35-55 bar and operating temperature between 200-300°C) in 1960's and now this is the only process that is used in methanol market [11, 12].

For a long time it was believed that methanol is produced by the carbon monoxide hydrogenation. However, after detailed studies, it was found out that methanol synthesis from synthesis gas involves hydrogenation of carbon oxides (CO and CO_2) according to following reactions. Water gas shift reaction also occurs over the copper-based catalyst [13]:

$$CO + 2H_2 \leftrightarrow CH_3OH + 90.7\ kJ/mol \quad (1)$$

$$CO_2 + 3H_2 \leftrightarrow CH_3OH + H_2O + 50.1\ kJ/mol \quad (2)$$

$$CO + H_2O \leftrightarrow CO_2 + H_2 + 41.2\ kJ/mol \quad (3)$$

Conversion of synthesis gas to methanol is highly effected by thermodynamic factors. The thermodynamic equilibrium limits the conversion per pass of the process -conversion favors the high pressure- and causes large recycle of unreacted gas for carbon monoxide hydrogenation reaction and also removal of water by reverse water gas shift reaction over the catalyst promotes the methanol synthesis. Since the CO and CO_2 hydrogenation reactions are exothermic, temperature increases during methanol production. To increase conversion, it is essential to remove the excess heat from the system. For this reason, the methanol synthesis reactors are designed according to three important aspects such as; high cooling around the reactors, low pressure drop and reasonable economy. Today, 60% of the world's total methanol production from synthesis gas is achieved by using series of adiabatic reactors with coolers placed between each reactor [12, 13].

3.1.2. Indirect Synthesis of Dimethyl Ether (DME) (Methanol Dehydration)

Synthesis of DME by dehydration of methanol over several solid acid catalysts is the traditional route for DME synthesis. This route needs two sequential reactors; the first reactor is for methanol formation and the second reactor is for dehydration of methanol. Moreover synthesis of DME by following indirect route having two reactors requires higher production cost [14]. The following reaction occurs in the methanol dehydration process to produce DME.

$$2CH_3OH \leftrightarrow CH_3OCH_3 + H_2O + 23.4\ kJ\ /\ DME\text{-}mol \quad (4)$$

A bimolecular Langmuir-Hinshelwood reaction mechanism is proposed in the literature for methanol dehydration process in which one methanol molecule adsorbs on a Brönsted acid site and the other methanol molecule adsorbs at adjacent Lewis basic sites with formation of the two surface species $[CH_3OH_2]^+$ and $[CH_3O]^-$ which give DME and water with condensation [15, 16]. The proposed mechanism contains the following reaction steps and the reaction (5) is considering as the rate limiting step [15].

$CH_3OH + H^+ \leftrightarrow [CH_3OH_2]^+$…….(5)

$CH_3O\text{-}H + O^{2-} \leftrightarrow [CH_3O]^- + [OH]^+$…….(6)

$[CH_3OH_2]^+ \leftrightarrow [CH_3]^+ + H_2O$……...(7)

$[CH_3]^+ + [CH_3O]^- \leftrightarrow CH_3OCH_3$……...(8)

Methanol dehydration reaction occurs easily over almost any dehydration catalyst at relatively low temperature ranges between 250-300°C in vapor phase and the reaction is pressure insensitive [14]. According to the researches that are done in order to analyze the kinetics of the methanol dehydration reaction, dissociative adsorption of the methanol by assuming surface reaction control is the most reliable one that fits with the experimental results and rate of dimethyl ether formation is reported to be proportional with the square root of the methanol concentration [17].

3.1.3. Direct Synthesis of Dimethyl Ether (DME) from Synthesis gases

Direct DME synthesis from syngas has increased the attention of many researchers and companies in recent years because of its thermodynamically and economically favorable production steps. There are mainly two overall reactions that occur in the direct DME production from synthesis gas. These reactions, reaction (9) and (10), are listed below.

$3CO + 3H_2 \leftrightarrow CH_3OCH_3 + CO_2 + 246.2$ kJ / DME-mol ……..…….(9)

$2CO + 4H_2 \leftrightarrow CH_3OCH_3 + H_2O + 205.0$ kJ / DME-mol..……...(10)

$2CO + 4H_2 \leftrightarrow 2CH_3OH + 181.6$ kJ / DME-mol (Methanol Synthesis Rxn.)……...……(11)

$CO + H_2O \leftrightarrow CO_2 + H_2 + 41.0$ kJ / DME-mol (Water-gas Shift Rxn.)……...……..(3)

$2CH_3OH \leftrightarrow CH_3OCH_3 + H_2O + 23.4$ kJ / DME-mol (Methanol Dehydration Rxn.)……....(4)

Reaction (9) occurs with the combination of three reactions, which are methanol synthesis reaction (11), methanol dehydration reaction (4) and water gas shift reaction (3). In the case when water gas shift reaction does not take place, only reactions (11) and (4) combine and give reaction (10). Although both of the reactions (9) and (10) give two moles of products from six moles of reactants, increasing the process pressure leads higher conversion. Methanol synthesis reaction is the equilibrium restricted reaction of the process [18, 19].

In addition to these, in the direct synthesis process, the equilibrium limitations which occur because of methanol formation can be eliminated by continuous removal of methanol from the reaction medium through its conversion to DME and the removal of methanol from the system prevents the reverse reaction of the methanol equilibrium by allowing more carbon monoxide conversion [20].

Reaction (9), which has a stoichiometric ratio H_2/CO of 1/1, has some advantages, over reaction (10). If coal-gasified gas is used as raw material, reaction (9) requires less adjustment in the feed gas composition. Moreover, if natural gas or coal based methane is used as raw material, carbon dioxide which is given off as the product, can be recycled to produce synthesis gas by reaction (12) given below and this process is less energy consuming when compared to removal of water from the system which occurs in reaction (10) [18].

$$CH_4 + CO_2 \leftrightarrow 2CO + 2H_2 \qquad (12)$$

Finally reaction (9) gives higher equilibrium conversion when compared to reaction (10) according to the observed conversion values in all different feed gas ratios (Figure 3) [21].

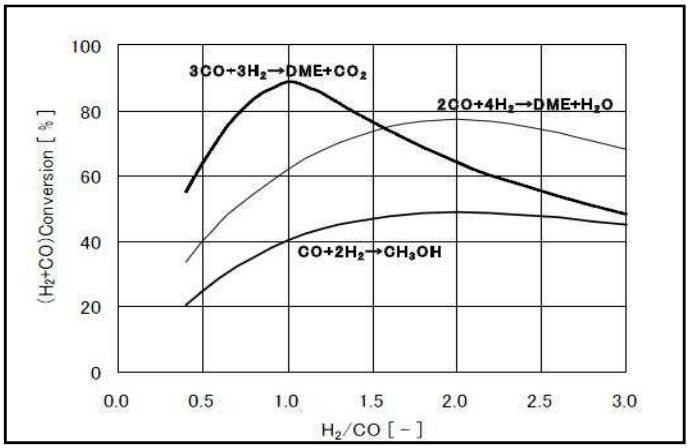

Figure 3. Equilibrium conversion of synthesis gas (260°C, 5MPa) [21]

Reaction (10) has a stoichiometric ratio of 2 for H_2/CO and this reaction requires adjustment in the feed gas composition when coal-gasified gas is used as raw material. It also gives lower equilibrium conversion (Figure 3). The increase of H_2/CO ratio suppresses water gas shift reaction and results in the accumulation of water in the reaction medium. Water accumulated near the catalyst medium decreases the life of the catalyst [18, 19]. However, the reaction which is dominant in DME synthesis mainly depends on the reactivity of the catalyst that is used in the reaction medium.

In direct synthesis of DME, a wide range of feed composition and operating conditions can be used. Feed gas composition, source of feed gas and catalyst selections are the important parameters of the process [22]. Typical reaction conditions of direct DME synthesis are tabulated in Table 2. [18].

Table 2. Reaction conditions of direct DME synthesis [18]

Reaction Conditions	
Temperature (°C)	240-280
Pressure (bar)	30-80
Feed (H_2 / CO) ratio	0.5-2.0
Catalyst loading ratio (W/F) [kg-cat.*h/ kg-mol]	3.0-8.0

Both Reaction (9) and Reaction (10) are highly exothermic so that removal of the heat and keeping the reactor temperature constant is important. Also removal of heat is necessary in order to prevent deactivation of catalyst at high temperatures. For this purpose a liquid phase slurry reactor (Figure 4) was proposed [23]. In this reactor, the catalysts particles are suspended in the solvent placed in the reactor. Gas reactant bubbles rise from bottom of the reactor to the top and reaction medium is full with solvent having high heat capacity, which absorbs the heat produced during the reaction. This reactor is mainly designed for the reaction having a stoichiometric ratio (H_2/ CO) of 1 [18, 19].

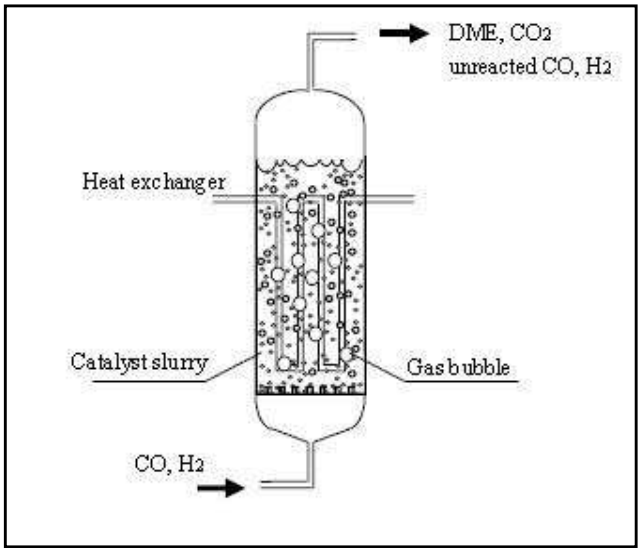

Figure 4. Conceptual diagram of a liquid phase slurry bed reactor for direct DME synthesis [23]

DME may also be synthesized directly from synthesis gas composed of CO_2 and H_2. Grzesik et al. [24] studied on the effects of feed gas composition, operating temperature (400-700K) and pressure (1-10 MPa) on equilibrium conversion of direct DME synthesis both from synthesis gases composed of CO and H_2 and composed of CO_2 and H_2. The reactions for DME synthesis from CO_2 are listed below:

$CO_2 + 3H_2 \leftrightarrow CH_3OH + H_2O$ ……..……...(13)

$CO_2 + H_2 \leftrightarrow CO + H_2O$.……...……(14)

$2CH_3OH \leftrightarrow CH_3OCH_3 + H_2O$ …….…...…….…...(15)

They concluded that both pressure and temperature had significant effects over the equilibrium conversion values of reactions (13)-(15). Pressure had high effects on equilibrium conversion for temperature values up to 550K and it showed nearly no effect at higher temperature values, for reactions (13) and (14). However, for reaction (15), effect of pressure only observed at the temperature values higher than 600K. In addition to these, at constant pressure, equilibrium conversion values decreased with increasing temperature for reactions (13) and (14), and increased for reaction (15).

CHAPTER 4

CATALYTIC FORMATION OF DIMETHYL ETHER (DME)

Direct conversion of synthesis gas to DME needs catalysts with two kinds of active sites; one for methanol formation and another for methanol dehydration. In this chapter, brief information about methanol synthesis catalysts and methanol dehydration catalysts are given. After giving information about these catalysts separately, the literature survey on bifunctional catalysts for direct DME synthesis is presented.

4.1. Catalytic Formation of Methanol

As it was previously mentioned in Chapter 3, methanol synthesis can be carried out via two different processes; the first one is methanol synthesis through high temperature/pressure process, proposed by BASF, over copper-free 'zinc-chromite type' (ZnO/Cr_2O_3) catalysts. These zinc-chromite type catalysts require high operating temperature and pressure ranges to give high activity. Also they produce methane and other light hydrocarbons with selectivity up to 2-5 wt. % [11, 25].

The second way of methanol synthesis is low temperature/pressure process, proposed by Imperial Chemical Industries (ICI), over copper-based catalysts containing zinc oxide (ZnO) on a support such as aluminum oxide [11-12, 25]. Copper is considered as the active metal for the reaction and it was reported that zinc is used for preventing agglomeration of copper in the catalyst structure. It improves the catalyst reactivity and decreases the high acidity of aluminum oxide support. The

incorporation ratios of the metal oxides into the catalyst structure are flexible and change for each producer. However, these ranges are limited between 40-80% for copper oxide, 10-30% for zinc oxide and 5-10% for aluminum oxide [1, 12].

Copper-based catalysts are active under lower temperature and pressure values. The decrease in the temperature increases the selectivity by decreasing the co-production of light hydrocarbons. In addition to these, economical requirements for the reaction process decreased with decreasing temperature and pressure [11, 25].

Recently, low temperature/pressure catalysts and their modifications to increase their activity with various metal oxides such as Zr, Cr, Ce, Co, Fe or Ti, have been widely studied by researchers working on methanol synthesis [25]. Among these metal oxides, researchers mainly focused on zirconium oxide. It is reported that Zr causes higher copper dispersion in the structure of the catalyst and increases the activity of the catalyst [1, 12].

Yang et al. [26] reported that ZrO_2 modified Cu-Zn oxide based catalysts are more active for both carbon monoxide and especially for carbon dioxide hydrogenation when compared to Cu-Zn oxide based catalysts. They also indicated that in ZrO_2 modified catalysts, active metals are highly dispersed and copper metal is in more interaction with other additive metals in the structure.

Moreover a study reported by Zhang et al. [27] gave similar results. They worked on methanol synthesis from CO_2 hydrogenation over Zr modified Cu/γ-Al_2O_3 type catalysts and they concluded that there is a strong interaction between CuO and ZrO_2 and addition of zirconium improves the catalytic performance by enhancing the CuO dispersion in the catalyst structure.

Sloczynski et al. [28] doped Cu/ZnO/ZrO_2 catalysts with different oxide additives (B, Ga, In, Gd, Y, Mg and Mn) for CO_2 hydrogenation and they reported that the additives showed significant changes in the catalyst activity and also they affected the activation energies and pre-exponential factors of methanol synthesis and water gas shift reactions. In addition to these, they also reported that among the additives, Ga_2O_3 gave the highest and In_2O_3 gave the lowest methanol yield. In other works of Sloczynski et al. [29, 30], they presented two studies again on doping Cu/ZnO/ZrO_2 type catalysts with Mn and Mg additives and they concluded that increase in the size of CuO crystallites decreased the catalytic activity and addition of MgO into the catalyst structure increased the copper dispersion and prevented

agglomeration in the catalyst structure and also they reported that the activity of the catalysts increased in CuZnZr < CuZnZrMg < CuZnZrMn order [30]. Moreover Chen et al. [31] investigated the activities of Manganese loaded $Cu/ZnO/Al_2O_3$ catalysts and similarly they indicated that Mn loading promoted the catalytic activity.

In the study of Huang et al. [32], they worked on the effect of Cr, Zn and Co additives on the performance of Cu-based catalysts and they found out that the addition of ZnO significantly promoted the catalytic performance of the Cu-based catalysts for methanol synthesis reactions. They also found that addition of Cr_2O_3 increased the activity slightly.

Melián-Cabrera et al. [33] investigated the effect of Pd over the catalytic performance of $Cu/ZnO/Al_2O_3$ catalysts for methanol synthesis from carbon dioxide. They reported that Pd doping into the catalyst structure increased both carbon dioxide conversion and methanol yield.

It was indicated in the study of Kilo et al. [34] that addition of chromium and manganese oxides to Cu/ZnO catalysts increased the thermal stability of the catalyst and also addition of them prevented the sintering of copper crystallites and stabilized the amorphous state of zirconia.

Ma et al. [35] also investigated the effects of rare earth oxides over the $CuO/ZnO/Al_2O_3$ catalysts and they reported that loading of Pr_2O_3 and Gd_2O_3 promoted methanol selectivity, loading of Eu_2O_3 increased the carbon dioxide conversion and Gd_2O_3 doped catalysts performed the best catalytic activity.

4.2. Catalytic Dehydration of Methanol to Dimethyl Ether (DME)

Methanol dehydration over solid acid catalysts is the conventional method for dimethyl ether (DME) synthesis and several catalysts, such as γ-alumina, zeolites, silica aluminums, mixed metal oxides and ion-exchange resins are tested for the methanol dehydration reaction.

Kim et al. [36] investigated the activities of Na-ZSM-5 and H-ZSM-5 type catalysts having different Si/Al ratios for methanol dehydration reaction. Methanol was supplied into the fixed-bed reactor, filled with solid acid catalysts, at atmospheric pressure and at the temperature of 250°C. They obtained 100% DME

selectivity because no by-products were observed in the experiments. H-ZSM-5 catalysts exhibited higher activity than Na-ZSM-5 catalysts and the catalytic performance of the H-ZSM-5 catalysts increased with decreasing Si/Al ratio. H-ZSM-5 catalyst with Si/Al ratio 30 showed the highest acidity and gave the best activity for methanol dehydration to DME reaction.

Vishwanathan et al. [37] reported that methanol dehydration reaction produced high amount of water as the by-product and over the γ-Al_2O_3 type catalysts methanol and water were captured by the same sites of alumina. Lewis acid sites on alumina had more tendencies to capture water molecules than methanol. The captured water decreased the activity of the catalyst by blocking the acid sites. For this reason, they also studied on the Na-modified H-ZSM-5 type catalysts having different Na contents, because water had less significant effect over H-ZSM-5 type catalysts. The catalyst were prepared by impregnation method and tested in a fixed-bed micro reactor at atmospheric pressure and in the temperature range between 230-340°C. According to the experiments, Na-modified H-ZSM-5 (Si/Al = 20) exhibited the highest catalytic activity and Na_{80}-H-ZSM-5 exhibited highest methanol conversion, 100% selectivity for DME and highest resistance against the water.

Yaripour et al. [38] investigated solid acid catalysts having different contents in a fixed bed reactor at 300°C under atmospheric condition. They worked with γ-Al_2O_3, silica–titania and modified-alumina with phosphorus type catalysts. They observed that phosphorus modified catalyst showed higher activity than γ-Al_2O_3. γ-Al_2O_3 type catalysts are good for methanol dehydration reaction but they are easily deactivated. In addition to these, among the phosphorus modified catalysts, the one with an Al/P molar ratio of 2 exhibited the highest methanol conversion without giving any by-product.

In the study of Xu et al. [39], γ-Al_2O_3, H-ZSM-5, amorphous alumina-silica and titanium modified zirconia type solid acid catalysts were tested with a plug-flow reactor at 280°C and they concluded that H-ZSM-5 with a Si/Al ratio of 25, was the best one with respect to activity but it gave low DME selectivity. However, the amorphous alumina-silica catalyst with 20% silica content showed the best catalytic performance in terms of activity, selectivity and conversion. In addition to these, they investigated the effect of water on the activities of the catalysts treated by adding different amounts of water into reactant gas stream. They indicated that increase in

the water partial pressure had a large negative effect on the catalytic activity for DME formation. In order to eliminate the negative effect of water, higher reaction temperatures were required. Negative effect of water was mostly observed on the catalytic activity of γ-Al_2O_3 and it showed the least negative effect on H-ZSM-5.

Kim et al. [40] studied on the boehmites particles prepared by sol-gel method having different acetic acid (AA)/aluminum iso-propoxide (AIP) and water/AIP ratios and different aging durations. Also, they prepared γ-Al_2O_3 powders from thermal decomposition (at 500°C for 5 h) of the boehmites particles. They observed that addition of acetic acid into the structure controlled the morphology of the catalysts. The pore size distribution of the catalyst shifted to mesoporous range when AA/AIP molar ratio increased from 0 to 0.5. The change in the water/AIP molar ratio exhibited less significant effect on the pore size distribution. Furthermore, increase in the AA/AIP molar ratio, promoted the surface area and surface acidity of the prepared materials. The prepared γ-Al_2O_3 type material with a AA/AIP molar ratio 0.5 showed the best catalytic activity and 100% selectivity in the dehydration reaction of methanol. Also the required reaction temperature for 50% conversion decreased with increasing acid sites promoted by larger surface area.

Fu et al. [41] investigated the effects of surface acidity on the methanol dehydration reaction over H-ZSM-5, steam de-aluminated H-Y zeolite (SDY), γ-Al_2O_3 and $Ti(SO_4)_2$ modified γ-Al_2O_3 type catalytic materials by microcalorimetric adsorption of ammonia and FT-IR spectra. They also performed conversion of isopropanol in order to characterize the acid strength of the materials. The dehydration reactions were carried out in a stainless steel fixed-bed micro reactor at atmospheric pressure at different temperatures. The results showed that at low temperatures H-ZSM-5 and SDY gave the best catalytic activity due to their strong Brönsted surface acidity. However, at higher temperatures, they observed hydrocarbons and coke formation over these zeolites. γ-Al_2O_3 showed low acidity with respect to its strong Lewis surface acidity because the presence of water. Water blocked the Lewis acid sites of the material and decreased its activity. Among the tested catalysts, $Ti(SO_4)_2$ modified γ-Al_2O_3 exhibited the best activity with no carbon deposition and no deactivation at high temperatures.

In another work, Raoof et al. [42] worked on the temperature and feed composition effects on methanol dehydration to DME reaction over γ-Al_2O_3 catalyst obtained from BASF (Kat.D10-10 S4). They performed the tests in an adiabatic fixed bed reactor at temperature ranges between 233-303°C, at constant atmospheric pressure. They observed that for feed gas temperature below 230°C, methanol conversion was not sustainable. At 250°C, the conversion increased to 85% and above this temperature, it remained constant. In addition to these, at 250°C they injected different feed gas compositions – pure methanol and methanol-water mixture - into the reactor system. They concluded that addition of water in the feed composition decreased the methanol conversion. These results indicated that water blocked the active sites of the catalyst and decreased the catalyst activity.

Kim et al. [43] worked on Na modified-ZSM-5 catalysts having γ-Al_2O_3 with different weight percents. They tested the catalysts in a fixed-bed reactor under 10 atm and the temperature of the reactor was changed between the ranges of 210°C to 380°C. In this study, an operative temperature range (OTR) was defined and it covered the values giving conversion higher than 50% and selectivity higher than 99%. According to the results obtained throughout the reactions, Na-ZSM-5 catalysts having 70% (wt.) γ-Al_2O_3 showed the best catalytic activity, because strong acid sites of zeolite were effectively eliminated in the structure of γ-Al_2O_3 and also no coke formation was observed in a wide OTR. It exhibited high stability for 15 days at 270°C with 80% DME yield.

Xia et al. [44] worked on the catalytic properties of NH_4F modified alumina particles with several concentrations (0.1, 0.2 and 0.5 mol/l) for the methanol dehydration to DME reaction in a fixed-bed reactor at atmospheric pressure and at relatively lower temperature ranges (250-280°C). The increase in the NH_4F concentration in the alumina structure decreased the surface area and acidity of the alumina. The catalyst having 0.1 molar NH_4F concentrations exhibited the best activity at all temperatures, because methanol dehydration is an acid-catalyzed reaction. The catalyst having highest surface acidity gave the highest conversion.

Xu et al. [45] studied on the dehydration of methanol to DME over 10 wt.-% Pd/Cab-O-Sil (fumed silica) catalyst prepared by impregnation method. They investigated the effects of hydrogen, helium and oxygen on the performance of the catalyst. For pure methanol as the only reactant, the methanol conversion of 27.9%

and 78.5% DME selectivity were obtained over the catalyst with CH_4 and CO as side products at 225°C. In the presence of hydrogen, methanol conversion decreased. However, the stability of the catalyst increased. In addition to these, replacement of hydrogen with helium increased the methanol conversion value from 32% to 37%.

4.3. Catalytic Formation of DME from Synthesis Gases

The direct synthesis of DME has been investigated for nearly ten years and it is getting more and more attention because of its thermodynamic and economic advantages. It requires a highly integrated catalyst system that combines the methanol synthesis and methanol dehydration catalysts in a close proximity, for optimum efficiency. Up to now, many studies have been performed in order to understand the mechanism of the direct synthesis reactions, however there is still no general agreement on their nature.

Generally, two different methods are used for the combination of the methanol synthesis and methanol dehydration catalysts. In the preparation of composite (bifunctional) catalysts; the components for the two functions of DME synthesis are combined together in a single step. The other approach is called as 'hybrid (admixed) catalysts', in which the two components are synthesized separately and then they mixed together by grinding or milling methods [46]. Both of these two methods are suggested in the literature but still there is no consensus on the superiority of method 1 or method 2.

In the literature there are several studies investigating different catalysts and preparation methods for DME synthesis.

Naik et al. [46] prepared DME synthesis catalysts with $ZnO/CuO/Al_2O_3$ as methanol synthesis component and SiO_2-Al_2O_3 (Si/Al=2) as methanol dehydration component. The aim of their work was to indicate the difference between the composite and hybrid catalysts preparation methods. They synthesized two composite catalysts (DM-1 and DM-2) by mixing the freshly precipitated precursors and co-precipitation methods respectively, methanol synthesis catalyst (MS-1), methanol dehydration catalyst (AS-1) and a hybrid catalyst (DM-3) composed of AS-1 and MS-1 catalysts in a weight ratio of 1:1. Then the prepared catalysts were tested

in a high-pressure tubular stainless steel fixed-bed reactor operating at 260°C and 735 psi. According to the reaction results, they concluded that the hybrid catalyst prepared by physical mixing of methanol synthesis and methanol dehydration catalysts gave the highest CO conversion of 20% at a high DME selectivity of 96%. The catalysts prepared by composite catalyst methodology gave poorer activity (CO conversion of 2%) because it was stated in the study that the active site in the methanol synthesis and methanol dehydration catalysts reacted during the synthesis step or calcination step and reactive species occurred over the catalyst which inhibited the catalyst activity.

Kim et al. [47] investigated the direct DME synthesis from coal based synthesis gas composed of CO and H_2 over commercial methanol synthesis catalysts obtained from Süd-Chemi having different copper, zinc and aluminum ratios and commercial γ-Al_2O_3 (DME-C-41, surface area: 218.0 m^2/g) as methanol dehydration catalyst. They prepared DME synthesis catalysts by physically mixing of methanol synthesis catalyst with methanol dehydration catalysts in the weight ratio of 1:1. In addition to these, they prepared two methanol synthesis catalysts (Cu/Zn molar ratio 1:1); one of them is prepared with acetate-based precursors (copper acetate, zinc acetate) was named as CZ-A and the other one is prepared with nitrate-based precursors (copper nitrate, zinc nitrate) by co-precipitation method. Then the prepared catalysts were mixed physically with commercial methanol synthesis catalysts in the weight ratio of again 1:1. The experiments were carried out in a fixed bed tubular stainless-steel reactor. The reaction was proceeded within the temperature ranges of 240-290°C and in the pressure range of 30-70 atm. Also, molar ratio of H_2/CO in the synthesis gas was changed between 0.5-2. The experimental results carried out at 260°C and 50 atm for commercial catalysts showed that the one having Cu/Zn/Al molar ratio of 5:4:1 (CZ-C-3) exhibited the best catalytic performance and the tests in order to analyze the effects of temperature and pressure were done over this catalyst. In the temperature dependency test CZ-C-3 catalyst showed the best activity at 260°C and started to decompose above 280°C. In the pressure dependency tests, it was observed that activity increased with pressure however the DME selectivity decreased. The optimum molar syngas ratio (H_2/CO) was found as 1:1. Finally, between the synthesized catalysts with different

metal precursors, the one prepared with acetate-based precursors showed higher reactivity than the catalyst prepared with nitrate-based precursors.

Kang et al. [48] investigated the direct synthesis of DME from biomass based synthesis gas, which has high CO_2 concentration-low CO/H_2 ratio, over composite catalysts containing for $Cu/ZnO/Al_2O_3$ (CZA) with weight ratios of 46:40:14 as methanol synthesis catalyst and Zr modified proton-type zeolites such as ferrierite (Si/Al = 25), ZSM-5 (Si/Al = 50) and Y (Si/Al = 2.3) as methanol dehydration catalyst which were synthesized by wet-impregnation and co-precipitation methods. In this study, they mainly focused on the effects of different zeolites over the catalytic performance. The activity tests were carried out in a tubular fixed bed reactor at 250°C and 4.0 MPa. According to the obtained results, CZA modified ferrierite catalyst gave the highest CO conversion (49.0%) and DME selectivity (58.2%). This catalyst exhibited low copper surface area but high acidity. It was stated that overall activity of the direct DME synthesis catalyst mainly depends on the surface area of active metals and acidity. However, the results showed that methanol dehydration over acid sites promoted DME synthesis more effectively than methanol formation over metallic coppers.

In another study, Venugopal et al. [49] prepared admixed catalysts for single step DME production. The admixed catalysts composed of Cu-Zn-Al modified with Ga, La, Y, Zr metals synthesized by conventional co-precipitation method, as methanol formation catalyst and γ-Al_2O_3 as methanol dehydration catalyst. The reaction was carried out in a fixed bed micro reactor at 600 psig, 250°C with feed gas molar ratio (H_2/CO) of 1.5. Results showed that Yttrium modified Cu-Zn-Al catalyst physically mixed with γ-Al_2O_3 gave the highest CO conversion and DME selectivity. Yttrium prevented the copper particle grain growth and increased the copper surface area, which was reported as an important factor for higher syngas conversion and promoted the direct DME synthesis.

Sun et al. [50] worked direct DME synthesis over bifunctional $CuO/ZnO/ZrO_2$/HZSM-5 type catalysts prepared with several ZrO_2 contents by coprecipitating sedimentation method. The catalytic tests carried in a fixed bed reactor showed that addition of ZrO_2 had an important effect and promoted the CO conversion and DME selectivity. Addition of ZrO_2 enhances both formation and stabilization of Cu^+, which is important for high DME selectivity and CO

conversion. Also, in this study it was stated that relation between Cu and Zn species in the catalyst structure has an important effect over catalytic performance.

Kim et al. [36] worked on the admixed catalysts composed of conventional $Cu/ZnO/Al_2O_3$ catalyst (ICI catalyst, KATALCO 33-5) physically mixed with H-ZSM-5 and Na-ZSM-5 catalysts having different Si/Al ratio. With increasing Si/Al ratio, the acid strength of the catalyst decreased significantly and for the ZSM-5 catalyst having Si/Al ratio of 100 gave no DME as a product in the reaction. Among the prepared catalysts, Na-ZSM-5 having Si/Al ratio of 30 showed the highest activity in the reaction tests performed in a stainless steel tubular reactor at 4.3 MPa.

In the study of Moradi et al. [51], direct DME synthesis catalyst were prepared by using seven different catalyst preparation techniques, such as co-precipitation by Na_2CO_3 and $NaAlO_2$, co-precipitation impregnation, co-precipitation sedimentation, sol-gel and a novel sol-gel impregnation techniques. $CuO/ZnO/Al_2O_3$ and γ-Al_2O_3 were used as methanol formation and methanol dehydration catalysts, respectively. Among the prepared catalyst, the one synthesized by a novel sol-gel impregnation method showed the best catalytic activity. In addition to these, catalysts containing different aluminum contents were synthesized by using sol-gel impregnation method and their performances were tested in a micro slurry reactor at 240°C, 40 bar and the optimum weight ratios for $CuO/ZnO/Al_2O_3$ were determined as 2:5:1, respectively.

Takeguchi et al. [52] also studied on the different preparation techniques and their effects on the catalytic activity in order to determine the effects of water on the acidic properties of the catalyst and on the reaction. The prepared hybrid catalysts composed of methanol synthesis catalyst ($CuO/ZnO/Ga_2O_3$) and silica-alumina catalysts, having different Si/Al contents, for methanol dehydration. They physically mixed these catalysts by two different methods. In one of them, the catalysts were milled, tabletted and pulverized together. In the other method, the catalysts tabletted and pulverized separately and then they mixed together. The catalysts were tested in a fixed-bed high-pressure flow reactor at a relatively low temperature (230°C) at 7.0 MPa. It is suggested that the catalysts having Brönsted acid sites became as the important active sites for direct DME synthesis. The catalysts prepared by dehydration catalyst having high silica content showed the best catalytic activity,

because it had Brönsted acid sites which were little affected by water and their activity remained high at relatively low temperatures.

Qing-li et al [53] worked on the bifunctional catalysts composed of conventional methanol synthesis catalyst (JC207, Jingjing Catalyst Plant, China) and CaO modified H-ZSM-5 (Si/Al=38) as methanol dehydration catalyst. They investigated the effects of CaO on the catalyst activity, in a fixed bed tubular reactor. The bifunctional catalyst modified by 0.5% CaO exhibited the best activity. The increase in the CaO content decreased DME selectivity significantly, especially above 3% because for excessive amount of CaO, Brönsted acid sites were turned into the Lewis acid sites which caused irregular acidity distribution and inhibited the synergetic effect for DME production.

In another study, MgO modified H-ZSM-5 type dehydration catalyst with different MgO contents physically mixed with $CuO/ZnO/Al_2O_3$ methanol synthesis catalysts were investigated for direct DME synthesis reaction by Mao et al. [54]. The experiments were conducted in a fixed-bed continuous flow reactor and effect of MgO was investigated. The results showed that MgO loading up to 5% decreased the formation of undesirable side products and removed the strong Brönsted acid sites and as a result increased the CO conversion and DME selectivity. In contrary, for MgO loading higher than 5%, the CO conversion and DME selectivity decreased significantly because the acidity of the catalyst decreased which is essential for methanol dehydration.

Khandan et al. [55] investigated the catalytic activity of hybrid catalysts composed of $Cu–ZnO–ZrO_2$ as methanol formation catalyst and Al-modified H-Mordenite having different Al contents as methanol dehydration catalysts in a slurry bed reactor. The effect of methanol synthesis catalyst to methanol dehydration ratio was investigated and the optimum ratio was found as 2:1. The results showed that conversion of the dehydration process highly depended on the total amount of catalyst acidity; however selectivity and stability of catalysts depended on the strength of acidic sites of the catalyst. Among the synthesized catalysts, the catalyst containing 8 wt.% aluminum oxide showed the best catalytic activity in terms of CO conversion (64%) and DME selectivity (78.8%).

In the study of Yoo et al. [56] for direct DME synthesis, admixed catalysts were prepared with commercial $Cu/ZnO/Al_2O_3$ (ICI catalyst, KATLCO 33-5) and the

SAPO catalysts with different compositions to analyze the optimum catalyst conditions. Catalytic reactions were carried out in a fixed-bed high pressure reactor with a gas mixture composed of H_2 and CO in the ratio of 1.5, at the pressure of 4.2 MPa and the temperature of 260°C. Among the prepared catalysts, SAPO-34 and SAPO-18 were easily deactivated. Also the effect of methanol formation catalyst to methanol dehydration ratio was investigated and it was observed that the increase of the methanol dehydration catalyst content, rapidly decreased the CO conversion so that the catalyst having 10% dehydration catalyst in its content showed the maximum catalytic activity in the reaction. In addition to these, SAPO-5 and SAPO-11 catalysts exhibited the best catalytic performance and stability in direct DME synthesis and it was observed that catalytic stability of methanol dehydration catalyst had an important effect over direct DME synthesis.

Mao et al. [57] studied the direct DME synthesis over hybrid catalysts composed of sulfate-modified (0–15 wt.%) γ-Al_2O_3 as methanol dehydration catalyst synthesized by impregnation method, physically mixed with $Cu/ZnO/Al_2O_3$ (Cu:Zn:Al=6:3:1 atomic ratio) as methanol synthesis catalyst in a fixed bed continuous flow reactor. Besides the effect of sulfate loading, the effect of calcination temperature was also investigated. Experimental results showed that sulfate modification up to 10 wt.% increased both CO conversion and DME selectivity. However, more increase in the sulfate content (up to 15 wt.%) decreased the catalytic performance, because strong acid sites appeared in the structure which promoted the by-product formation and also they increased the carbon dioxide formation by enhancing the water reforming reactions of methanol and DME.

Furthermore, the effect of calcination temperature was investigated and they found out that the increase in the temperature up to 550°C promoted the CO conversion and DME selectivity and inhibited the CO_2 formation. However, further increase in the calcination temperature decreased the catalytic activity and also DME selectivity and CO conversion. According to the obtained results, the catalyst having 10 wt.% sulfate content and calcined at 550°C showed the best catalytic performance among the synthesized catalysts.

Ramos et al. [14] investigated the effect of dehydration acid catalyst properties with commercial methanol synthesis and methanol dehydration catalysts (alumina, HZSM-5, tungsten–zirconia and sulfated-zirconia) for direct DME

synthesis. Among the prepared catalysts, the one composed of HZSM-5 as methanol dehydration catalyst showed the best catalytic activity and also it was found out that the methanol dehydration reaction was strongly affected by the number of acid sites and acid strength of the catalyst.

CHAPTER 5

M41S MOLECULAR SIEVE MATERIALS

According to the patent literature, ordered mesoporous material synthesis procedure was firstly described in 1969, however, due to inadequate analysis techniques, the remarkable properties of these materials were not recognized sufficiently until 1992 [58, 59]. In 1992, Mobil Research and Development Corporation researchers worked on the conventional templating strategy of zeolites and by using long-chain surfactants as templates, they found out a new family of periodic mesoporous silicates named as M41S [60,61]. M41S family members have long range order and high surface area values above 800 m^2/g. These properties make them attractive catalyst supports and they are very promising for catalytic applications in petrochemical industry. [62].

MCM-41, MCM-48 and MCM-50 are the members of the M41S family. Although these materials are synthesized from same chemical substances, their structures exhibit different properties according to their synthesis conditions [63].

In this chapter, brief descriptions of the porous materials, properties and characterization of M41S family members and modifications of M41S molecular sieves materials for catalytic applications are given in detail, respectively.

5.1. Classification of Porous Solids

Porous solids are usually used as adsorbents, catalysts and catalyst support materials because of their high surface areas and ordered structures [64]. Porous solids are classified into three categories in terms of their pore diameter (Figure 5), according to International Union of Pure and Applied Chemistry (IUPAC) definition;

- **Microporous materials:** The pore diameters of microporous materials are less than 2 nm. Pillared clays, anodic alumina, carbon nanotubes are examples to microporous materials. Zeolites are the well-known examples of this class. They have attractive catalytic properties however, because of their relatively small pore sizes, their application areas are limited. [64, 65]

- **Mesoporous materials:** The pore diameters of mesoporous materials are between the ranges of 2-50 nm. Breakthrough in mesoporous materials came in the form of materials called M41S family in 1992. Depending on the synthesis conditions, different M41S family members can be synthesized such as; MCM-41 (hexagonal phase), MCM-48 (cubic phase) and MCM-50 (non-stable lamellar phase) [66, 67].

- **Macroporous materials:** The pore diameters of macroporous materials are greater than 50 nm. Porous glasses and alumina membranes are examples of this class [64-67].

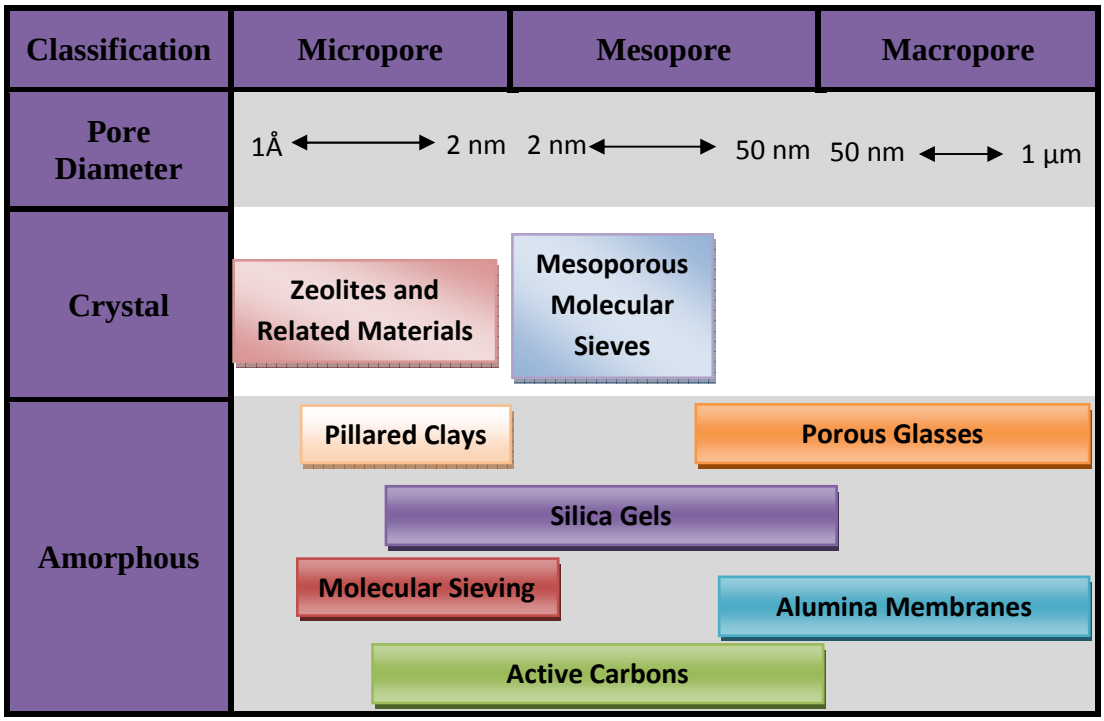

Figure 5. Classification of porous materials according to their pore diameters (Adapted from [67])

5.2. Properties and Formation Mechanism of MCM-41

MCM-41 is synthesized by four main components [65]; a source of silica, a structure-directing surfactant, a solvent and acid or base. Researchers of Mobil Research and Development Corporation found out that the final pore structure of the materials mainly depends on the relative amounts of the components used in the synthesis procedure. The variations in the surfactant to silica molar ratio in the synthesis procedure cause to obtain different members of M41S family as the final product. These products are [68]:

1. Surfactant / Silica < 1 → Hexagonal Structure (MCM-41)
2. Surfactant / Silica between 1-1.5 → Cubic Structure (MCM-48)

3. Surfactant / Silica between 1.2-2 → Lamellar Structure (MCM-50)

4. Surfactant / Silica > 2 → Cubic Octomer

Mobil Composition of Matter No.41 which has the short form as 'MCM-41' shows structure like honeycomb as a result of highly ordered hexagonal array of unidimensional pore sizes with narrow pore size distribution [69]. Depending on the alkyl chain length of the surfactants, the pore size of the MCM-41 can be changed and experimental studies exhibited that increase in the surfactant chain length increases the pore diameter of MCM-41 [60, 61].

MCM-41 synthesis was conventionally carried out under basic conditions in water medium. Organic molecules and surfactants are forming an organic-inorganic material as templates and the surfactant is removed from the material by leaving the porous silicate network behind after calcination process [70].

The formation mechanism of MCM-41 was investigated in several studies and some inconsistencies were observed between the proposed mechanisms in these studies. Beck et al. [61] proposed a mechanism, which was called as 'liquid-crystal templating mechanism (LCT)', (Figure 6) was supposed to cover all the previously proposed mechanisms. In this study two possible routes for the formation of MCM-41 were proposed. In the first route, the surfactant molecules are acting as a template and they are ordered into a liquid crystalline. Then around the hydrophilic parts of the surfactants, rigid shells occurred and the silicate species penetrated into these rigid shells. For first route to be functional, liquid structure is formed when the concentration of the surfactant molecules became as low as critical micelle concentration (CMC). In the second route, the silicate species play a more important role in the formation of MCM-41 structure. The addition of silicate species into the structure results in the ordering of the sub-layer silicates which are surrounded surfactant micelles [61, 64, 71].

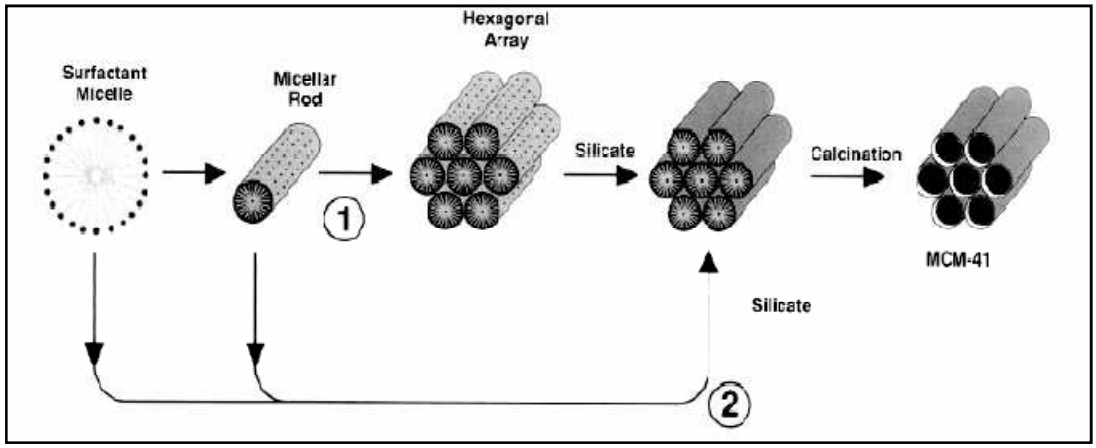

Figure 6. Liquid Crystal Templating (LCT) Mechanism proposed by Beck et al. [61] representing two possible formation routes of MCM-41: (1) liquid-crystal- initiated and (2) silicate-initiated.

5.2.1. MCM-48

MCM-48 is another member of M41S family. It has a complex, cubic Ia3d symmetrical structure with two independent intertwined channel networks, creating two three-dimensional pore systems. The intertwined channels line along the [111] and [100] directions and they have no interactions (Figure 7). MCM-48 type materials are attractive candidates for various catalytic applications because of their three-dimensional pore structure [71-73].

Synthesis reagents for MCM-48 are; an inorganic silica reagent, an alkylammonium hydroxide and a halide containing surfactant in an aqueous medium. The process can be carried out in a single step or in multiple steps (addition of surfactant after mixing silica and alkyammonium hydroxide) [73, 74].

Although MCM-48 materials are attractive because of their three-dimensional pore structure, they have not been widely preferable because of difficulties in the synthesizing procedure and they are not consistently reproducible [73].

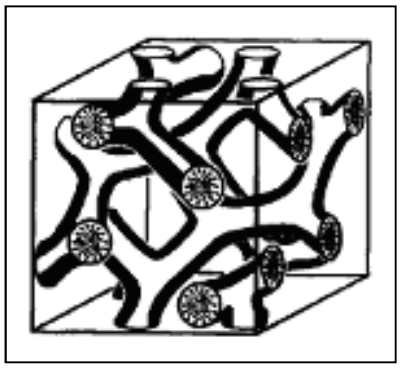

Figure 7. The schematic representation of proposed model of MCM-48 [74]

5.2.2. MCM-50

MCM-50 materials are other members of M41S family and they have non-stable lamellar arrangement of surfactant and silica layers (Figure 8). Since they are non-stable, their structure deforms through the calcination process [63].

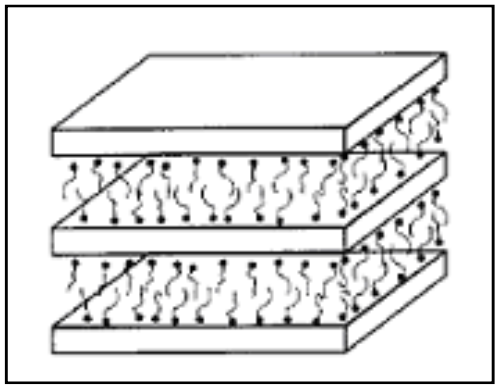

Figure 8. The schematic representation of proposed model of MCM-50 [66]

5.3. Characterization Methods for MCM-41 Mesoporous Materials

Many different characterization techniques have been utilized to characterize the properties of mesoporous materials. The most valuable methods for structure analysis are powder X-ray diffraction (XRD), transmission electron microscopy (TEM), and nitrogen adsorption measurements.

5.3.1. X-Ray Diffraction (XRD)

X-ray diffraction is one of the most important techniques for characterizing the structure of ordered materials and this technique gives the direct information about the architecture of the materials. The diffraction patterns for mesoporous materials only gives peaks at the low angle range, meaning 2θ value is less than 10. At higher angles, no reflection peaks occur which shows that pore walls of the mesoporous materials are mainly amorphous. However, the surfaces of the pore walls show crystalline-like behavior.

The XRD peaks do not result from crystal structure in the atomic range, but from the ordered channel walls of the mesoporous material. MCM-41 shows a X-Ray diffraction pattern containing typically 3-5 peaks between 2θ=2° and 5° which can be indexed to a hexagonal lattice as; a sharp (100) plane diffraction peak and the diffraction peaks of higher Miller Index planes, (110), (200) and (210) [61, 65, 75]. In Figure 9, a typical X-Ray powder diffraction data for a calcined sample of MCM-41 is given [72].

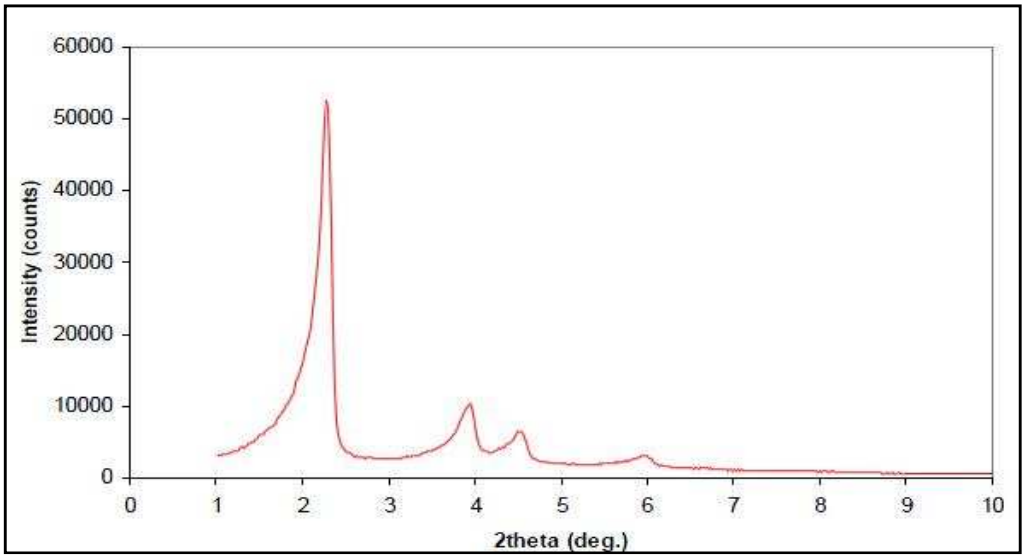

Figure 9. XRD pattern of calcined MCM-41 (Adapted from [72])

5.3.2. Transmission Electron Microscopy (TEM)

Transmission Electron Microscopy is a useful tool to visualize different pore orderings of the materials. By using TEM characterization technique, dislocations and other crystallographic defects character can be determined. The high-energy electron beam transmits the sample grids and captures an image of the structure of MCM-41, the channels, pores and the hexagonal structure of the material [65].

5.3.3. Nitrogen Physisorption

Adsorption techniques are used to determine the porosity and specific surface area of materials. The MCM-41 materials have uniform mesopores, between the ranges of 1.5 to 10 nm, and have been usually characterized by N_2 physisorption. According to the IUPAC definition, mesoporous materials show a Type IV adsorption-desorption isotherm [67, 68]. In Figure 10, nitrogen adsorption isotherm of pure MCM-41 synthesized by hydrothermal synthesis procedure is given [72].

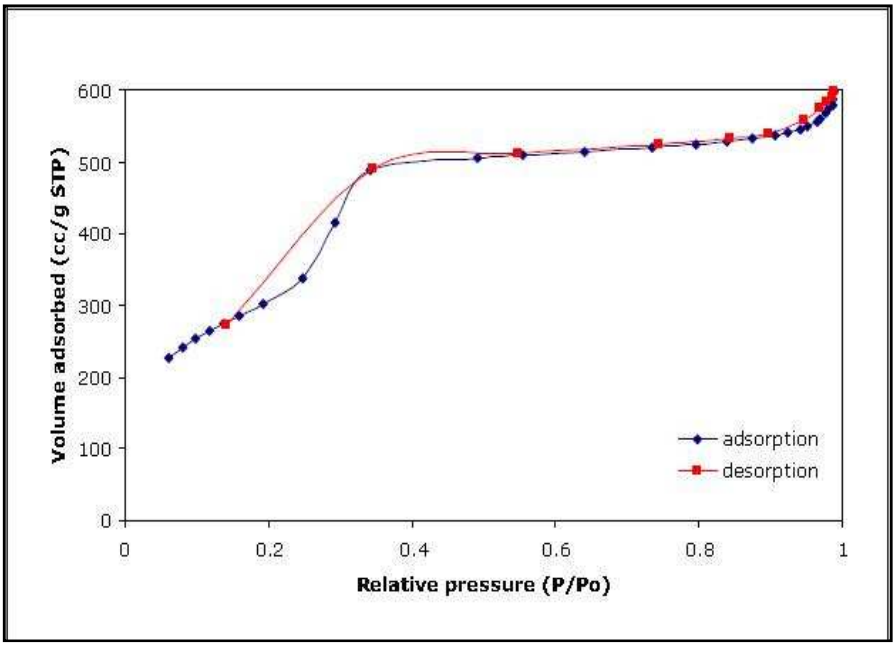

Figure 10. Nitrogen Adsorption Isotherm for pure MCM-41 [72]

Depending on the pore size, a sharp increase is seen at relative pressures from 0.25 to 0.5 which indicates the capillary condensation of nitrogen in the mesopores. It is stated that the sharpness of the inflection shows the uniformity of pore sizes and the height of the inflection gives the pore volume of the material. When pore diameter is higher than 4 nm, a hysteresis loop is usually observed for nitrogen adsorption-desorption isotherms [64, 65].

Combination of the results obtained from X-Ray diffraction patterns and nitrogen adsorption characterization techniques, the wall thickness of the material can be estimated by calculating the difference between the lattice parameter ($a = 2d_{(100)}/\sqrt{3}$) obtained from XRD and the pore size obtained from nitrogen adsorption [64].

5.4. Modification of M41S Molecular Sieves Materials for Catalytic Applications

M41S family members have large surface areas which makes these materials very attractive for catalytic applications. However, ordered mesoporous materials are not always used as catalysts themselves. More frequently, the materials are modified by additional catalytic functions such as; incorporation of active sites in the silica walls or deposition of active sites on the inner surface of the material. Relatively large pores of the mesoporous materials enhance the mass transfer during the catalytic reactions and the very high surface areas of the materials allows a high concentration of active sites per mass of material [69].

Up to now incorporation of various metals and metal oxides into the MCM-41 structure has been studied by many researchers.

Incorporation of aluminium metal into the MCM-41 structure and effects of the Si/Al ratios over the catalytic activity of the material have been widely investigated in many studies. MCM-41 materials show weak acidity so that modification of MCM-41 structure with aluminium metal increases the acidity of the structure and the synthesized Al-MCM-41 based materials were tested in a large numbers of petroleum refining processes [64, 76]. Moreover, in order to increase the acidity of Al-MCM-41 type materials for alkylation and alcohol dehydration reactions, heteropolyacids which obtain high Brönsted acid sites, incorporated into the mesoporous materials' wall structure [76, 77].

Copper modified MCM-41 type catalytic materials are also investigated in different applications. Copper is a metal which shows redox properties and incorporation of copper ions into the mesoporous silicates can be done by means of ion exchange, impregnation and grafting methods. Cu-MCM-41 based materials are also studied in phenol oxidation reactions [78], steam reforming of ethanol for hydrogen production [79] and they exhibit attractive catalytic properties in H_2S removal processes in petroleum refining industries [80]. In addition to these applications, copper and zinc modified MCM-41 type materials are studies for the selective oxidation reactions of alcohols to aldehydes [81].

Transition metals such as; vanadium and titanium modified mesoporous materials are also investigated as redox catalysts for selective oxidation reactions of paraffins, olefins and alcohols [65, 77].

CHAPTER 6

PREPARATION METHODS OF CATALYTIC MATERIALS

Preparation of solid catalysts includes many different complex processes and preparation steps. Starting materials have an important effect on the characteristics of final product. The main aim of catalyst preparation is to synthesize reproducible, stable, active and selective catalysts that are also having high surface area that reactants could interact with large number of active sites, good porosity and mechanical strength.

There are too many ways to prepare catalytic materials. In order to reduce the numbers of alternatives, the preparation methods are grouped according to similar processes take place during the synthesis. They are grouped according to following issues [82];

- ✓ Chemical and physical changes in the structure and the scientific laws that control these changes
- ✓ The process parameters such as temperature, pressure, time, pH and concentration
- ✓ Properties of the product
- ✓ Equipments required for the process

However some preparation methods include more than one issue that is listed above so that classification according to these properties is inadequate. More limitations are required to classify the preparation methods, such as [83];

1. Bulk catalysts and their supports (Precipitation, gelation, hydrothermal synthesis, filtration, washing, drying, calcination, forming operation)
2. Impregnated catalysts (Impregnation, precipitation)
3. Mixed-agglomerated catalysts (Crushing and grinding, mixing, activation)

In this chapter two of the described preparation methods will be discussed in detail that were used for catalyst preparation in this study. These methods are; hydrothermal synthesis including filtration, washing, drying and calcination steps, and impregnation. In addition to these methods, some catalysts were prepared by using precipitating agent modified hydrothermal synthesis. For this reason, in Section 6.3, properties and usage purposes of precipitating agents were presented.

6.1. Hydrothermal Synthesis

The hydrothermal synthesis has been used in various applications such as synthesis of molecular sieves, zeolites and also single phase crystalline solids. By this method, the active phase is distributed uniformly in the structure. In hydrothermal synthesis method, the prepared gels or precipitates modifications are carried out usually in liquid phase (mainly water) under relatively low temperatures (100-300°C). The morphological changes occur in the catalyst structure, occurs in the direction that promotes a decrease in the free energy of the system under the control of thermodynamic laws, can be classified as follows [82-83];

- ✓ Small crystals turn into large crystals
- ✓ Small amorphous particles turn into large amorphous particles
- ✓ Amorphous solids turn into crystalline
- ✓ Crystalline structure of a particle turn into different crystalline structure
- ✓ Gels having high porosity turn into gels having low porosity

Besides temperature; pressure, pH of the solution, concentration and time are also important parameters that can change the characteristics of final product in hydrothermal synthesis. Hydrothermal synthesis is carried out in special reactors. In this study, teflon-lined stainless steel autoclaves were used for hydrothermal synthesis process. After hydrothermal treatment, obtained solid product undergoes

several operations such as filtering, washing, drying and calcination. In all these processes, physical and chemical transformations occur and these transformations caused changes in the structure and surface composition of the final product. These operations will be discussed in details in the following sections.

6.1.1. Washing Process

In the washing process, the main aim is to remove some of the surfactant and to clean the product from the materials that are not entered into the structure and also from impurities. Particle size of the solid product is the main issue of washing process. Washing is easy for crystalline precipitates, difficult for flocculates and not useful for hydrogels [82]. In the washing step of flocculates, too much washing cause problems. After each washing step, purified flocculate requires more time to settle down and elimination of counter-ions repeatedly turns flocculate to sol. This transformation is known as peptization and the peptized flocculates can pass through the filter.

The other aim of washing step is to exchange the unwanted ions with the ones that can be decomposed in the calcination process. For this application, high temperature (100°C) water can be used in order to increase the ion exchange rate [50].

During the washing step, the solid is filtered and prepared for the drying step. In the filtration step, filtration paper choice should be done carefully according to the particle size of the solid product.

6.1.2. Drying & Calcination Processes

Removal of solvent from the pores of the solid product is known as drying process. This is a traditional and useful treatment for crystalline solids. However, it can cause structural deformation for hydrogels having 90% water in its structure.

Drying process can be proceeded under vacuum at low temperatures for the conservation of the amorphous or glassy structure of the solids having low melting temperatures.

Further heat treatment after drying process is known as calcination. Calcination can be done in the flow of different gases (usually dry air) at temperature higher than the reaction temperature that the catalyst will be used. In the calcination step, various chemical modifications occur and these can be listed as below [85,88]:

- ✓ Elimination of chemically bonded water or carbon dioxide
- ✓ Changes in the morphology of the catalyst (small crystals or particles transform into bigger ones)
- ✓ Changes in the structure of the catalyst (change in the calcination temperature effects the pore size distribution)
- ✓ Generation of active phases
- ✓ Stabilization of mechanical properties

6.2. Impregnation

Contacting the active materials in a solution with a support material is known as impregnation method. In this method, firstly a previously synthesized solid material is used as a support material and then for a period of time catalytically active materials in a solution interacted with the support and stabilized on it. After that, excess liquid phase is removed and in the end, obtained final solid product activated by suitable heat treatments such as calcination or reduction, if necessary. According to the amount of solution, impregnation can be done in two ways; wet impregnation (soaking or dipping) and dry impregnation (impregnation to incipient wetness) [82].

In the wet impregnation, the amount of the solution is higher than the pore volume of the support. The previously prepared support placed into an excess amount of solution and after the time necessary for total impregnation is passed, the solid is separated and dried to get rid of excess water. The wetting time and drying step have important effects over the catalytic characteristics of the final product.

In the dry impregnation, the amount of solution is equal or less than the pore volume of the support. If support-active material interaction is weak in the prepared solid; drying process can be followed after dry impregnation in order to increase the active metal loading into the support structure which is also limited by the active

material solubility in the solution. However drying process can cause improper distribution of active materials and in the final product there would be a support material inhomogenously covered by active materials [82, 83].

In impregnation techniques, temperature is the main variable that controls the active material solubility and the aqueous solution viscosity. Also the mass transfer conditions in the pores of the support strongly effect the active material distribution in the structure of the final catalyst and its mechanical properties. In addition to temperature, process time has an important effect on the final characteristics of the synthesized solid product.

6.3. Precipitating Agent

Precipitating agent in the synthesis procedure is used in order to obtain a precipitated solid from a homogenous liquid. The formation of precipitated solid phase can occur through physical or chemical transformations. These transformations occur in the basis of three steps; supersaturation, nucleation and growth or agglomeration of the particles.

In the supersaturation region, the system is unstable and pH and temperature are the main functions that affect the system. In this region, particles may occur by nucleation and growth. For example, in the high saturation region crystal growth rate is slower than nucleation rate so large amounts of small particles are formed in the solution. However the characteristics of the precipitated particles mainly depend on the Ostwald ripening (crystal growth) and Brownian motion (agglomeration of colliding particles) processes that occur in the solution [82-84].

The main aim of using precipitating agent in preparing supported catalysts is to obtain mixed catalyst components with the formation of small crystallites or mixed crystallites containing the active materials by the following process [82]:

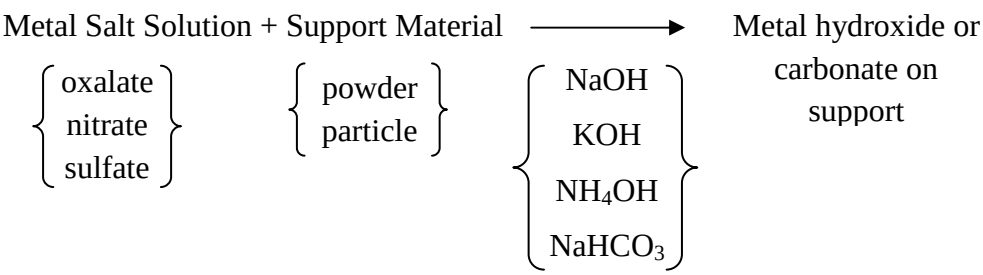

As it is mentioned in the process, hydroxides and carbonates are used as precipitating agent according to following reasons [83]:

1. Due to low solubility of salts of the transition metals, small precipitate particle sizes can be obtained.
2. By heat treatment, these precipitating agents can easily decomposed to oxides having high surface area by causing no catalyst poison.
3. Poisoning gas release from the calcination is minimum.

CHAPTER 7

THERMODYNAMIC ANALYSIS OF DIRECT DME SYTNHESIS REACTIONS

As mentioned in Chapter 3, direct synthesis of DME from syngas, is a reaction which requires high pressure (50 bars and above) and high temperature (200°C-400°C). In order to decide on the reaction parameters that are going to be used during the experimental studies, thermodynamic analyses of the direct DME synthesis reactions were done and under the light of obtained results; the feed ratio of the reactants, the pressure and temperature values of the experiment were decided.

Direct synthesis of DME from synthesis gases can be achieved by two different reactions mainly related to the stoichiometric ratios of the reactants.

$3CO + 3H_2 \leftrightarrow CH_3OCH_3 + CO_2 + 246.2$ kJ / DME-mol ……..(9)

$2CO + 4H_2 \leftrightarrow CH_3OCH_3 + H_2O + 205.0$ kJ / DME-mol ……...(10)

For reaction (9) the stoichiometric ratio of the reactants (H_2/CO) is one and this ratio is two for reaction (10). In this chapter, thermodynamic analyses for both of the reactions were done for the feed (H_2/CO) ratio of one. This ratio was kept constant throughout the experimental studies in this work. By using the obtained results conversion versus temperature graphs at different pressure values were plotted.

For the first step, heat capacity (C_p) value of each reactant and product should be calculated. Heat capacity is a function of temperature and it can be calculated from equation 16.

$$Cp_{,T}\,(\text{in J/mol.K}) = a + bT + cT^2 + \ldots \quad (16)$$

For the calculation of C_p, molar heat capacity coefficients of the species that are produced or consumed during the reaction are needed. These coefficients are listed in Table 3 for each of the reactants and products.

Table 3. Molar Heat Capacity Coefficients [85]

Species	**a**	**b x 10^2**	**c x 10^5**
CO	28.142	0.167	0.537
H_2	29.088	-0.192	0.4
CH_3OCH_3	17.02	17.91	-5.234
CO_2	22.243	5.977	-3.499
H_2O	32.218	0.192	1.055

For the second step, formation enthalpy and Gibbs free energy values at 298.15 K for each reactant and product involved the reaction are needed. These values are listed in Table 4.

Table 4. Standard Enthalpies and Gibbs Energies of Formation at 298.15 K for One Mole of Each Substance [86]

Species (gas state)	ΔH^{o}_{f} (kJ/mol)	ΔG^{o}_{f} (kJ/mol)
CO	-110.5	-137.2
H_2	0	0
CH_3OCH_3	-184.2	-113.0
CO_2	-393.5	-394.4
H_2O	-241.8	-228.6

By using these listed values, reaction enthalpy and Gibbs free energy values were calculated with the equations listed below;

$$\Delta H^{\circ}_{rxn} = \sum_i \nu_i \Delta H^{\circ}_{fi} = \sum_{products} |\nu_i| \Delta H^{\circ}_{fi} - \sum_{reactants} |\nu_i| \Delta H^{\circ}_{fi} \quad (17)$$

$$\Delta G^{\circ}_{rxn} = \sum_i \nu_i \Delta G^{\circ}_{fi} = \sum_{products} |\nu_i| \Delta G^{\circ}_{fi} - \sum_{reactants} |\nu_i| \Delta G^{\circ}_{fi} \quad (18)$$

Finally, in order to calculate the reaction enthalpy at any temperature values equation 19 was used.

$$\Delta H^{o}_{R,T} = \Delta H^{\circ}_{298} + \int_{298}^{T} (\Delta a + \Delta b T + \Delta c T^2)\, dT \quad (19)$$

7.1. Equilibrium Constant Calculations for the Reaction

Equilibrium constant calculations for the reaction were done by using the following equations. While writing the equations, non-ideal gas behavior was taken into the consideration.

$$K_{298} = \exp(-\Delta G^{o}_{298} / RT) \tag{20}$$

$$\frac{d \ln K}{d\left(\frac{1}{T}\right)} = -\frac{\Delta H^{o}_{R,T}}{R} \tag{21}$$

$$K = K_{f/P} \times K_P \tag{22}$$

$K_{f/P}$ and K_P values of the reactions (9) and (10) were calculated by the equations listed in Table 5.

Table 5. Equations of $K_{f/P}$ and K_P for reactions (9) and (10)

Reaction (9)	**Reaction (10)**
$K_{f/P} = \frac{(f/P)_{CH3OCH3} \times (f/P)_{CO2}}{(f/P)^3_{H2} \times (f/P)^3_{CO}}$	$K_{f/P} = \frac{(f/P)_{CH3OCH3} \times (f/P)_{H2O}}{(f/P)^4_{H2} \times (f/P)^2_{CO}}$
$K_P = \frac{(y_{CH3OCH3}P) \times (y_{CO2}P)}{(y_{H2}P)^3 \times (y_{CO}P)^3}$	$K_P = \frac{(y_{CH3OCH3}P) \times (y_{H2O}P)}{(y_{H2}P)^4 \times (y_{CO}P)^2}$

Finally, the f/P ratios for each species were determined for each temperature value by Peng-Robinson equation. In order to find the fugacity coefficients, the critical temperature and pressure values of each species are needed (Table 6). By taking the literature survey into consideration, the calculations were done between the temperature intervals, 400K-700K by using MATHCAD software program. The fugacity coefficient values of each species are given in Appendix A.

Table 6. Critical temperature and critical pressure values for each species [86]

Chemical species	T_c (K)	P_c (bar)
CH_3OCH_3	400.05	53.70
CO_2	304.40	73.97
H_2	33.15	12.97
CO	133.10	34.94
H_2O	647.30	220.48

The molar flow rates of the species at equilibrium conversion and their molar compositions are determined as shown in Table 7. For the calculations, the inlet molar compositions of the reactants are taken as 50% H_2 and 50% CO, (H_2 / CO = 1), and total inlet flow rate was taken 100 kmol /hr as basis.

Table 7. Flow rates and molar compositions of the species at equilibrium

Species	Reaction (9)		Reaction (10)	
	F_i	y_i	F_i	y_i
CO	$50(1-x_{eq})$	$50(1-x_{eq})/(100-200/3x_{eq})$	$50(1-(x_{eq}/2))$	$50(1-(x_{eq}/2))/50(2-x_{eq})$
H_2	$50-50x_{eq}$	$50-50x_{eq}/(100-200/3x_{eq})$	$50(1-x_{eq})$	$50(1-x_{eq})/50(2-x_{eq})$
CH_3OCH_3	$50x_{eq}/3$	$(50/3)x_{eq}/(100-200/3x_{eq})$	$50x_{eq}/4$	$(50x_{eq}/4)/50(2-x_{eq})$
CO_2	$50x_{eq}/3$	$(50/3)x_{eq}/(100-200/3x_{eq})$	-	-
H_2O	-	-	$50x_{eq}/4$	$(50x_{eq}/4)/50(2-x_{eq})$
Total	$100-(200/3)x_{eq}$	1.0	$50(2-x_{eq})$	1.0

The procedure to determine the equilibrium curve is to calculate the equilibrium conversions (x_{eq}) of DME synthesis reactions at different temperature (T) values in the range 400-700 K by equating the two expressions of equilibrium constant given in equations (21) and (22). Finally for both of the reactions conversion-temperature graphs at different pressure values for feed ratio (H_2/CO) of one, were plotted and given in Figures 11 and 12.

It can be clearly observed from the graphs that reactions are highly pressure dependent. In both of the reactions, conversion increases with pressure. Also when compared the reactions, for the same feed ratio, equilibrium conversion of the reaction having stoichiometric ratio of one is slightly higher than the reaction with ratio of two.

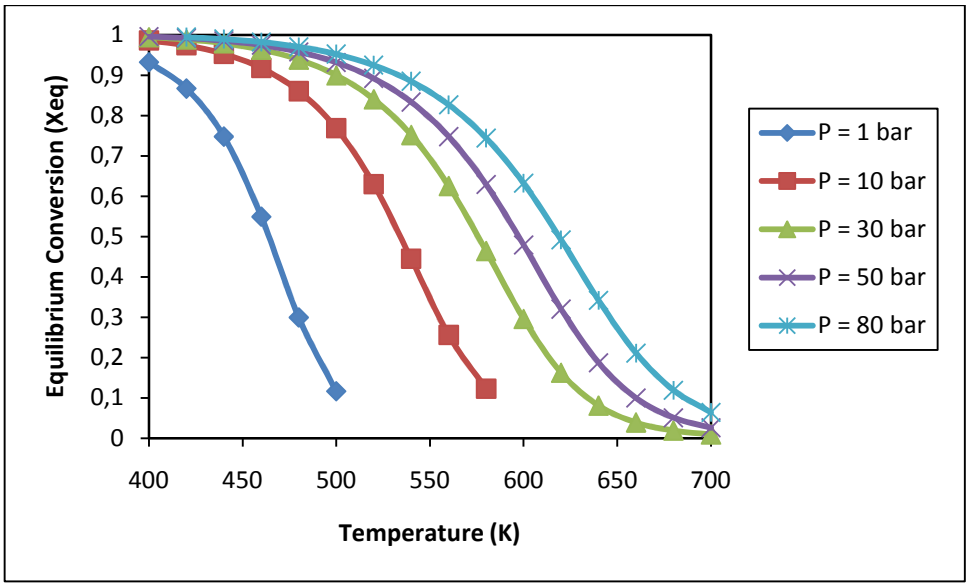

Figure 11. The equilibrium curve for direct DME synthesis with feed ratio (H_2/CO) of 1 [considering reaction (9): $3CO + 3H_2 \rightarrow CH_3OCH_3 + CO_2$]

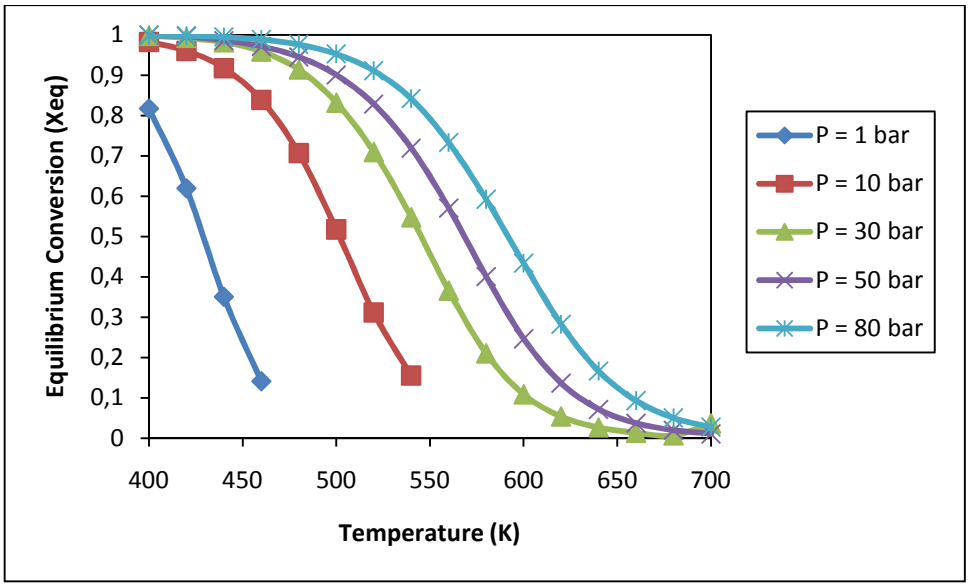

Figure 12. The equilibrium curve for direct DME synthesis with feed ratio (H_2/CO) of 1 [considering reaction (10): $2CO + 4H_2 \rightarrow CH_3OCH_3 + H_2O$]

By considering all of these results and also safety conditions and economical aspects, 50 bars was chosen as our operating pressure and it was decided to keep constant during the experiments. In addition to this, reactant feed ratio was adjusted to one and the temperature range for the analyses was taken between 200-400°C.

CHAPTER 8

EXPERIMENTAL STUDIES

In this chapter, synthesis procedures of bifunctional DME synthesis catalysts by using one-pot hydrothermal synthesis, impregnation and physical mixing methods are explained in detail. Moreover, the characterization techniques that were used for the analysis of chemical and physical properties of the synthesized catalysts are described and finally the experimental set-up which is built in Chemical Reaction Engineering Laboratory to carry out the direct DME synthesis reactions with synthesized catalysts is described in detail.

8.1. Synthesis of Catalysts

Direct synthesis of DME from syngas requires bifunctional catalysts having two different active sites; one for methanol formation (Cu/ZnO) and the other for methanol dehydration. As it was stated in Chapter 3, Copper (Cu) is the active metal for methanol formation reaction. In addition to this, Zinc (Zn) prevents agglomeration of copper and increases its stability. Another metal, Zirconium (Zr) which was also used in catalyst preparation, causes higher dispersion of copper in the catalyst structure. On the other hand, for the methanol dehydration reaction, catalysts having Brönsted acid sites are needed.

In this work, for the preparation of bifunctional catalysts, weight ratios of metal oxides ($CuO/ZnO/Al_2O_3$) were chosen as (50:40:10 wt %) respectively and these ratios were kept constant for all of the catalysts. Also Al/Si weight ratio was

determined as 0.03. In addition to these catalysts, in the synthesis of one catalyst, Silicatungstic acid (STA) was used instead of aluminum oxide. W/Si weight ratio was taken as 0.4.

In the following sections of this chapter synthesis of bifunctional catalysts were described step by step.

8.1.1. Synthesis of CuO-ZnO-Al_2O_3-MCM-41 Type Mesoporous Catalysts by One-pot Hydrothermal Synthesis Method (HS1 & HS5)

CuO-ZnO-Al_2O_3-MCM-41 type catalytic materials were synthesized by following acidic and basic one-pot hydrothermal synthesis routes. MCM-41 synthesis was proceeded according to the procedure described by Sener [72] with modifications. The catalyst synthesized by basic hydrothermal synthesis route was named as HS1 and the one synthesized by acidic hydrothermal synthesis route was named as HS5.

8.1.1.1. Synthesis Procedure

For the synthesis of the catalysts, the following chemical reagents were used;

- Source of Surfactant: N-Cetyl-N,N,N-trimethylammonium bromide (CTMABr), $C_{16}H_{33}(CH_3)_3NBr$, (99% pure powder, MW: 364.46 g/mol, Merck)
- Source of Solvent: Deionized water (Millipore Ultra-Pure Water System, Milli-QPlus)
- Source of Silica: Tetraethylorthosilicate (TEOS), $C_8H_{20}O_4Si$ (Merck)
- Source of Zinc: Zinc nitrate tetrahydrate, $Zn(NO_3)_2.6H_2O$, Merck
- Source of Copper: Copper nitrate trihydrate, $Cu(NO_3)_2.3H_2O$, Merck

- Source of Aluminium: Aluminium nitrate nanohydrate, $Al(NO_3).9H_2O$, Merck
- Source of base: 1M Sodium Hydroxide (NaOH), Merck

In the synthesis procedure of the HS1 & HS5 catalysts, five steps were followed; preparation of synthesis solution, hydrothermal synthesis, washing and filtration, drying and calcination. The schematic representation of these steps was given in Figure 13 and they were explained in details in the following sections.

a) Preparation of Synthesis Solution

13.2 grams of surfactant was dissolved in 87 ml of deionized water. The solution was heated up to 30°C in order to obtain a complete dissolution of surfactant and the clear solution was stirred for half an hour with magnetic stirrer keeping the temperature between 30-35°C. Then 15.64 ml of silica source was added drop-wise to the clear solution with continuous stirring. In this preparation step of HS1 catalyst, the pH value of the obtained clear solution was adjusted to 11 by adding 1M NaOH. The final pH value of MCM-41 synthesis solution for HS5 was measured as 3.4. Finally, the resulting solutions were stirred for one more hour.

During the preparation of the MCM-41 synthesis solution, preparation of metal nitrate solutions was also started. Pre-determined amounts of metal nitrates were dissolved in deionized water at different bakers and then they mixed together and stirred for an hour. The pH value of final metal nitrate solution was measured as 2.5. After one hour mixing, the obtained metal nitrate solution was added drop-wise into the prepared MCM-41 synthesis solution and after one more hour mixing pH values of final solutions obtained for HS1 and HS5 were measured 8.0 and 3.2, respectively.

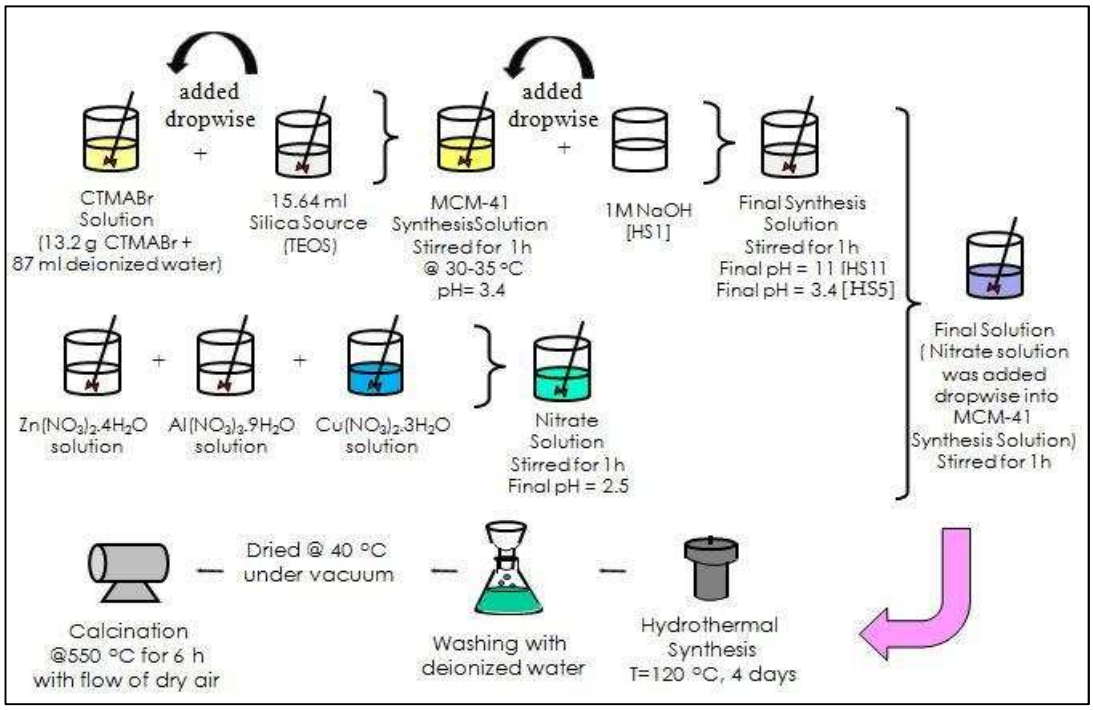

Figure 13. Synthesis procedures of HS1 and HS5 catalysts

b) Hydrothermal Synthesis

After one hour mixing, the obtained light blue homogenous solution was transferred to a Teflon bottle, which was placed in a stainless-steel autoclave. The hydrothermal synthesis was carried out at 120°C for 96 hours under the vapor pressure of the solution occurred in the closed stainless-steel autoclave.

c) Washing with Deionized Water and Filtration

At the end of 96 hours, the resultant solids having blue color (for both of the catalysts) were taken into bakers and waited in 300 ml of deionized water for three to five days. Then obtained materials were washed with deionized water six times for HS1 and five times for HS5 to remove the sodium ions and excess template from the material. After each washing step, the obtained solid was taken from the filtration paper, put in a baker and stirred with 300 ml of deionized water for half an hour. This

washing procedure was continued until the pH value of the residual washing liquid remained constant. The pH value of washing liquid was measured 7.2 for HS1 and 5.9 for HS5. After washing steps were completed, the obtained catalytic materials were dried at 40°C in an oven for 24 hours under vacuum.

d) Calcination

Calcination is the final step of the one-pot hydrothermal synthesis. The aim of calcination procedure is to remove the surfactant from the pores of the obtained material. After drying, obtained solid material was calcined in a quartz tubular reactor placed in a tubular furnace by heating from ambient temperature to 550°C at a rate of 1°C/min and was kept at 550°C for 6 hours in a flow of dry air, having a flow rate of about $1dm^3$/min. The quartz reactor has a membrane in the middle and this membrane prevents solids from removing in the flow of dry air. The exit of the reactor was connected to ventilation with a pipe to discharge the gas products. At the end of the 6 hours, heater of the tubular furnace was turned off and the flow of dry air was continued until the reactor temperature decreased to nearly 200°C.

8.1.2. Synthesis of CuO-ZnO-(Al_2O_3/SiO_2) Type Mesoporous Catalyst by Impregnation Method (IMP1)

CuO-ZnO-(Al_2O_3/SiO_2) type mesoporous catalyst was synthesized by impregnation method. The obtained catalyst was denoted as IMP1. Details of the synthesis route were described in the following parts of this section.

8.1.2.1. Synthesis Procedure

The chemical reagents that were used for the synthesis procedure were listed below;

- Source of Solvent: Deionized water (Millipore Ultra-Pure Water System, Milli-QPlus)
- Source of Zinc: Zinc nitrate tetrahydrate, $Zn(NO_3)_2.6H_2O$, Merck

- Source of Copper: Copper nitrate trihydrate, $Cu(NO_3)_2.3H_2O$, Merck
- Active mesoporous component: Alumina silicate, Al_2O_3/ SiO_2, Sigma Aldrich

Mainly three steps were followed in the synthesis procedure of IMP1. These steps were preparation of synthesis solution, evaporation and drying, and finally calcination. A schematic representation of the synthesis procedure was given in Figure 14.

a) Preparation of Synthesis Solution

Aluminum silicate was used as the supporting material for the preparation of IMP1 catalysts. It was obtained from commercial suppliers and its Al/Si weight ratio is 3%. Before starting the synthesis procedure, 2 grams of Al_2O_3/ SiO_2 was taken and dried at 100°C for 2 hours in order to remove the moisture from the structure. Then dried Al_2O_3/SiO_2 was weighted again and amounts of metal sources were decided according to final weight. After that, obtained Al_2O_3/SiO_2 and 35 ml deionized water was mixed in a baker and stirred for 2 hours with magnetic stirrer at 350 rpm. Meanwhile, copper nitrate and zinc nitrate used as copper and zinc sources respectively. Pre-determined amounts of metal nitrate sources weighted and dissolved in 10 ml of deionized water separately. After complete dissolution, they mixed together and stirred for two hours.

At the end of two hours, nitrate solution was added drop-wise into the Al_2O_3/SiO_2 suspension while stirring. Then obtained mixture was stirred for 24 hours at room temperature in order to achieve a homogenous dispersion of metals inside the pores of support material.

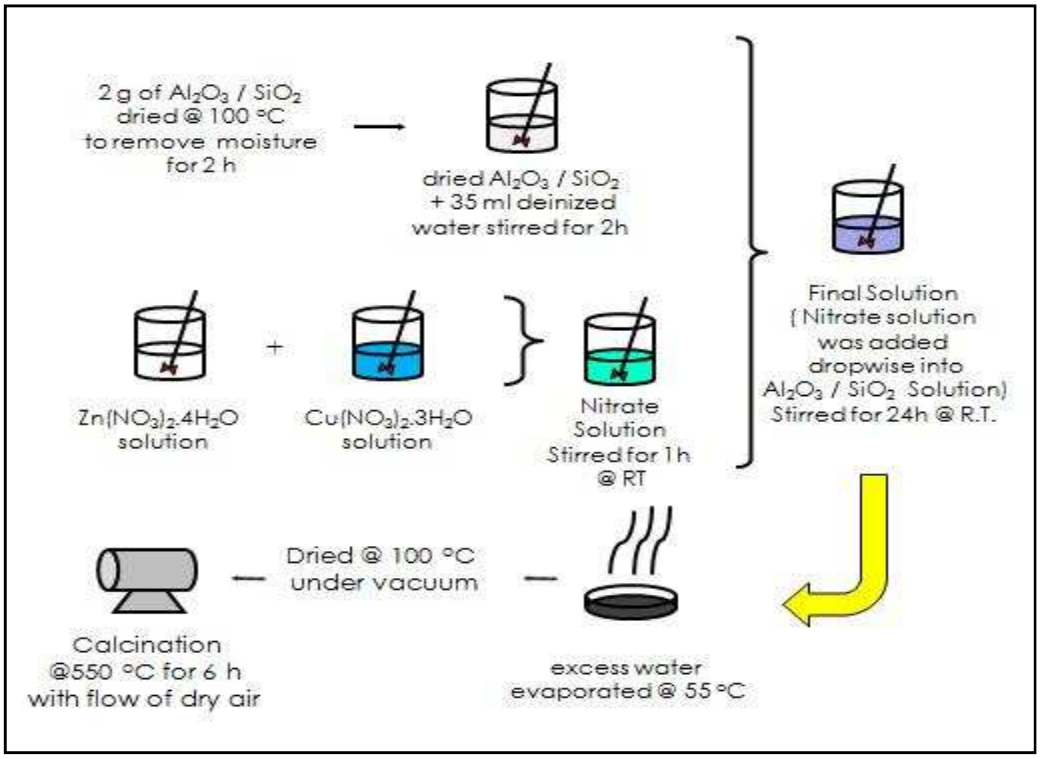

Figure 14. Synthesis procedure of IMP1 type mesoporous catalyst

b) Evaporation and Drying

After 24 hours mixing, excess water in the final solution was evaporated at 55°C and obtained solid material after evaporation dried in an oven at 100°C for 24 hours under vacuum.

c) Calcination

In the impregnation method, the aim of calcination is to remove the nitrates coming with metal sources, from the catalyst structure. Calcination procedure was performed at 550°C through the same procedure as it was described in Section 8.1.1.1. part a.

The experimental conditions of synthesized HS1, HS5 and IMP1 catalysts are listed in Table 8.

Table 8. Experimental conditions of the catalysts synthesized by one-pot hydrothermal synthesis and impregnation methods

Notation	Al/Si (wt. %)	Cu/Si (wt. %)	Zn/Si (wt. %)	Synthesis Route	pH of the solution
HS1	0.027	0.21	0.18	Basic one-pot hydrothermal synthesis	11.0
HS5	0.027	0.21	0.18	Acidic one-pot hydrothermal synthesis	3.4
IMP1	0.027	0.21	0.18	Impregnation	-

8.1.3. Synthesis of CuO-ZnO-Al_2O_3-MCM-41 Type Mesoporous Catalysts by Na_2CO_3 Modified One-pot Hydrothermal Synthesis Method (HS3 & HS4)

CuO-ZnO-Al_2O_3-MCM-41 type catalytic materials were synthesized by following sodium carbonate (Na_2CO_3) modified one-pot hydrothermal synthesis routes. In this procedure, Na_2CO_3 was used as the precipitating agent in the mixed metal nitrate solution in order to achieve closer connection between ingredients and to form mixed crystallites containing metal oxides in the nitrate solution [82]. In addition to this, hot deionized water (363 K) was used during the washing step in order to minimize the effects of remaining sodium ions on the activity of the catalyst [50]. The catalysts synthesized by using this procedure named as HS3 and HS4.

8.1.3.1. Synthesis Procedure

For the synthesis of the catalysts, the following chemical reagents were used;

- Source of Surfactant: N-Cetyl-N,N,N-trimethylammonium bromide (CTMABr), $C_{16}H_{33}(CH_3)_3NBr$, (99% pure powder, MW: 364.46 g/mol, Merck)

- Source of Solvent: Deionized water (Millipore Ultra-Pure Water System, Milli-QPlus)
- Source of Silica: Tetraethylorthosilicate (TEOS), $C_8H_{20}O_4Si$ (Merck)
- Source of Zinc: Zinc nitrate tetrahydrate, $Zn(NO_3)_2.6H_2O$, Merck
- Source of Copper: Copper nitrate trihydrate, $Cu(NO_3)_2.3H_2O$, Merck
- Source of Aluminium: Aluminium nitrate nanohydrate, $Al(NO_3).9H_2O$, Merck
- Precipitating Agent: 0.5M Sodium Carbonate (Na_2CO_3), Merck (prepared in the laboratory)

In the synthesis procedure of the HS3 & HS4 catalysts, five steps were followed; preparation of synthesis solution, hydrothermal synthesis, washing and filtration, drying and calcination.

a) Preparation of Synthesis Solution

13.2 grams of surfactant was dissolved in 87 ml of deionized water. The solution was heated up to 30°C in order to obtain a complete dissolution of surfactant and the clear solution was stirred for half an hour with magnetic stirrer keeping the temperature between 30-35°C. Then 15.64 ml of silica source was added drop-wise to the prepared solution with continuous stirring. The final pH value of MCM-41 synthesis solution was measured as 3.2. Meanwhile, preparation of metal nitrate solutions was also started. Pre-determined amounts of metal nitrates were dissolved in deionized water at different bakers and then they were mixed together and stirred for an hour. The pH value of final metal nitrate solution was measured as 2.6. After one hour mixing, 0.5M Na_2CO_3 solution was added drop-wise into the nitrate solution until the pH value of 8 was obtained. From this point slightly different procedures were followed for HS3 and HS4.

In the preparation procedure of HS3, after the addition of Na_2CO_3 the obtained precipitated nitrate solution (white color suspensions in blue liquid) was stirred for two more hours and after one hour stirring homogenous solution was obtained. Then the obtained nitrate solution was added drop-wise into the prepared MCM-41 synthesis solution. The pH value of final solution was measured as 5.6.

In the preparation procedure of HS4, after the addition of Na_2CO_3 the obtained precipitated nitrate solution aged for 12 hours at room temperature and washed with hot (363K) deionized water. The pH value of washing water was measured as 7.4. Then the remaining part over the filtration paper was added into the MCM-41 solution and after an hour mixing, homogenous solution was obtained with the pH value of 6.4. The schematic representations of the preparation methods of HS3 and HS4 catalysts were illustrated at Figures 15 and 16, respectively.

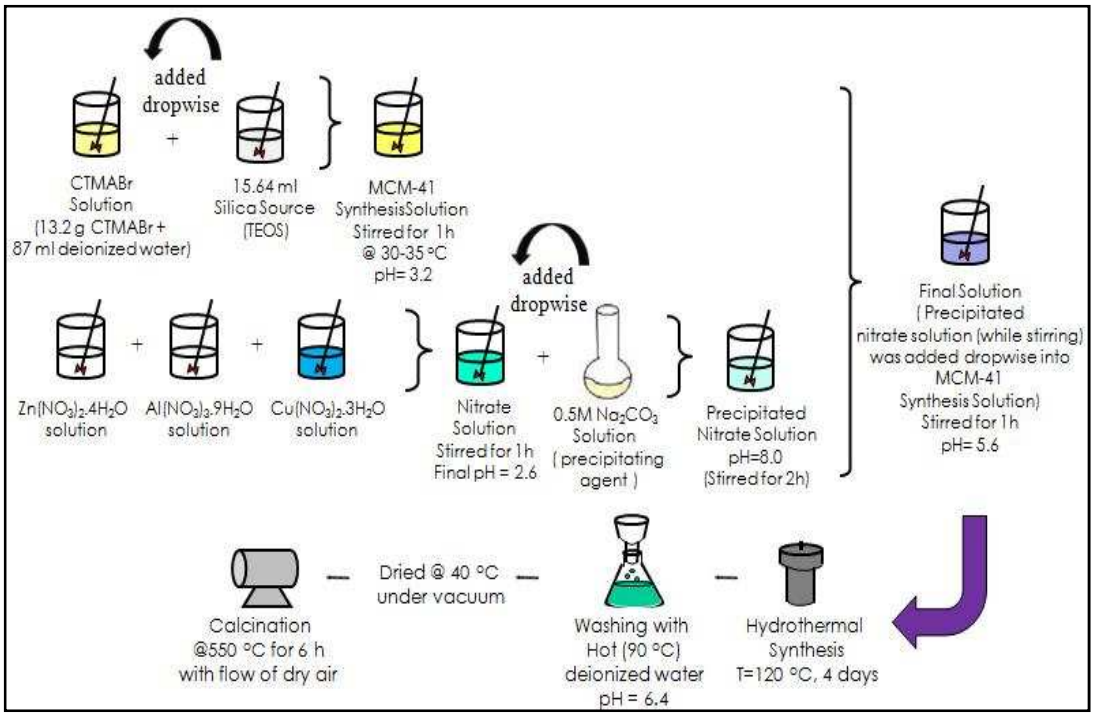

Figure 15. Synthesis procedure of HS3 type mesoporous catalyst

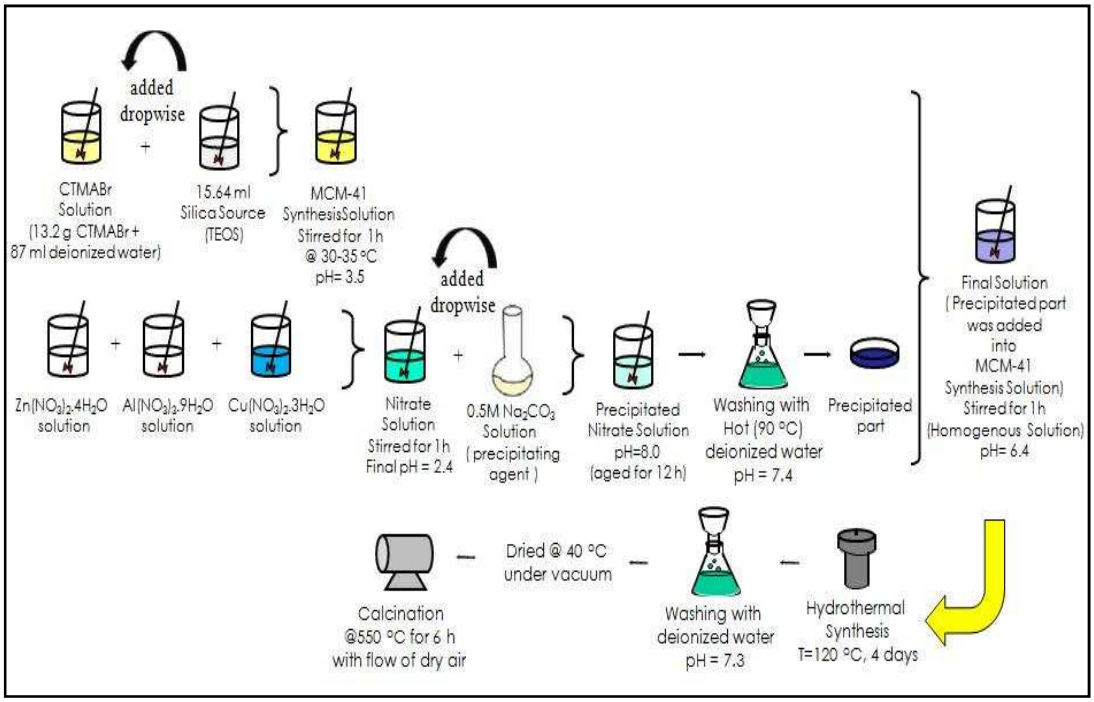

Figure 16. Synthesis procedure of HS4 type mesoporous catalyst

b) Hydrothermal Synthesis

After one hour mixing, the obtained solutions were transferred to a Teflon bottle and placed in a stainless-steel autoclave. The hydrothermal synthesis was carried out at 120°C for 96 hours.

c) Washing with Deionized Water and Filtration

At the end of 96 hours, the resultant solids were taken out from the autoclave and waited for 5 days in 300 ml deionized water. HS3 was washed with hot deionized water and final pH value of washing water measured 6.4. HS4 was washed with deionized water at room temperature and washing water pH value was measured as 7.3. After washing step, obtained solid parts were dried at 40°C in an oven for 24 hours under vacuum.

d) Calcination

After drying, obtained solid materials were calcined in a quartz tubular reactor placed in a tubular furnace by heating from ambient temperature to 550°C at a rate of 1°C/min and was kept at 550°C for 6 hours in a flow of dry air.

The experimental conditions of the catalysts synthesized by Na_2CO_3 modified one-pot hydrothermal synthesis method are presented in Table 9.

Table 9. Experimental conditions of the catalysts synthesized by Na_2CO_3 modified one-pot hydrothermal synthesis

Notation	**Precipitating Agent**	**Treatment (nitrate solution)**	**Temperature of washing water (after hydrothermal synthesis)**
HS3	Na_2CO_3	Precipitated + stirred for 2h	90°C
HS4	Na_2CO_3	Precipitated + aged for 12 hours + washed with hot(90°C) deionized water	Room temperature

8.1.4. Synthesis of ZrO_2 modified CuO-ZnO-Al_2O_3-MCM-41 Type Mesoporous Catalysts by One-pot Hydrothermal Synthesis Method (Zr-1, Zr-2 & Zr-3)

ZrO_2 modified CuO-ZnO-Al_2O_3-MCM-41 type catalytic materials were synthesized by following acidic and neutral one-pot hydrothermal synthesis routes. As it was previously mentioned in Chapter 3, Zirconium (Zr) causes higher dispersion of Copper (Cu) in the catalyst structure. In this section effects of

Zirconium with different weight ratios and effects of acidic and neutral hydrothermal synthesis routes were investigated.

8.1.4.1. Synthesis Procedure

For the synthesis of the catalysts, the following chemical reagents were used;

- Source of Surfactant: N-Cetyl-N,N,N-trimethylammonium bromide (CTMABr), $C_{16}H_{33}(CH_3)_3NBr$, (99% pure powder, MW: 364.46 g/mol, Merck)
- Source of Solvent: Deionized water (Millipore Ultra-Pure Water System, Milli-QPlus)
- Source of Silica: Tetraethylorthosilicate (TEOS), $C_8H_{20}O_4Si$ (Merck)
- Source of Zinc: Zinc nitrate tetrahydrate, $Zn(NO_3)_2.6H_2O$, Merck
- Source of Copper: Copper nitrate trihydrate, $Cu(NO_3)_2.3H_2O$, Merck
- Source of Aluminium: Aluminium nitrate nanohydrate, $Al(NO_3).9H_2O$, Merck
- Source of Zirconium: Zirconyl nitrate monohydrate, $ZrO(NO_3)_2.H_2O$, Aldrich
- Source of base: 1M Sodium Hydroxide (NaOH), Merck

Main steps followed through the synthesis procedure of the catalysts were; preparation of synthesis solution, hydrothermal synthesis, washing and filtration, drying and calcination. The schematic representation of these steps was given in Figure 17 and they were explained in details in the following sections.

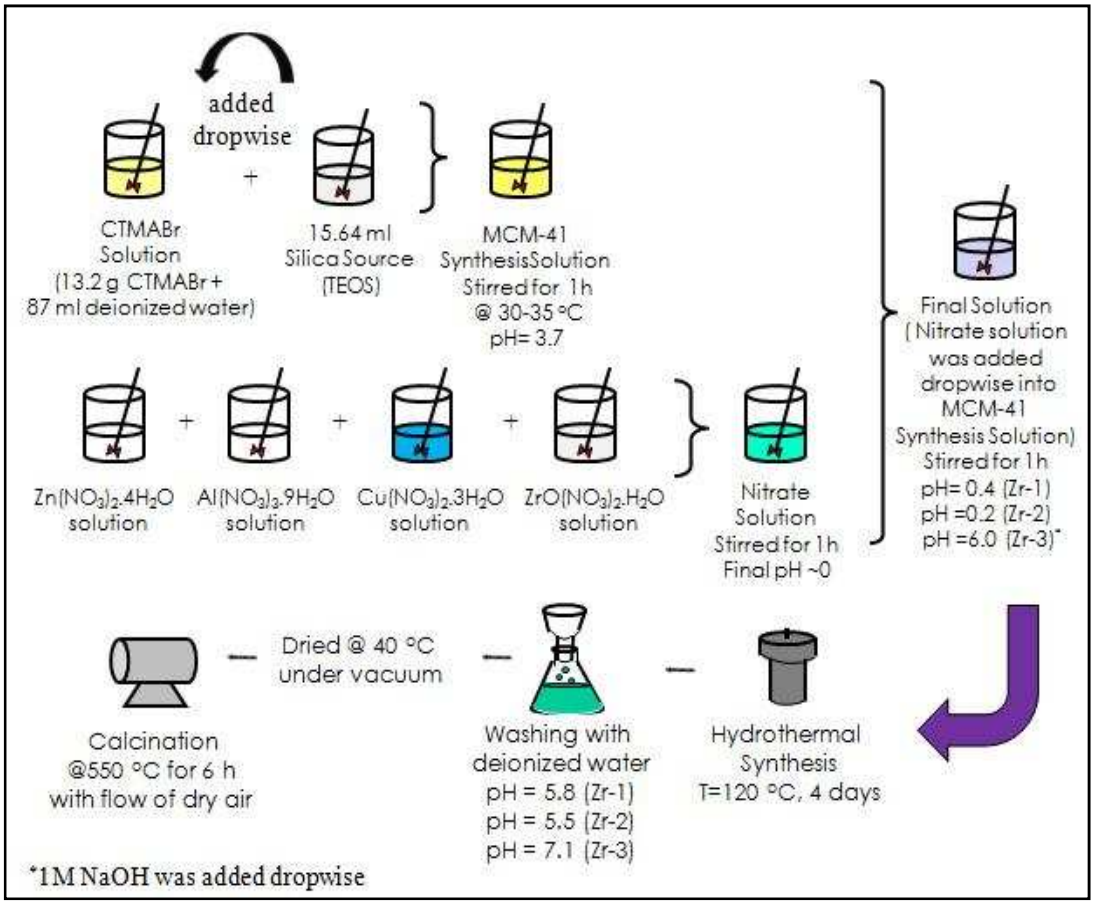

Figure 17. Synthesis procedures of Zr-1, Zr-2 and Zr-3 mesoporous catalysts

a) Preparation of Synthesis Solution

For the preparation of synthesis solutions of the catalysts, the same one-pot hydrothermal synthesis procedure was followed which was described in section 8.8.1.1. The only difference is addition of Zirconium source into the nitrate solution. Due to the high acidity of Zirconium source, the final pH value of nitrate solution was suddenly decreased to almost zero. After addition of nitrate solution to the MCM-41 solution, for Zr-3 1M NaOH was added drop-wise into the final solution until pH value of 6 was obtained.

b) Hydrothermal Synthesis

After one hour mixing, final solutions were transferred to a Teflon bottle and placed in a stainless-steel autoclave. The hydrothermal synthesis was carried out at 120°C for 96 hours.

c) Washing with Deionized Water and Filtration

After hydrothermal synthesis, washing step was conducted as it was described in previous sections. The final pH values of washing waters of the catalysts Zr-1, Zr-2 and Zr-3 were measured as 5.8, 5.6 and 7.1, respectively. Final products were dried at 40°C in an oven for 24 hours under vacuum.

d) Calcination

After drying, obtained solid materials were calcined in a quartz tubular reactor placed in a tubular furnace by heating from ambient temperature to 550°C at a rate of 1°C/min and was kept at 550°C for 6 hours in a flow of dry air.

The experimental conditions of the catalysts synthesized by ZrO_2 modified one-pot hydrothermal synthesis procedure are given in Table 10.

Table 10. Experimental conditions of the catalysts synthesized by ZrO_2 modified one-pot hydrothermal synthesis

Notation	ZrO_2/ (CuO-ZnO-Al_2O_3) (wt.%)	Synthesis Route	pH of the solution
Zr-1	10	Acidic	0.4
Zr-2	20	Acidic	0.2
Zr-3	20	Neutral	6.0

8.1.5. Synthesis of Methanol Dehydration Catalysts to be Physically Mixed with Commercial Methanol Reforming Catalyst (HiFUEL-R120)

Commercial methanol reforming catalyst and prepared methanol dehydration catalysts were physically mixed for testing in direct DME synthesis reactions. Commercial methanol reforming catalyst was obtained from HIFUEL R120, Alfa Aesar. A methanol reforming catalyst is represented by general formula $(CuO)_w(ZnO)_x(Al_2O_3)_yM_z$ where M is indicating one of the oxides selected from the group of lanthanum oxide, gallium oxide, cerium oxide and chromium oxide. Since methanol synthesis reaction is favorable over the catalysts comprising copper, zinc and aluminum metals, this commercial methanol reforming catalyst was decided to use for the preparation of direct DME synthesis catalysts by physical mixing. Commercial catalysts were in the pellet form (5.2mm x 3.0mm) so that required amount of catalyst was crushed into smaller particles (~0.2 mm) before syntheses.

For methanol dehydration two different catalysts were used. The first one of them is alumina modified MCM-41 having an Al/Si ratio of 0.03 which was prepared by hydrothermal synthesis route (Al-MCM-41). The second one, which was denoted as TRC75(L), is silicotungstic acid(STA) modified MCM-41 having a W/Si ratio of 0.4. This catalyst was synthesized by Ciftci [91] for methanol dehydration. In the DME synthesis reaction, these dehydration catalysts were mixed with the commercial methanol reforming catalyst with a weight ratio of 1:1.

8.1.5.1. Synthesis Procedures of Dehydration Catalysts

For the synthesis of the catalysts, the following chemical reagents were used;

- Source of Surfactant: N-Cetyl-N,N,N-trimethylammonium bromide (CTMABr), $C_{16}H_{33}(CH_3)_3NBr$, (99% pure powder, MW: 364.46 g/mol, Merck)
- Source of Solvent: Deionized water (Millipore Ultra-Pure Water System, Milli-QPlus)
- Source of Silica: Tetraethylorthosilicate (TEOS), $C_8H_{20}O_4Si$, Merck

- Source of Aluminium: Aluminium nitrate nanohydrate, $Al(NO_3).9H_2O$, Merck
- Silicotungstic acid (STA), (Sigma-Aldrich)
- Commercial Methanol Synthesis Catalyst (HIFUEL R120, Alfa Aesar)

a) Preparation of Methanol Dehydration Catalysts

For the preparation of the catalysts, MCM-41 synthesis solution was prepared as it was described in the previous sections. In Al-MCM-41, Aluminum was used as active component and in TRC75(L), STA was used as the active component. Separately prepared active component solutions with deionized water were added drop-wise into the MCM-41 synthesis solution and the final solutions were stirred one more hour. After that, final solutions were transferred to a Teflon bottle and placed in a stainless-steel autoclave. The hydrothermal synthesis was carried out at 120°C for 96 hours. Then obtained solid materials were washed, filtrated and dried at 40°C in an oven for 24 hours under vacuum. Al-MCM-41 was calcined at 550°C and TRC75(L) was calcined at 350°C. Details of the TRC75(L) synthesis procedure were given by Ciftci [87].

b) Preparation of Direct DME Synthesis Catalysts by Physical Mixing

- *Preparation of Al-MC-1:* 2 grams of synthesized Al-MCM-41 catalyst was suspended in deionized water and in the meantime 2 grams of commercial HiFUEL-R120 catalyst was also suspended in deionized water in separate vessel. These suspensions were stirred for an hour and after one hour stirring they mixed together. The mixture stirred for 24 hours at room temperature, excess water was evaporated at 55°C and dried at 100°C in an oven for 24 hours under vacuum. In the preparation of Al-MC-1 wet physical mixing was used in order to obtain more homogenous distribution.

- *Preparation of TRC75(L)-C:* One gram of TRC75(L) was mixed with one gram of commercial HiFUEL-R120 catalyst by using dry physical mixing method. Before mixing, their particle sizes were adjusted to ~0.2 mm by

crushing. Then they mixed together in a baker and stirred until observing a homogenous distribution.

The schematic representations of preparation procedures were given in Figure 18 and the experimental conditions of the prepared catalysts by physical mixing method were summarized in Table 11.

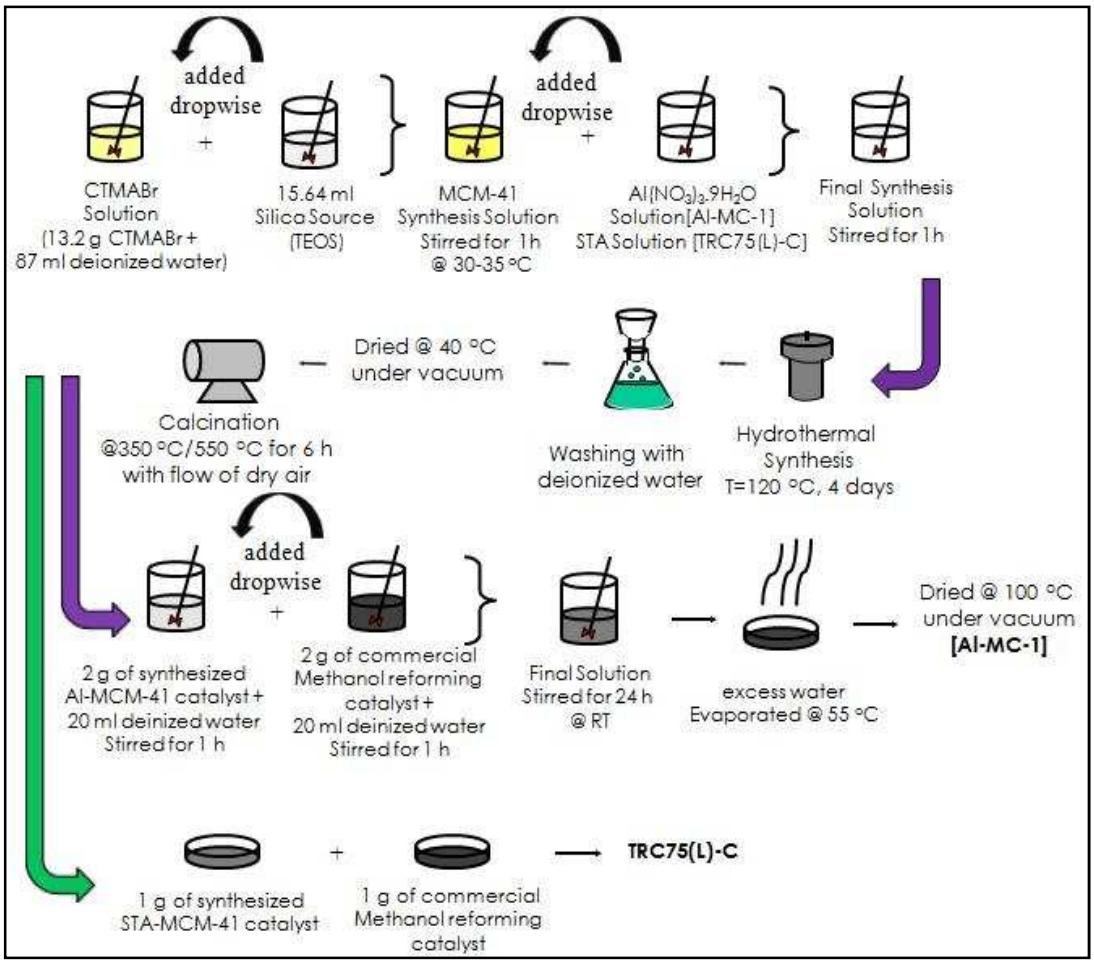

Figure 18. Synthesis procedures of Al-MC-1 and TRC75(L)-C catalysts

Table 11. Comparison of catalysts prepared by physical mixing method

Notation	MRC*	MDC**	Weight ratio (MRC / MDC)	Active component (MDC)	Acitve comp. / Silica ratio (MDC)	Calc. temp. (MDC)	Prep. Route
Al-MC-1	Commercial MRC HIFUEL R120	Al-MCM-41	1/1	Aluminum	Al/Si = 0.03	550°C	Wet Physical Mixing
TRC75L-C	Commercial MRC HIFUEL R120	TRC75L	1/1	STA	W/Si = 0.4	350°C	Dry Physical Mixing

*MRC: Methanol Reforming Catalyst
**MDC: Methanol Dehydration Catalyst

8.2. Material Characterizaton Techniques

Different characterization techniques were used in order to analyze the physical and chemical properties of the synthesized catalysts. In this study X-ray diffraction (XRD), energy dispersive spectroscopy (EDS), scanning electron microscopy (SEM), nitrogen physisorption and Diffuse Reflectance Infrared Fourier Transform Spectroscopy (DRIFTS) of Pyridine Adsorption techniques were employed for the characterization of the prepared materials.

8.2.1. X-Ray Diffraction (XRD)

X-Ray diffraction provides us information about the pore structure of the materials [88]. In this study, XRD patterns of all synthesized materials were performed by the Rigaku D/MAX2200 diffractometer with a CuK radiation source with a 2θ scanning range between 1°- 80° at a step size of 0.02.

8.2.2. N_2 Physisorption

Nitrogen adsorption-desorption analyses of the synthesized catalysts were done by the Quantachrome Autosorb-1-C/MS instrument in the METU Central Laboratory. Each sample was degassed at 110°C for 16 hours before analyses and characterization was performed at a relative pressure range of $5x10^{-2}$ to 0.99 at liquid nitrogen temperature. The results of the characterization gave information about multipoint BET surface area values, BJH adsorption and desorption pore diameters and pore volumes of the samples.

8.2.3. Scanning Electron Microscopy (SEM)

The morphologies of the synthesized materials were determined by using a Scanning Electron Microscope, JSM-6400 (JEOL) equipped with NORAN system Six in Metallurgical and Materials Engineering. Samples containing Zirconium were coated with carbon and the others were coated with gold for analysis.

8.2.4. Energy Dispersive Spectroscopy (EDS)

Energy Dispersive Spectroscopy (EDS) analyses were carried out in METU Metallurgical and Materials Engineering Department by a JSM-6400 (JEOL) instrument equipped with NORAN System Six in order to determine the near surface composition of the materials.

8.2.5. Diffuse Reflectance Infrared Fourier Transform Spectroscopy (DRIFTS) of Pyridine Adsorption

DRIFT Spectra of pyridine adsorption is used to analyze the acid sites of the synthesized materials. DRIFTS of pyridine adsorption analyses were carried out by

using a Perkin Elmer Spectrum One instrument in the Kinetic Laboratory in METU Chemical Engineering Department. Before the analyses, samples were dried at 110°C for 16 hours and then 1 mL of pyridine was added drop-wise on the samples. After waiting for two hours, pyridine adsorbed samples were weighted and 0.035 g of each sample was mixed with 0.07 g KBr. Same procedure was followed for the preparation of fresh catalysts. A reference spectrum was recorded with KBr. And finally, the spectra of the fresh samples were subtracted from the spectra of the pyridine adsorbed samples in order to determine the relative intensities of Lewis and Brönsted acid sites of the synthesized materials.

Pyridine adsorption of FT-IR spectrum analyses of Zr-1, Zr-2 and Zr-3 catalysts were carried out by using Perkin Elmer Spectrum One instrument in Gazi University Chemical Engineering Department. Helium was used as carrier gas and its flow rate was adjusted to 100 ml/min. The same procedure was followed for the preparation of pyridine adsorbed and fresh catalysts. Then the prepared samples pelletized under 1000 psia for five minutes and again the same procedure was followed for determination of Lewis and Brönsted acid sites of the materials.

8.3. Experimental Set-up of Direct DME Synthesis Reaction System

Direct DME synthesis reaction was carried out in a pressurized fixed bed flow reactor system. The system was built in the Chemical Reaction Engineering Laboratory. Reactants were fed into the system from a pressurized tank containing 50% hydrogen and 50% carbonmonoxide. Since there was a pressurized gas flow in the system, construction materials of all elements in the system were chosen as stainless–steel. An on-off valve was placed before the reactor in order to stop the flow from tube through the system, in case of any unexpected situation. A metering valve was placed on the line to the reactor to adjust the pressure. A pressure gauge was placed on the gas flow line just before the reactor to read the pressure of gas entering into the reactor. Reactants are fed into the stainless steel differential reactor (¼ in.) placed in a temperature controlled tubular furnace. Synthesized catalysts were placed to the middle of the reactor and supported with quartz wool from both ends. A metering valve was placed at the exit of the reactor in order to adjust the flow rate of

the exit stream. After that, an on-off valve was also placed before the gas chromatograph.

The products and the unreacted gases were analyzed on-line by a SRI 3680 Multigas #1 GC equipped with Carbosphere column and a thermal conductivity detector (TCD). Helium was used as the reference gas for the GC and its flow rate was adjusted to 20ml/min. All the connection lines before and after the reactor were heated up to 150°C to pre-heat the reactants before the reactor and to prevent condensation of any condensable product formed in the reactor. A soap bubble flow meter was connected to the gas exit of GC in order to measure the flow rate. For all the experiments, total flow rate of the reactants was adjusted to 50 ml/min (at atmospheric pressure). The TCD detector was heated to 200°C. A temperature ramped-program was designed in order to separate the gases in the exit stream of the reactor. Details of this programme are given in Table 12 and the schematic representation of the experimental set-up is given in Figure 19.

Table 12. The programme information of Gas Chromatograph

Programme	**Initial Temperature (°C)**	**Time (min)**	**Ramp (°C/min)**	**Final Temperature(°C)**
Step 1	130	7	-	130
Step 2	130	3	40	250
Step 3	250	18	-	250

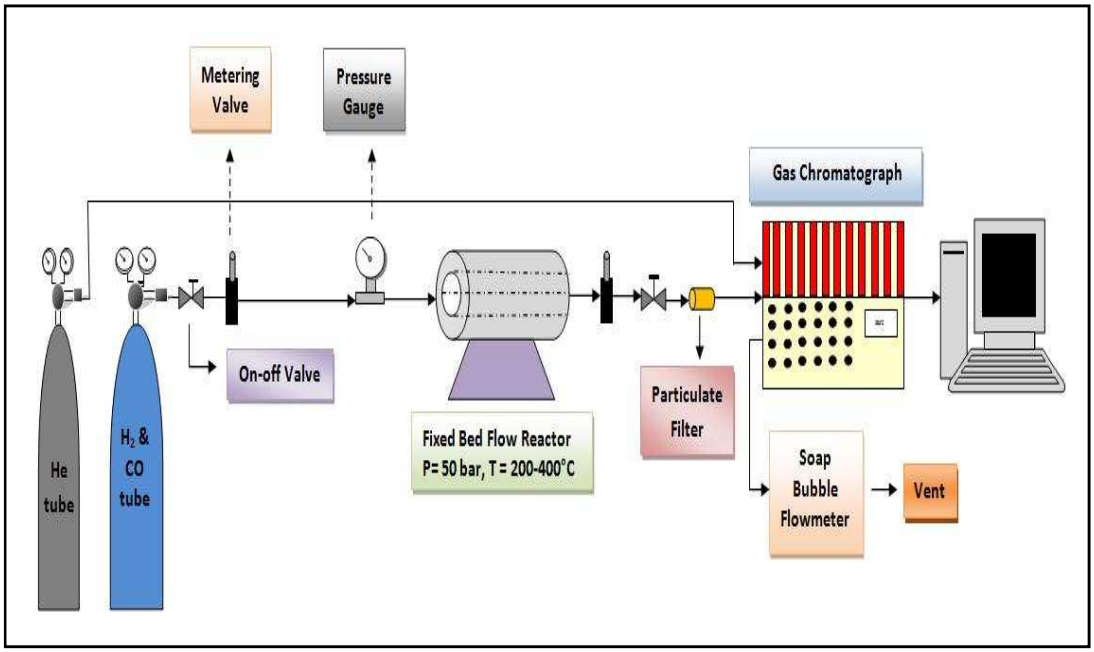

Figure 19. Schematic representation of experimental set-up

Before starting catalyst testing experiments, calibration experiments were carried out by preparing related mixtures of possible products in order to determine their retention times and the calibration factors. The calculations for calibration factors are given in Appendix B.

Catalyst testing experiments were carried out between the temperature range of 200-400°C and the pressure was kept at 50 bars in all the reactivity tests. The amount of catalyst charged to the reactor was 0.2 g in all the experiments. Space time was calculated by dividing catalyst weight placed in the reactor by total flow rate of the reactants. The value of the space time as evaluated at atmospheric pressure and room temperature was 0.24 g.s/ml. However, the actual space time at 50 bars and at the reaction temperature is expected to be quite different.

In each catalyst testing experiment, at least four successive steady state data points were taken of each temperature and the average value of these data was used for the calculations of selectivity and conversion values. Relations used for evaluation of selectivity and conversion are presented in Appendix B.

CHAPTER 9

RESULTS AND DISCUSSION

In this chapter characterization results of the synthesized catalysts are presented. In addition to these, results of direct DME synthesis reaction and effects of operation temperature on conversion, selectivity and yield of the products are discussed.

9.1. Characterization Results of the Catalysts

9.1.1. Characterization Results of CuO-ZnO-Al_2O_3-MCM-41 Type Mesoporous Catalysts Synthesized by One-pot Hydrothermal Synthesis and Impregnation Methods

9.1.1.1. X-Ray Diffraction

The X-Ray diffraction patterns of synthesized HS1, HS5 and IMP1 catalyst having Al/Si weight ratios of 0.03, were analyzed between $2\theta=1^o$-80^o and they were presented in Figure 20. A typical synthesized MCM-41 material is expected to have a major peak at $2\theta = 2.20^o$ and three reflections corresponding to 3.90^o, 4.42^o and 5.90^o [72]. In the XRD patterns of all three catalysts, major peaks corresponding to MCM-41 type materials were observed and in the XRD pattern of IMP1 catalyst in addition to major peak, two reflections were observed at 3.90^o and 4.42^o. These results

indicating that mesoporous structure was preserved in IMP1 catalyst substantially however for HS1 and HS5 catalysts, absence of the reflections was indicating a distortion in the long range ordering of mesoporous structure.

In XRD patterns of HS1 and IMP1, peaks were observed at higher 2θ values. In Table 14, 2θ and d-values of these peaks and also XRD data obtained from the literature [89] were listed. When compared with the literature data, results indicated that all the peaks observed in the XRD patterns of HS1 and IMP1 belonged to CuO in the tenorite structure. The absence of peaks corresponds to aluminum and zinc or their compounds showed that they were well-dispersed in the catalyst structure.

In the XRD pattern of HS5 catalyst, no peaks were observed at higher 2θ values which showed that the catalyst had an amorphous structure and all metals were well-dispersed in the catalyst structure without forming crystallites.

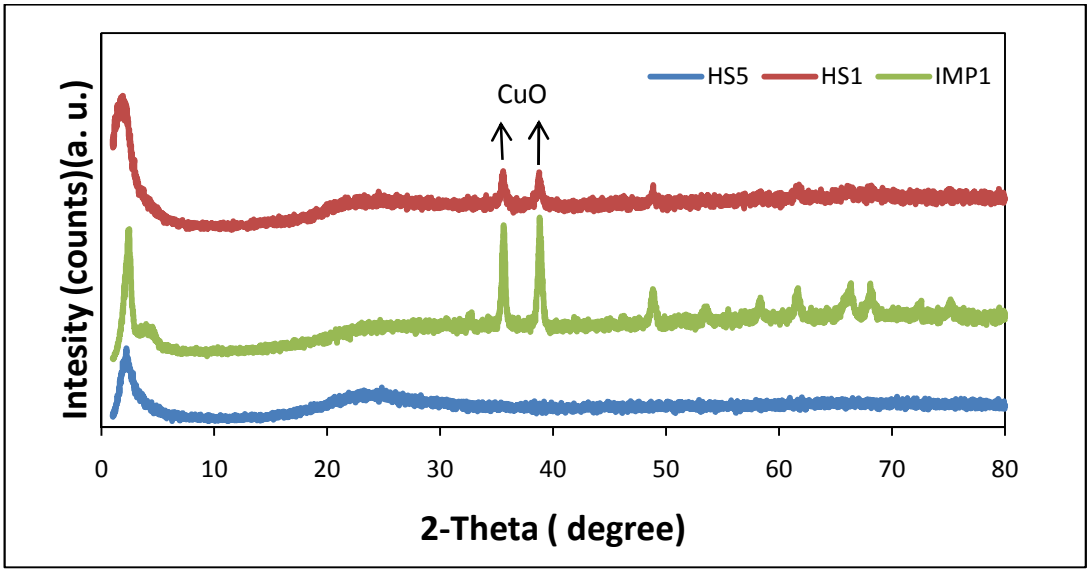

Figure 20. XRD Patterns of HS1, HS5 and IMP1 catalysts

Thicknesses of the biggest CuO crystallites observed in the XRD patterns of HS1 and IMP1 catalysts were calculated by Scherrer's equation [90] given below and the results were presented in Table 13. The calculations were done according to the peaks observed at 2θ =38.68^o for HS1 and 2θ =35.62^o for IMP1 and they were given in Appendix C.

$$t = \frac{K \times \lambda}{B \times \cos\theta}$$

t = thickness of crystallite

K = constant dependent on crystallite shape (0.89)

λ = X-ray wavelength

B = FWHM (full width at half max) or integral breadth

θ = Bragg Angle

Table 13. Crystallites Thickness of HS1 and IMP1 catalysts

Catalyst	**Crystallite Thickness (nm)**
HS1	11
IMP1	18

Table 14. Comparison of XRD pattern data of HS1 and IMP1 catalysts with literature data [89]

Peaks	Literature			HS1			IMP1		
	2θ	d-value (Å)	I/Io	2θ	d-value (Å)	I/Io	2θ	d-value (Å)	I/Io
MCM-41 peaks	2.2	39.8	100	2.26	39.06	100	2.44	36.18	94
	3.9	22.9	6.7	-	-	-	3.90	22.63	22
	4.42	19.8	3.3	-	-	-	4.74	18.63	15
	5.9	14.9	2.5	-	-	-	-	-	-
CuO Tenorite peaks	32.51	2.75	8	-	-	-	32.50	2.75	10
	35.44	2.53	60	-	-	-	-	-	-
	35.54	2.52	100	35.52	2.52	100	35.60	2.52	95
	38.94	2.31	100	38.76	2.32	94	38.78	2.32	100
	48.74	1.87	25	48.68	1.87	32	48.82	1.86	33
	53.47	1.71	7	-	-	-	53.38	1.71	14
	58.31	1.58	12	-	-	-	58.28	1.58	19
	61.55	1.51	16	61.52	1.51	33	61.64	1.50	26
	65.82	1.42	12	-	-	-	65.74	1.42	17
	66.28	1.41	14	66.16	1.41	22	66.34	1.41	33
	67.93	1.38	9	-	-	-	-	-	-
	68.15	1.37	14	-	-	-	68.10	1.38	25
	72.44	1.30	6	-	-	-	72.50	1.30	11

9.1.1.2. Energy Dispersive Spectroscopy (EDS)

The results obtained from EDS analyses were given in Table 15. As expected EDS results of IMP1 catalyst showed that metals incorporated into the catalyst structure successfully. When compare the EDS results of the catalysts synthesized by one-pot hydrothermal synthesis route, metals incorporated into the catalyst structure in HS1 successfully which was synthesized by following basic hydrothermal synthesis route. However, in HS5 which was synthesized by acidic hydrothermal synthesis route nearly all of the zinc and one-third of copper was lost from the catalyst structure during the washing step. EDS results clearly indicated that pH value of the synthesis solution was highly effective on the final physical structure of the catalyst.

Table 15. EDS results of HS1, HS5 and IMP1 catalysts

Sample ID	Al/Si (wt %)		Cu/Si (wt %)		Zn/Si (wt %)	
	Prepared	Obtained (EDS)	Prepared	Obtained (EDS)	Prepared	Obtained (EDS)
HS1	0.027	0.03	0.21	0.18	0.18	0.18
HS5	0.027	0.026	0.21	0.13	0.18	trace
IMP1	0.027	0.03	0.21	0.20	0.18	0.17

9.1.1.3. Scanning Electron Microscopy (SEM)

SEM analyses were performed in order to determine the surface morphologies of synthesized materials. In Figure 21, 100 times magnified SEM image of HS1 was presented and its average particle size was determined as nearly

200 μm. Agglomeration on the particle surface can be easily detected from the 3000 times magnified image of the material given in Figure 22.

A hundred and five hundred times magnified SEM images of HS5 catalyst are given in Figure 23 and Figure 24, respectively. Average particle size was found as ~150 μm from Figure 23.

Finally, in Figures 25 and Figure 26, SEM images of IMP1 catalyst are presented. The average particle size was determined as 20 μm from a thousand times magnified image presented in Figure 25.

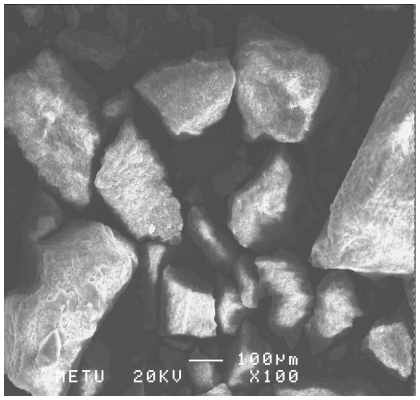

Figure 21. SEM image of HS1 (magnified 100 times)

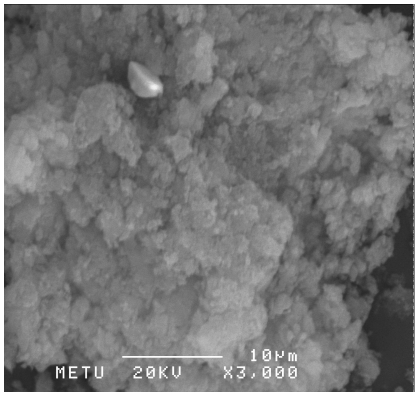

Figure 22. SEM image of HS1 (magnified 3000 times)

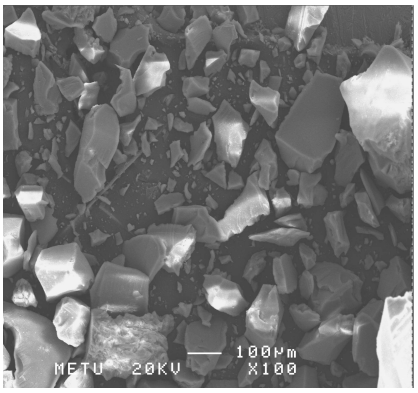

Figure 23. SEM image of HS5 (magnified 100 times)

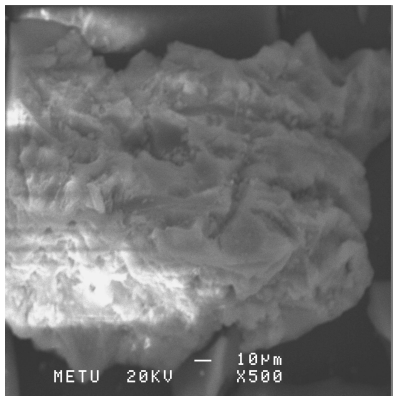

Figure 24. SEM image of HS5 (magnified 500 times)

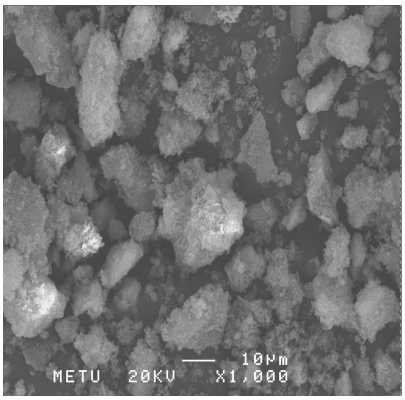

Figure 25. SEM image of IMP1 (magnified 100 times)

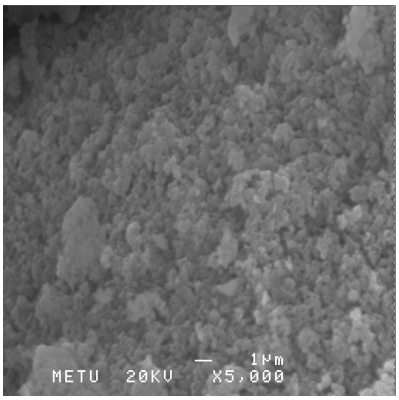

Figure 26. SEM image of IMP1 (magnified 5000 times)

9.1.1.4. Nitrogen Physisorption

The multipoint BET and BJH surface areas, average pore diameters and pore volumes of the HS1, HS5 and HS1 catalysts obtained from nitrogen physisorption analyses are presented in Table 16.

The pore volumes of the synthesized catalysts were found to be between 0.73-1.6 cm^3/g. Their BJH desorption average pore diameters were calculated in the range of 0 to 50 nm and found between 3.7-8.9 nm. The multipoint BET and BJH desorption surface areas of the catalysts were also obtained from nitrogen physisorption analyses. The BET surface areas were found between 669-722 m^2/g and BJH surface areas were found between 771-902 m^2/g.

The results indicated that more successive incorporation of metals into the structures of IMP1 and HS1 catalysts slightly decreased their surface areas. In addition to these, the surface area results showed that metals and their compounds penetrated into the catalysts frameworks successfully without blocking the pores of silica based mesoporous structures.

Table 16. Physical properties of synthesized catalysts

Sample ID	Surface Area (m^2/g)		Avg. Pore Diameter (nm) (BJH Desp.)*	Pore Volume (cm^3/g)
	BET	BJH Desp.		
HS1	722	902	8.9	1.6
HS5	804	904	6.6	1.4
IMP1	669	771	3.7	0.73

* BJH Interpolated Cumulative Desorption average pore diameter for pores in the range of 0 to 50 nm in diameter

The nitrogen adsorption-desorption isotherms of the catalysts are given in Figure 27. According to the IUPAC physisorption isotherm classification, adsorption-desorption isotherms of HS1 and HS5 showed Type IV isotherms indicating their mesoporous structures. In addition to this, again according to the UIPAC hysteresis loop classification, HS1 and HS5 catalysts showed H3 and H2 type hysteresis loops, respectively. Hysteresis loops occur due to capillary condensation in the mesoporous structures. H2 type hysteresis loops are also seen in the isotherms of porous adsorbents. Since there is no common consensus on the formation mechanisms of H2 type hysteresis loops, these hysteresis loops are generally observed for mesoporous materials having significant interconnection between the pores in the material structure. H3 type hysteresis loops are usually obtained by the aggregates of platy absorbents containing slit-shaped pores [91].

The nitrogen adsorption-desorption isotherm of IMP1 catalyst showed Type IV isotherm indicating its mesoporous structure.

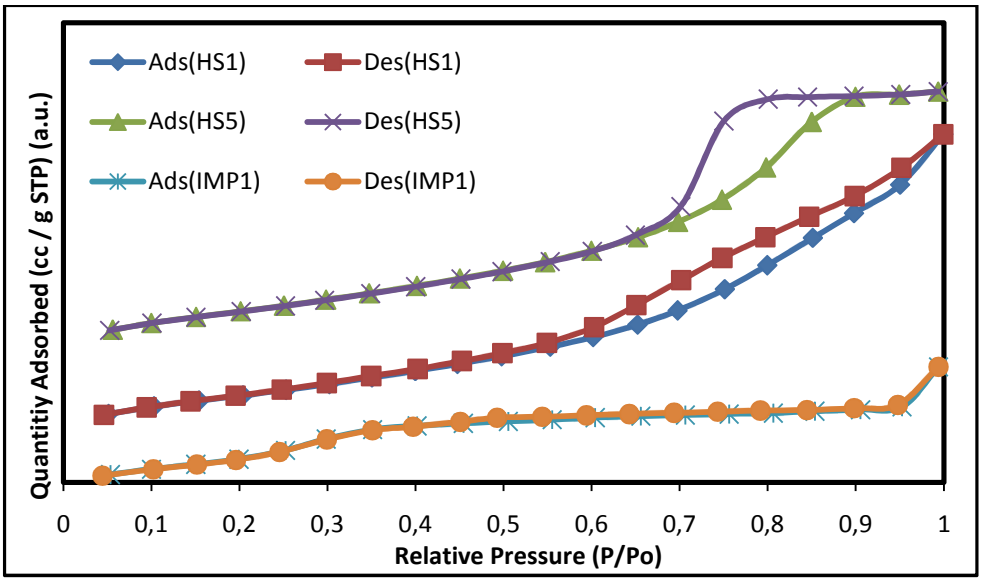

Figure 27. Nitrogen adsorption-desorption isotherms of HS1, HS5 and IMP1 catalysts

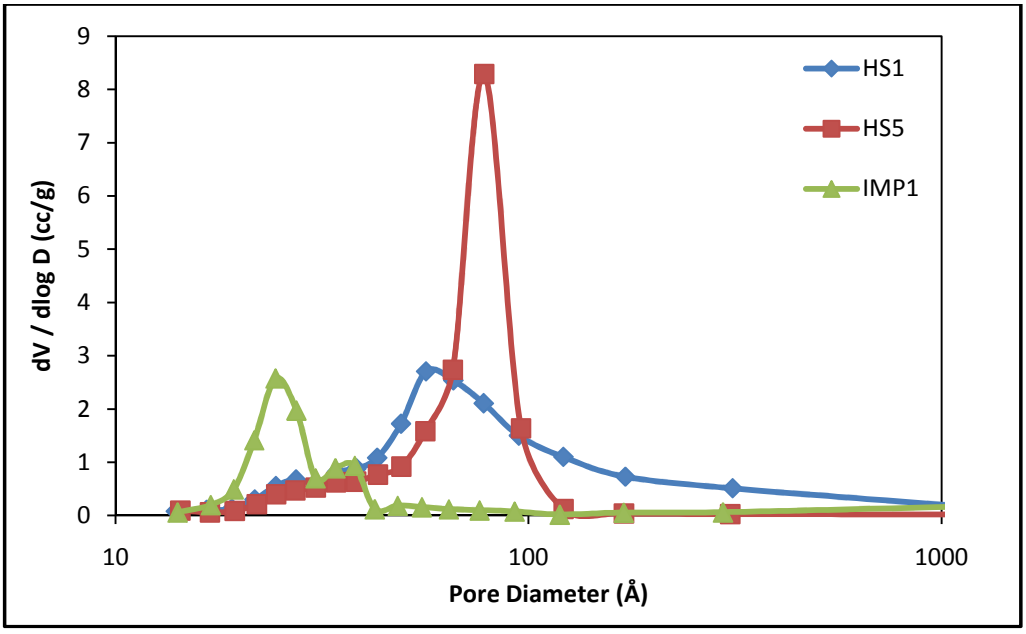

Figure 28. Pore size distributions of HS1, HS5 and IMP1 type catalysts

Pore size distributions of the synthesized catalysts were obtained from BJH desorption method and they are given in Figure 28. The results showed that catalysts having narrow pore size distribution were synthesized successfully.

9.1.1.5. DRIFT Spectra of Pyridine Adsorption

Differences of diffuse reflectance FT-IR (DRIFTS) results obtained from pyridine adsorbed catalysts and fresh catalysts are given in Figure 29. IR spectroscopy is the basic and most direct way to get information about acidity characteristic of a material from the distribution of Lewis and Brönsted acid sites on the surface [92].

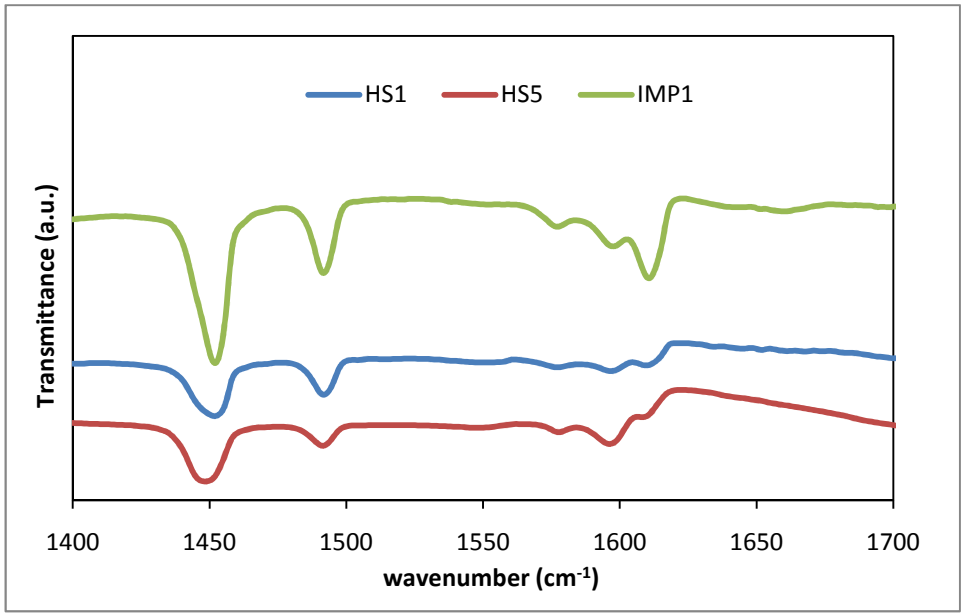

Figure 29. DRIFTS spectra of HS1, HS5 and IMP1 catalysts

The bands observed at 1453 cm^{-1}, 1576 cm^{-1}, 1597 cm^{-1} and 1612 cm^{-1} were due to Lewis acid sites [93]. A band would be expected at 1540 cm^{-1} if our materials had Brönsted acid sites. However, pyridine adsorbed DRIFTS analysis showed negligibly small band at this wave number. This result indicated that HS1, HS5 and IMP1 catalysts had very low Brönsted acidity.

DRIFTS results of the catalysts showed that the intensities of IR bands observed due to Lewis acid sites were higher for IMP1 catalyst relative to HS1 and HS5 catalysts. Brönsted acid sites are superior to Lewis acid sites for methanol dehydration reaction. For the synthesized catalysts, relative intensity of IR band due to Brönsted acid site was very low when compared to IR bands observed due to Lewis acid sites. Results indicated that acidity of the catalysts might be inadequate for conversion of methanol to DME and this conclusion was also supported by reactivity results obtained with IMP1 catalyst presented in Section 9.2.

9.1.2. Characterization Results of CuO-ZnO-Al_2O_3-MCM-41 Type Mesoporous Catalysts Synthesized by Na_2CO_3 Modified One-pot Hydrothermal Synthesis Method

9.1.2.1. X-Ray Diffraction

The XRD patterns of HS3 and HS4 catalysts synthesized by Na_2CO_3 modified one-pot hydrothermal synthesis method are presented in Figure 30. The major peak at $2\theta=2.20^o$ corresponds to MCM-41 type catalytic materials was observed only in the XRD pattern of HS3 catalyst however absence of the reflection peaks indicated that the long range ordering of mesoporous structure was highly destroyed. Similarly, in the XRD pattern of HS4 catalyst, no peaks indicating the formation of mesoporous structure was observed.

Peaks observed at around $2\theta =35.54^o$ and $2\theta =38.94^o$ were the major peaks of copper oxide. The 2θ and d-values of the major and reflection peaks of copper oxide

observed in the structure of the synthesized catalysts and their literature values were listed in Table 18. Results obtained from XRD analyses showed that copper oxide was in the crystallite form in the catalyst structure and the thicknesses of these crystallites were calculated by Scherrer's equation. The peaks observed at $2\theta = 38.80^{o}$ and at $2\theta = 38.78^{o}$ in the XRD patterns of HS3 and HS4 catalysts were used in the calculations, respectively. The results were tabulated in Table 17 and the sample calculations were presented in Appendix C. The thicknesses of CuO crystallites observed in HS3 and HS4 catalysts structures were smaller than the crystallite thicknesses values observed in HS1 and IMP1 catalysts. These results indicated that better dispersion of copper in the catalyst structure was achieved by Na_2CO_3 modified one-pot hydrothermal synthesis.

The absence of the peaks corresponding to aluminum, zinc or their derivatives indicated that they were well-dispersed in the catalyst structure.

Table 17. Crystallites Thickness of HS3 and HS4 catalysts

Catalyst	Crystallite Thickness (nm)
HS3	8
HS4	12

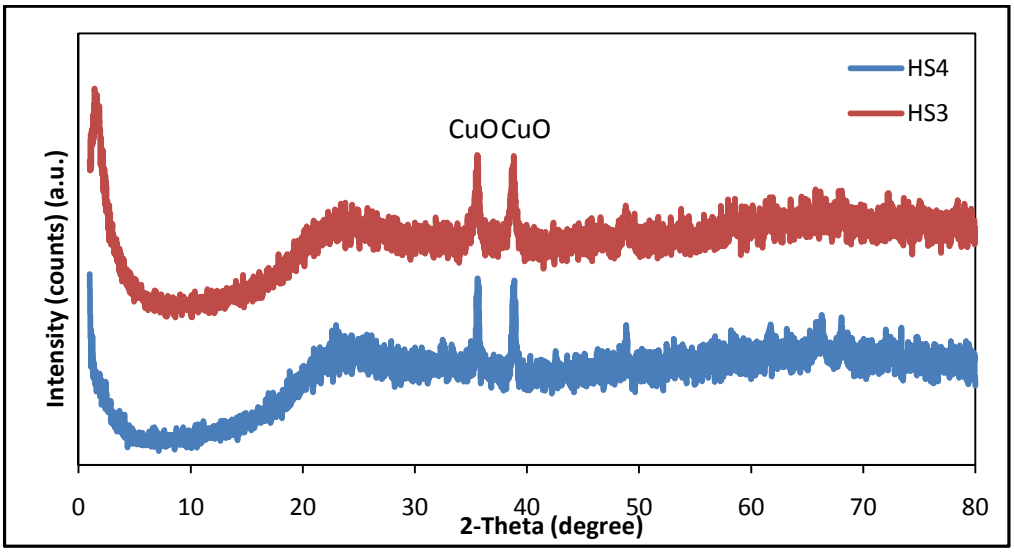

Figure 30. XRD Patterns of HS3 and HS4 catalysts

Table 18. Comparison of XRD pattern data of HS3 and HS4 catalysts with literature data [89]

Peaks	Literature			HS3			HS4		
	2θ	d-value (Å)	I/Io	2θ	d-value (Å)	I/Io	2θ	d-value (Å)	I/Io
MCM-41 peaks	2.2	39.8	100	2.2	40.12	100	-	-	-
	3.9	22.9	6.7	-	-	-	-	-	-
	4.42	19.8	3.3	-	-	-	-	-	-
	5.9	14.9	2.5	-	-	-	-	-	-
CuO Tenorite peaks	32.51	2.75	8	-	-	-	32.66	2.74	17
	35.44	2.53	60	-	-	-	-	-	-
	35.54	2.52	100	35.52	2.52	95	35.62	2.52	95
	38.94	2.31	100	38.78	2.32	100	38.80	2.32	100
	48.74	1.87	25	48.72	1.87	29	48.84	1.86	28
	53.47	1.71	7	-	-	-	-	-	-
	58.31	1.58	12	58.28	1.58	28	58.36	1.58	22
	61.55	1.51	16	61.58	1.50	28	61.66	1.50	23
	65.82	1.42	12	-	-	-	-	-	-
	66.28	1.41	14	66.22	1.41	28	66.36	1.41	21
	67.93	1.38	9	67.98	1.38	36	-	-	-
	68.15	1.37	14	-	-	-	68.06	1.38	22
	72.44	1.30	6	-	-	-	72.42	1.30	15

9.1.2.2. Energy Dispersive Spectroscopy (EDS)

The results of EDS analyses are given in Table 19. Results showed that all three metals were incorporated into the catalysts structures successfully without any lost during the synthesis steps.

Table 19. EDS results of HS3 and HS4 catalysts

Sample ID	Al/Si (wt %)		Cu/Si (wt %)		Zn/Si (wt %)	
	Prepared	Obtained (EDS)	Prepared	Obtained (EDS)	Prepared	Obtained (EDS)
HS4	0.027	0.03	0.21	0.22	0.18	0.17
HS3	0.027	0.03	0.21	0.23	0.18	0.15

9.1.1.3. Scanning Electron Microscopy (SEM)

SEM analyses of synthesized HS3 catalyst are presented in Figure 31 and Figure 32. The average particle size was determined from 1000 times magnified SEM image presented in Figure 31 and found as ~15 μm.

In Figures 33 and 34, SEM images of HS4 catalyst are presented. The average particle size for HS4 catalyst was determined nearly 10 μm.

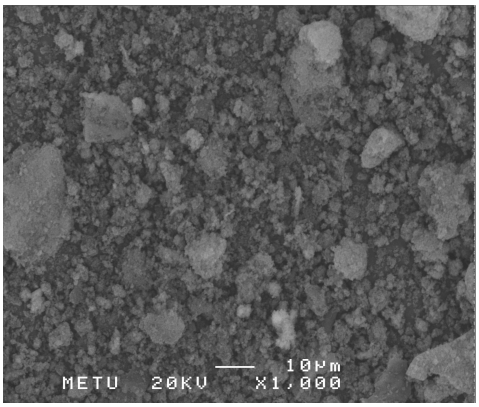

Figure 31. SEM image of HS3 (magnified 1000 times)

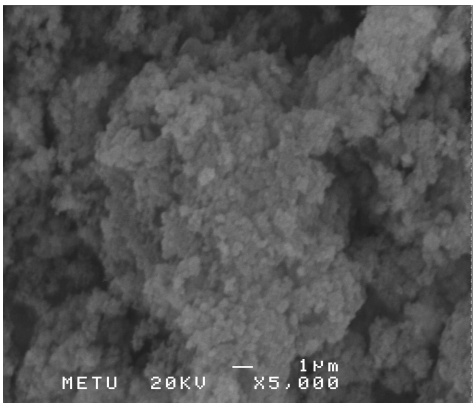

Figure 32. SEM image of HS3 (magnified 5000 times)

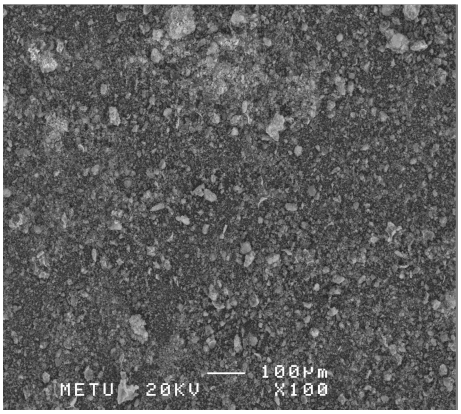

Figure 33. SEM image of HS4 (magnified 100 times)

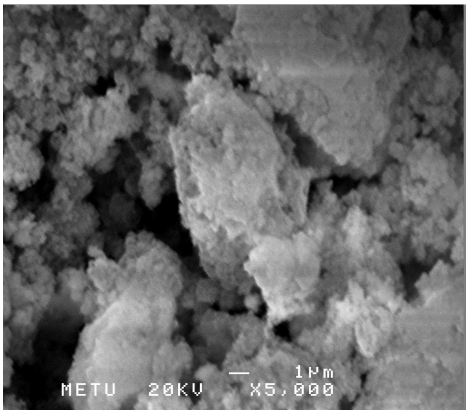

Figure 34. SEM image of HS4 (magnified 5000 times)

9.1.2.4. Nitrogen Physisorption

The multipoint BET and BJH desorption surface areas, average pore size diameters and pore volumes of HS3 and HS4 catalysts obtained from nitrogen physisorption analyses are presented in Table 20. The BET surface areas of the catalysts were found as 207 m^2/g and 353 m^2/g for HS4 and HS3 catalysts, respectively. In the synthesis procedures of the catalysts, Na_2CO_3 was used as the precipitating agent during the synthesis of mixed metal nitrate solutions and formation of mixed crystallites including all metal oxides in the nitrate solution was

expected. The surface area results when compared to the surface areas of HS1 and HS5 catalysts (722 m^2/g and 804 m^2/g respectively), clearly indicated that pores of the MCM-41 structure was blocked with mixed metal crystallites. Due to blocking of the pores, the surface areas of the catalysts were decreased significantly and also the mesoporous structure of MCM-41 was destroyed significantly as previously discussed for the XRD pattern analyses of the catalysts.

The results also showed that the surface area of HS3 catalyst was higher than HS4 catalyst. The addition of metal nitrates into the MCM-41 solution after washing with hot deionized water blocked the pores more than addition of metal nitrates without washing step and decreased the surface area of the HS4 catalyst.

Table 20. Physical properties of the synthesized catalysts

Sample ID	**BET Surface Area (m^2/g)**		**Avg. Pore Diameter (nm) (BJH Desp.)***	**Pore Volume (cm^3/g)**
	BET	**BJH Desp.**		
HS4	207	234	12	0.74
HS3	353	400	11	1.24

* BJH Interpolated Cumulative Desorption average pore diameter for pores in the range of 0 to 50 nm in diameter

The nitrogen adsorption-desorption isotherms of the catalysts were given in Figure 35. The obtained isotherms of the catalysts were between type III and type IV isotherms and they showed H3 type hysteresis loop. This type of hysteresis loop is usually seen for the plate-like particles having slit-shaped pores and these materials do not have absorption limit at high p/p_o values [91]. These isotherms also indicated the presence of macropores in the catalysts structures.

The pore size distribution graphs of the synthesized catalysts obtained by BJH desorption method data are presented in Figure 36. The results also indicated that catalysts containing mesopores and macropores in their structure were synthesized by using Na_2CO_3 modified one-pot hydrothermal synthesis. The average pore diameters of the catalysts were calculated for the pores having diameter in the range of 0-50 nm and given in Table 20.

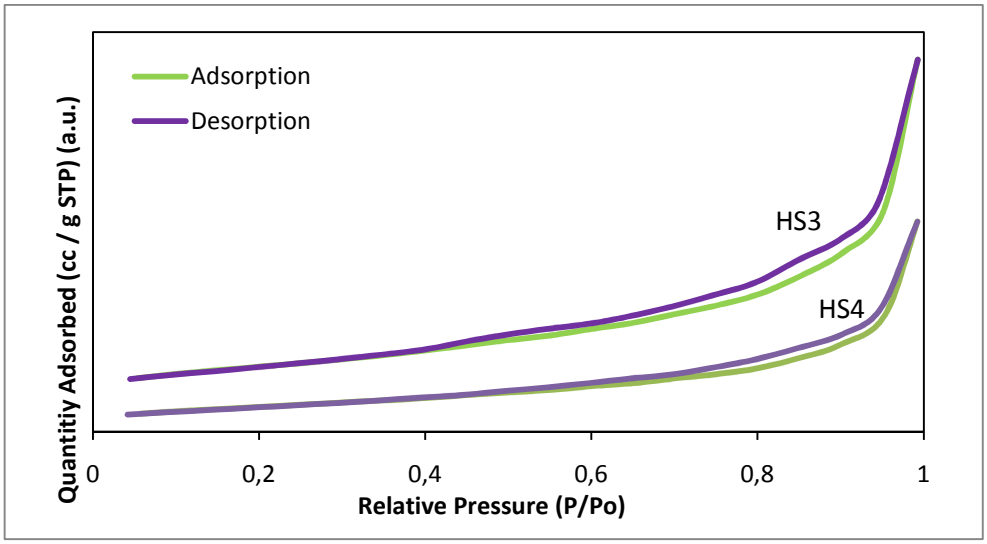

Figure 35. Nitrogen adsorption-desorption isotherms of HS3 and HS4 catalysts

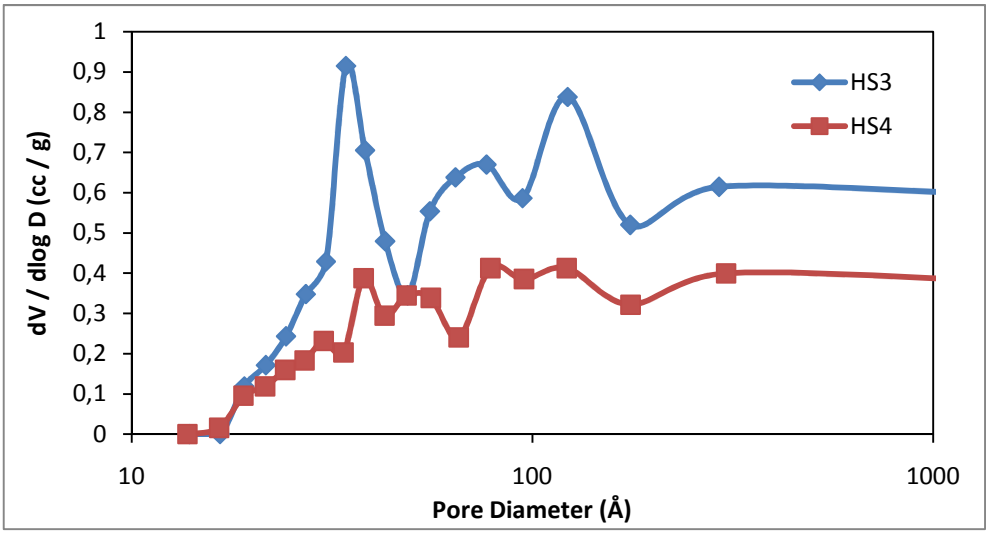

Figure 36. Pore size distributions of HS3 and HS4 catalysts

9.1.2.5. DRIFT Spectra of Pyridine Adsorption

The DRIFT Spectra of pyridine adsorbed HS3 and HS4 catalysts are given in Figure 37. Similar to the DRIFTS results of the catalysts discussed in Section 9.2.1.5., the bands observed at 1453 cm^{-1}, 1581 cm^{-1}, 1600 cm^{-1} and 1613 cm^{-1} were due to Lewis acid sites. The broad and weak band observed at 1540 cm^{-1} was corresponded to pyridinium ion formed by the interaction of Brönsted acid sites and the peak observed at 1494 cm^{-1} indicated the contribution of both Brönsted and Lewis acid sites. The relative intensities of the IR bands observed in the DRIFTS analyses of HS3 catalyst were higher than the ones observed for HS4 catalyst. However, low intensities of Brönsted acid sites showed that methanol dehydration reaction to DME was not favorable for these catalysts and these results were also confirmed by the reactivity test results of HS4 catalyst.

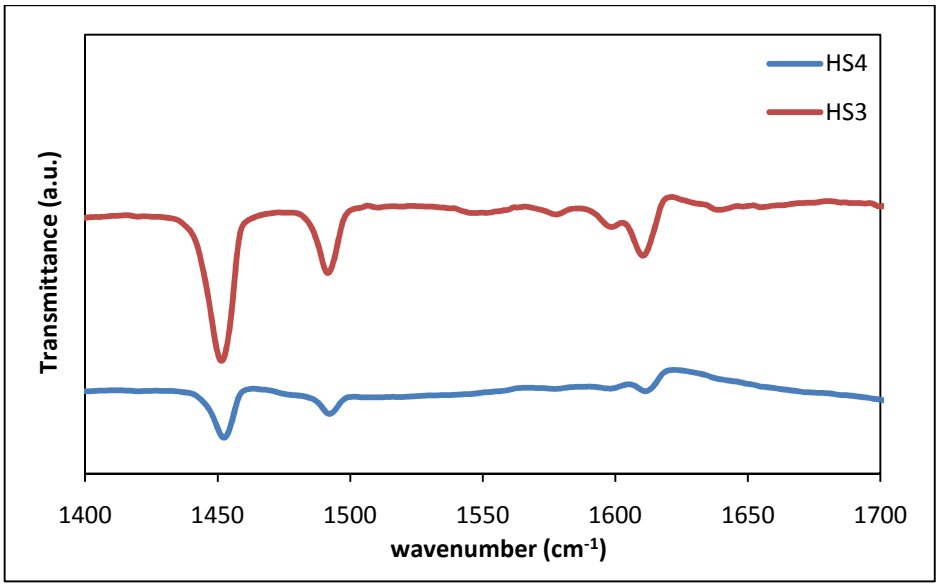

Figure 37. DRIFTS spectra of HS3 and HS4 catalysts

9.1.3. Characterization Results of ZrO_2 modified CuO-ZnO-Al_2O_3-MCM-41 Type Mesoporous Catalysts by One-pot Hydrothermal Synthesis Method

9.1.3.1. X-Ray Diffraction

The XRD patterns of Zr-1 and Zr-2 catalysts synthesized by ZrO_2 modified one-pot hydrothermal synthesis method by acidic route are presented in Figure 38. The XRD pattern of Zr-3 synthesized by neutral one-pot hydrothermal synthesis route is presented in Figure 39. The XRD patterns of the Zr-1 and Zr-2 catalysts showed that catalysts had amorphous structure and the metal oxides were well-dispersed in the structure. The major peak at $2\theta=2.14^{o}$ corresponds to MCM-41 type catalytic materials was observed without its reflections indicated that mesoporous structure of MCM-41 was destroyed. The broad peak observed between $2\theta=20\text{-}30^{o}$ indicated amorphous silica.

In the XRD pattern of Zr-3 catalyst, major peaks of CuO and their reflections were observed. The results showed that final pH value of the synthesis solution had great effects on the crystalline structure of the synthesized material.

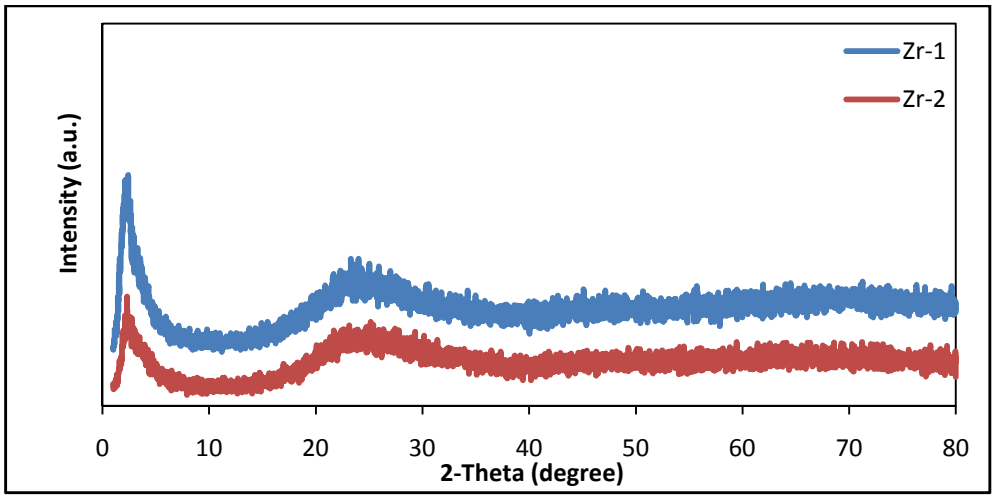

Figure 38. XRD Patterns of Zr-1 and Zr-2 catalysts

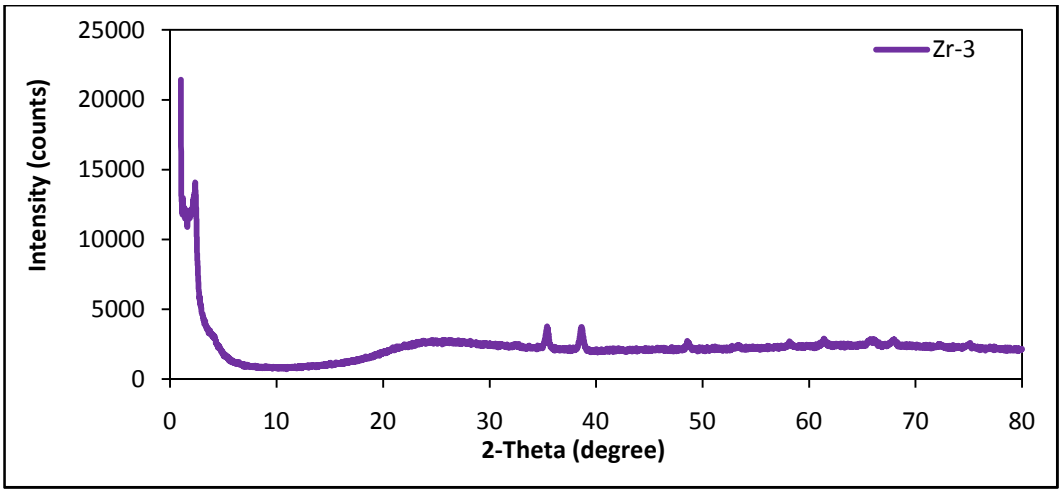

Figure 39. XRD Pattern of Zr-3 catalysts

9.1.3.2. Energy Dispersive Spectroscopy (EDS)

The results of EDS analyses are given in Table 21. Results showed that in Zr-3 catalyst all metals were incorporated into the catalyst. However for the catalysts Zr-1 and Zr-2 synthesized by acidic route, almost all zinc and nearly half of the copper metals were lost from the structure in the washing and calcination steps. The results indicated that increase in the pH value favors the incorporation of the metals into the MCM-41 framework.

Table 21. EDS results of Zr-1, Zr-2 and Zr-3 catalysts

Sample ID	Al/Si (wt %)		Cu/Si (wt %)		Zn/Si (wt %)		Zr/Si (wt %)	
	Prep.	Obt. EDS	Prep.	Obt. EDS	Prep.	Obt. EDS	Prep.	Obt. EDS
Zr-1	0.027	0.026	0.21	0.11	0.18	Trace	0.08	0.07
Zr-2	0.027	0.03	0.21	0.07	0.18	0.02	0.16	0.14
Zr-3	0.027	0.031	0.21	0.20	0.18	0.18	0.16	0.13

9.1.3.3. Scanning Electron Microscopy (SEM)

SEM analyses of synthesized catalysts are presented in Figure 40 and Figure 41 below.

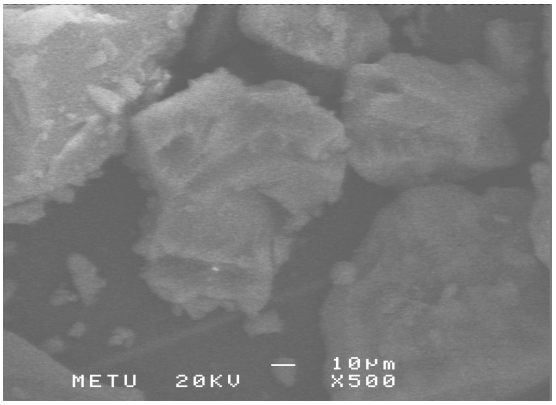

Figure 40. SEM image of Zr-1 (magnified 500 times)

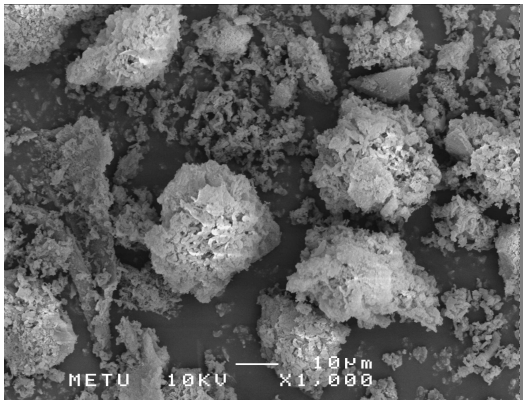

Figure 41. SEM image of Zr-3 (magnified 1000 times)

9.1.3.4. Nitrogen Physisorption

The multipoint BET and BJH desorption surface areas, average pore size diameters and pore volumes of the synthesized catalysts obtained from nitrogen physisorption analyses are presented in Table 22. The BET surface areas of the catalysts were found between 858-958m^2/g. The results showed that incorporation of zirconium into the catalysts structure prevented copper from agglomeration and increased the surface areas of the catalysts.

Table 22. Physical properties of the synthesized catalysts

Sample ID	BET Surface Area (m^2/g)		Avg. Pore Diameter (nm) (BJH Desp.)	Pore Volume (cm^3/g)
	BET	BJH Desp.		
Zr-1	858	986	7.9	1.7
Zr-2	958	1102	7.8	1.6
Zr-3	869	1079	7.5	1.6

* BJH Interpolated Cumulative Desorption average pore diameter for pores in the range of 0 to 50 nm in diameter

The nitrogen adsorption-desorption isotherms of the catalysts were given in Figure 42. Isotherms of the Zr-1 and Zr-2 catalysts showed type IV isotherm and H2 type hysteresis loop. Isotherm of Zr-3 catalyst also showed Type IV isotherm and H3 type hysteresis loop. The pore size distribution graphs obtained by BJH desorption method data were presented in Figure 43. The results showed that all catalysts had narrow pore size distribution in their structure.

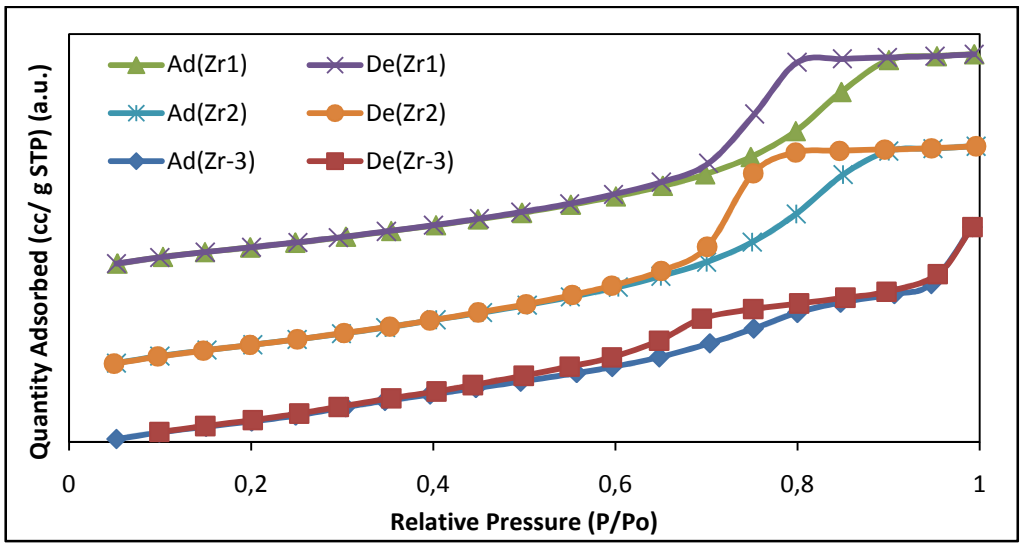

Figure 42. Nitrogen adsorption-desorption isotherms of Zr-1, Zr-2 and Zr-3 catalysts

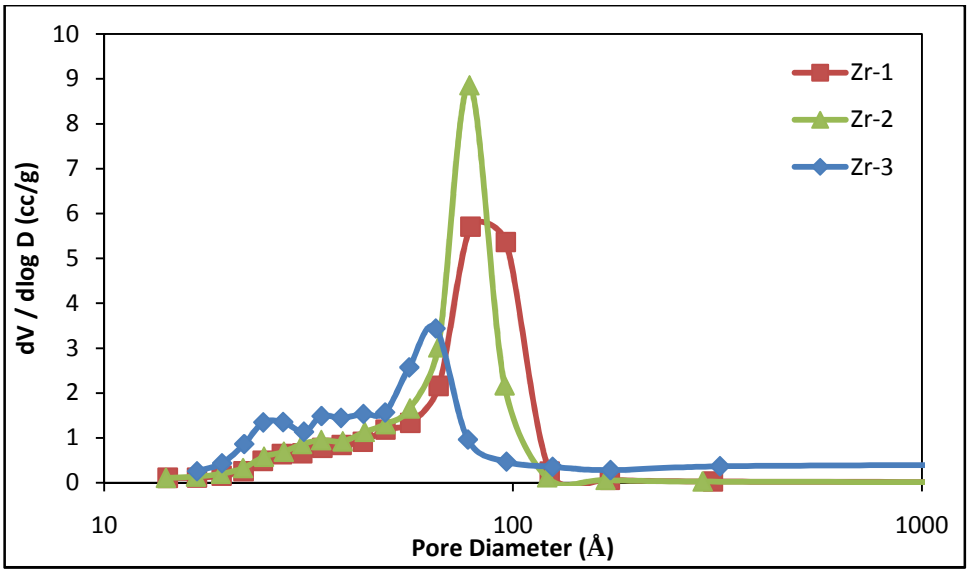

Figure 43. Pore size distributions of Zr-1, Zr-2 and Zr-3 catalysts

9.1.3.5. DRIFT Spectra of Pyridine Adsorption

The DRIFT Spectra of pyridine adsorbed Zr-1, Zr-2 and Zr-3 catalysts are given in Figure 44. The peaks observed at 1453 cm^{-1}, 1581 cm^{-1}, 1600 cm^{-1} and 1613 cm^{-1} wave numbers were due to Lewis acid sites. The peak observed at 1494 cm^{-1} indicated the contribution of both Brönsted and Lewis acid sites. The relative intensities of the IR bands observed in the DRIFTS analyses of Zr-3 catalyst were higher than the ones observed for Zr-1 and Zr-2 catalysts.

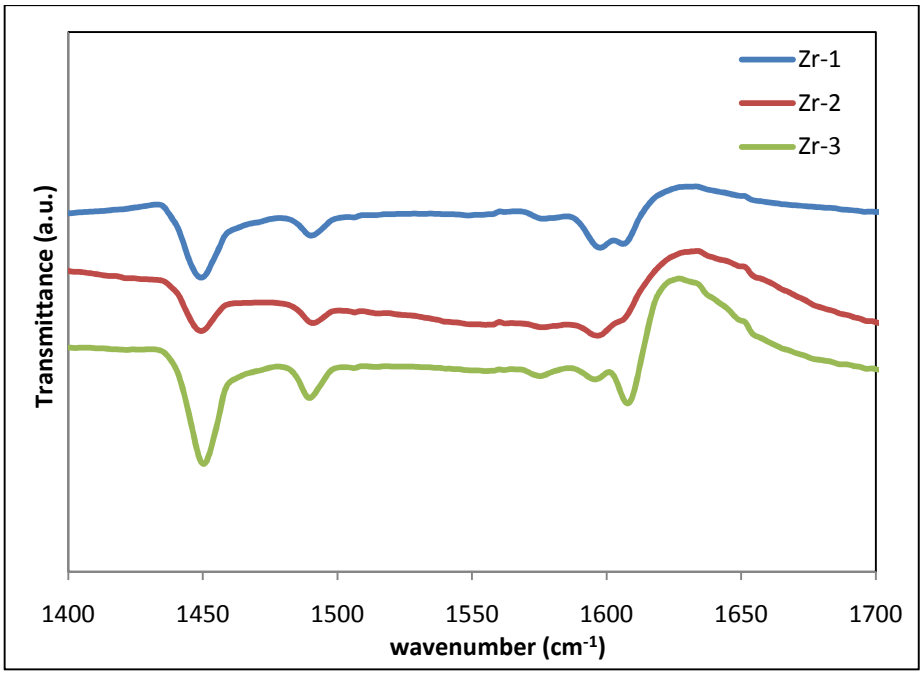

Figure 44. DRIFTS spectra of Zr-1, Zr-2 and Zr-3 catalysts

The properties of catalysts synthesized by one-pot hydrothermal synthesis method following different synthesis routes are presented in Table 23.

Table 23. Summary of the catalysts prepared by one-pot hydrothermal synthesis method

Notation	Synthesis Method	Synthesis Route	EDS Results (wt%)				BET Surface Area (m_2/g)	Avg. Pore Diameter (nm) (BJH Desp.)*	XRD Results
			Al/Si	Cu/Si	Zn/Si	Zr/Si			
HS1	One-pot hydrothermal synthesis	Basic	0.03	0.18	0.18	-	722	8.9	Formation of CuO Crystallites
HS5	One-pot hydrothermal synthesis	Acidic	0.026	0.13	trace	-	804	6.6	Amorphous Structure
IMP1	Impregnation	-	0.03	0.20	0.17	-	669	3.7	Formation of CuO Crystallites
HS3	Na_2CO_3 modified one-pot hydrothermal synthesis	Neutral	0.03	0.22	0.17	-	353	12	Formation of CuO Crystallites
HS4	Na_2CO_3 modified one-pot hydrothermal synthesis	Neutral	0.03	0.23	0.15	-	207	11	Formation of CuO Crystallites
Zr-1	ZrO_2 modified one-pot hydrothermal synthesis	Acidic	0.026	0.11	trace	0.07	858	7.9	Amorphous Structure
Zr-2	ZrO_2 modified one-pot hydrothermal synthesis	Acidic	0.03	0.07	0.02	0.14	958	7.8	Amorphous Structure
Zr-3	ZrO_2 modified one-pot hydrothermal synthesis	Neutral	0.031	0.20	0.18	0.13	869	7.5	Formation of CuO Crystallites

* BJH Interpolated Cumulative Desorption average pore diameter for pores in the range of 0 to 50 nm in diameter

9.1.4. Characterization Results of the Catalysts Prepared by Physical Mixing Method

9.1.4.1. X-Ray Diffraction

The X-Ray diffraction patterns of synthesized Al-MCM-41, TRC75(L) and commercial methanol reforming catalysts are presented in Figure 45 and Figure 46, respectively. The major peak of MCM-41 structure was observed in the XRD pattern of Al-MCM-41 having Al/Si ratio of 0.03. However, in the XRD pattern of TRC75(L) having W/Si ratio of 0.4, no peaks corresponding to MCM-41 structure was observed.

In Figure 46, XRD pattern of commercial methanol reforming catalyst was given. The peaks observed at $2\theta = 35.54^{o}$ and $2\theta = 39.14^{o}$ showed the CuO crystallites in the catalyst structure and also the sharp peak observed at $2\theta = 26.64^{o}$ showed the silica crystallite in the structure.

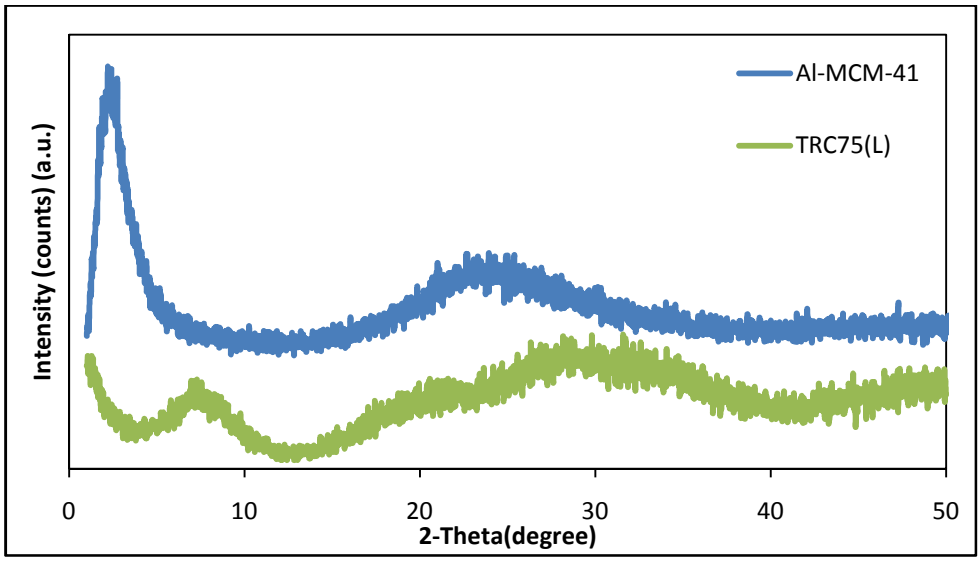

Figure 45. XRD Patterns of Al-MCM-41 and TRC75(L) catalysts

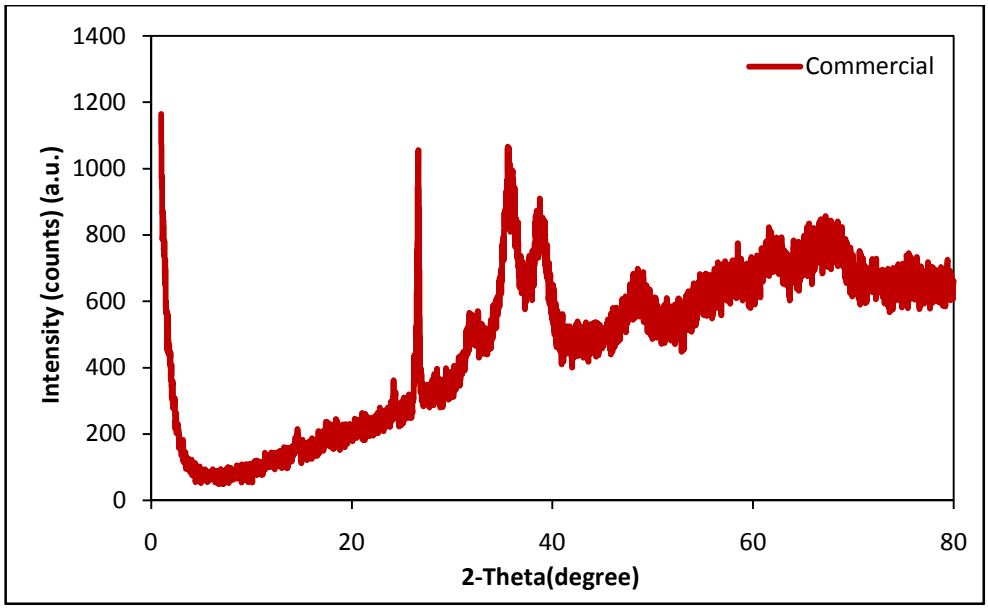

Figure 46. XRD Pattern of commercial methanol reforming catalyst

9.1.4.2. Energy Dispersive Spectroscopy (EDS)

The results of EDS analyses are given in Table 24. EDS results of commercial catalyst showed that the weight ratios of metals in the structure are almost same with the ratio of the metals taken for the synthesis of the catalysts in this study. In the commercial catalyst the weight ratios Al:Cu:Zn found as 9:56:35 and this ratio was taken as 10:50:40 in this study. However the commercial catalyst contains essentially no silica.

Table 24. EDS results of the catalysts

Sample ID	Al (wt%)	W (wt%)	Si (wt%)	Cu (wt%)	Zn (wt%)
	Obtained from EDS				
Al- MCM-41	2.35	-	97.65	-	-
TRC75(L)	-	68.52	31.48	-	-
Commercial	9.19	-	0.17	56.14	34.5

9.1.4.3. Scanning Electron Microscopy (SEM)

SEM analyses of commercial methanol reforming and TRC75(L) catalysts are presented in Figure 47 and Figure 48.

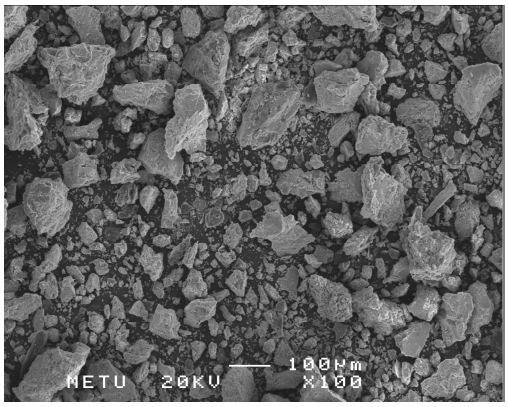

Figure 47. SEM image of Commercial Methanol Reforming Catalyst

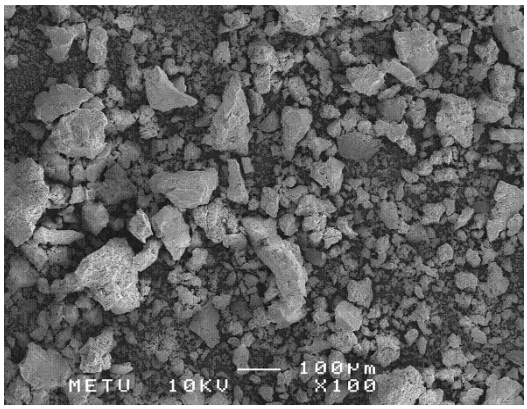

Figure 48. SEM image of TRC75(L) [87]

9.1.4.4. Nitrogen Physisorption

The multipoint BET and BJH desorption surface areas, average pore size diameters and pore volumes of the catalysts obtained from nitrogen physisorption

analyses were presented in Table 25. The BET surface areas of the Al-MCM-41 and TRC75(L) were found 1189m^2/g and 252m^2/g, respectively .

Table 25. Physical properties of the synthesized catalysts

Sample ID	BET Surface Area (m^2/g)		Avg. Pore Diameter (nm) (BJH Desp.)	Pore Volume (cm^3/g)
	BET	BJH		
Al- MCM-41	1189	1396	3.9	1.7
TRC75(L)	252	-	7.8	0.37
Commercial	383	594	7.9	0.8

* BJH Interpolated Cumulative Desorption average pore diameter for pores in the range of 0 to 50 nm in diameter

The nitrogen adsorption-desorption isotherms of the catalysts were given in Figure 49. Isotherms of the Al-MCM-41 and TRC75(L) catalysts showed type IV isotherm. According to the UIPAC hysteresis loop classification, they showed H2 and H1 type hysteresis loops, respectively. The pore size distribution graphs obtained by BJH desorption method data were presented in Figure 50.

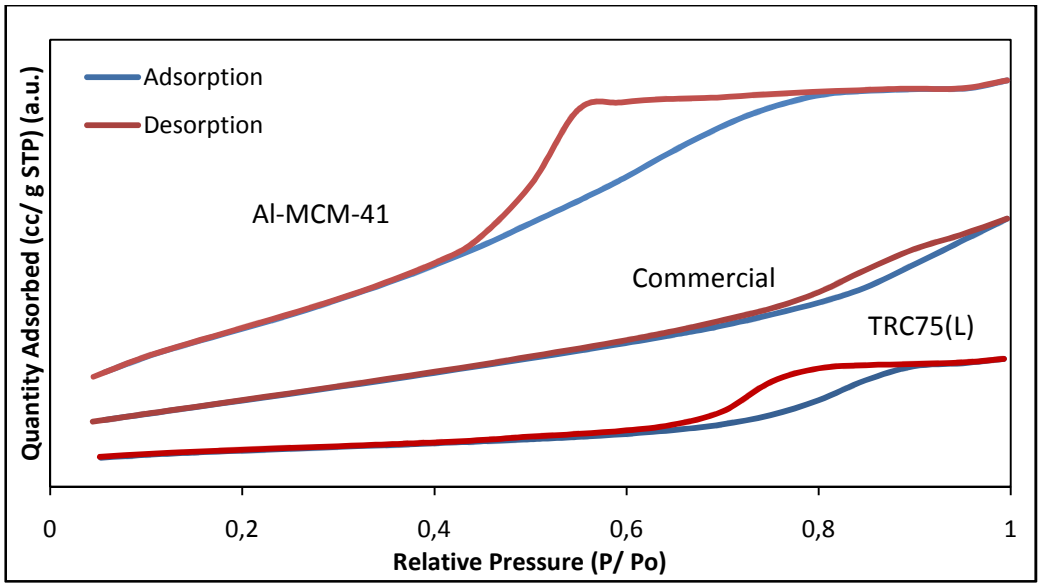

Figure 49. Nitrogen adsorption-desorption isotherms of Al-MCM-41, TRC75(L) and commercial methanol reforming catalysts

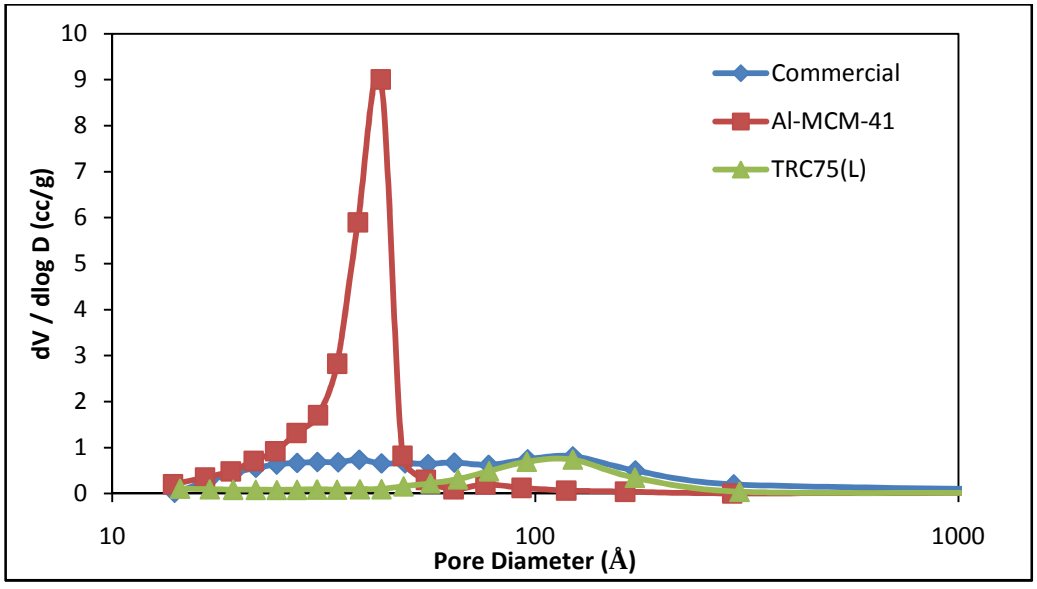

Figure 50. Pore size distributions of of Al-MCM-41, TRC75(L) and commercial methanol reforming catalysts

9.2. Activity Results of the Synthesized Catalysts

In this section, the activity test results of the synthesized IMP1, HS4, Zr-1, Zr-2, Zr-3 and TRC75(L)-C catalysts in direct synthesis of DME from synthesis gas, are given. The carbon monoxide conversion and selectivity values of the products are plotted as a function of temperature.

9.2.1. Activity tests of IMP1 catalyst

IMP1, which was prepared by impregnation method, has a BET surface area 669 m^2/g. It has BJH adsorption pore volume and pore diameter of 0.73 cm^3/g and 3.7 nm, respectively. The weight ratio of aluminum to silica was taken as 0.03.

The catalytic activity tests of IMP1 catalyst were investigated in direct dimethyl ether synthesis reactions in the experimental set-up described in Section 8.3. Feed stream composed of carbon monoxide and hydrogen with a molar ratio of 1:1 was used. Total flow of the mixture was adjusted to 50 ml/min (at atmospheric pressure). The amount of IMP1 catalyst was 0.2 grams and it was placed in the middle of the differential fixed bed reactor. The reaction was carried out between the temperature ranges of 200-400°C.

No carbon monoxide conversion was observed when reactor temperature was 200°C. The IMP1 catalyst showed activity at the temperatures between 250-400°C and carbon monoxide conversion increased with increasing temperature. The obtained results are presented in Figure 51. The conversion value at 400°C was found around 8%.

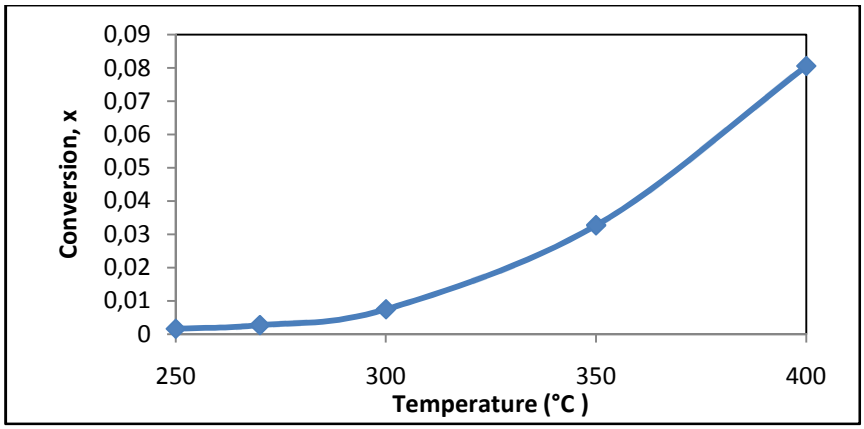

Figure 51. The variation in carbon monoxide conversion with 0.2 g of IMP1 catalyst (Feed stream molar ratio (H_2/CO=1)

When product distribution was investigated, formation of methane and carbondioxide was observed together with methanol and ethanol. No DME was formed with this catalyst. This is considered to be due to low Brönsted acidity of this catalyst. It was interesting to observe that ethanol was also formed together with methanol (Figure 52) especially at higher temperatures. Selectivities of methanol and ethanol were about 0.17 and 0.3 at 400°C, respectively.

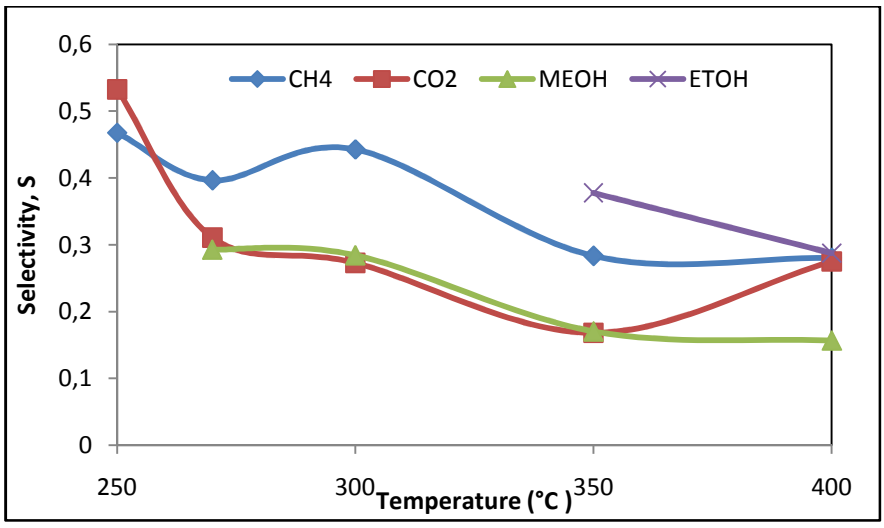

Figure 52. The variation of selectivities of products with 0.2 g of IMP1 catalyst (Feed stream molar ratio (H_2/CO=1)

Decrease of methanol selectivity with temperature is considered to be mainly due to thermodynamic limitations. Formation of CH_4 and CO_2 was considered to be due to reverse dry reforming reaction (Reaction 23) and some of the formed CO_2 was expected to be used in reverse water gas shift reaction (Reaction 25).

$2CO + 2H_2 \leftrightarrow CH_4 + CO_2$ (reverse dry reforming of methane) (23)

$CO + 2H_2 \leftrightarrow CH_3OH$ (methanol synthesis) (1)

$2CO + 4H_2 \leftrightarrow C_2H_5OH + H_2O$ (ethanol synthesis) (24)

$H_2 + CO_2 \leftrightarrow CO + H_2O$ (reverse water-gas shift) (25)

Dry reforming of methane reaction is a reversible reaction and methane reforming occurs at high temperature values above 600°C. At low temperature values reaction goes to right hand side and methane was produced from carbonmonoxide and hydrogen. This catalyst is not appropriate for DME synthesis. However, it can be considered as a potential catalyst for the synthesis of ethanol and methanol from synthesis gas. In order to increase the selectivities of alcohols, formation of methane should be eliminated. This might be achieved by using CO_2 in the feed stream (Reaction 23).

9.2.2 Activity Tests of Zr-1, Zr-2 and Zr-3 Catalysts

Zr-1, Zr-2 and Zr-3 catalysts were synthesized by Zirconium modified one pot hydrothermal synthesis method. Zr-1 and Zr-2 catalysts were synthesized in acidic synthesis conditions (pH=0.2 and pH=0.4, respectively) and Zr-3 was synthesized in neutral conditions (pH=6.0). 0.2 grams of each catalyst were placed in the differential tubular reactor separately. Carbon monoxide conversion results are given in Figure 53. No carbon monoxide conversion was observed in the activity test of Zr-1 catalyst. The characterization results showed that only difference between the

Zr-1 and Zr-2 catalysts was incorporation of very small amount zinc metal into the catalyst structure. No zinc was clanged to the structure of Zr-1 catalyst however a small amount of zinc was observed in the EDS results of Zr-2 which showed some carbon monoxide conversion. The conversion values obtained with Zr-3 was much higher than the corresponding values obtained with Zr-2 and also with IMP1. As it was stated in the literature, presence of Brönsted acid sites is very important for methanol dehydration reaction. However, intensities of Brönsted acid sites observed in the pyridine adsorbed DRIFT spectra of Zr-3 catalyst were negligibly small. The DME formation over this catalyst could be due to high intensities of its Lewis acid sites when compared with Zr-2. Due to the high Lewis acidity of the surface, methanol molecule could be adsorbed on the catalyst surface by the following mechanism:

$CH_3OH + S_1 \leftrightarrow CH_3\text{-}O\text{-}S_1 + H\text{-}S_1$ (Adsorbed methoxy)

$CH_3OH + S_2 \leftrightarrow CH_3OH\text{--}S_2$ (Adsorbed methanol)

$CH_3\text{-}O\text{-}S_1 + CH_3OH\text{--}S_2 \leftrightarrow CH_3O\text{-}CH_3 + S_1 + OH\text{--}S_2$

$H\text{-}S_1 + OH\text{--}S_2 \leftrightarrow H_2O + S_1 + S_2$

A similar mechanism was reported in the literature for DME [15], and diethyl ether (DEE) production [77]. This mechanism predicts that methanol is adsorbed on one surface in methoxy form by dissociation of one hydrogen atom and also adsorbed on another surface surface in methanol molecule form.

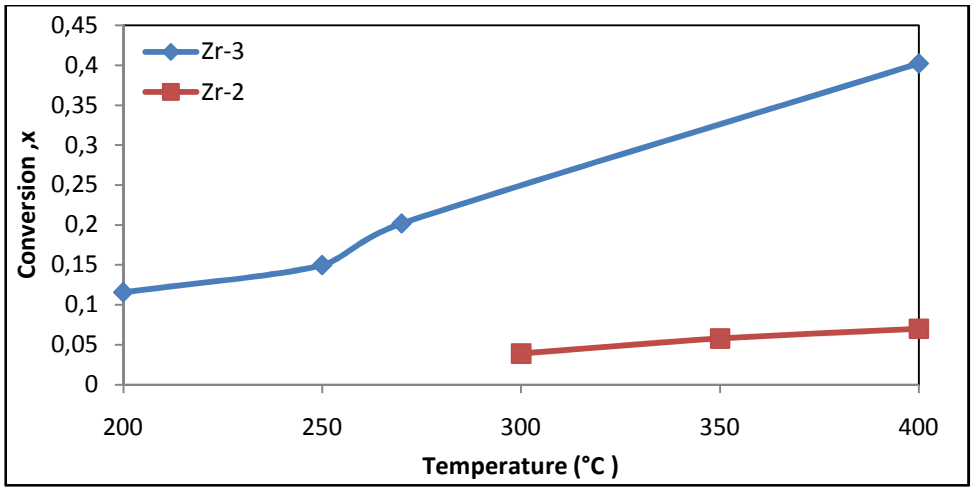

Figure 53. The variations in CO conversions with 0.2 g of Zr-2 and Zr-3 catalysts (Feed stream molar ratio (H_2/CO=1)

Zr-2 catalyst showed activity at the temperatures higher than 300°C and carbon monoxide conversion was obtained around 7 %. On the other hand Zr-3 catalyst showed activity at all temperature values and carbon monoxide conversion was around 40 % at 400°C.

As it was stated before, the main difference between Zr-2 and Zr-3 catalyst was the pH value of synthesis solution. In Zr-3, all metals incorporated into the catalyst structure and in Zr-2 nearly all zinc and one-third part of the copper was lost during the synthesis procedure. However, when compared the IMP1 activity results it can be clearly seen that besides the incorporation of the metals into the structure, addition of Zirconium was the main reason for high conversion.

The product selectivity results of Zr-2 and Zr-3 catalysts are presented in Figure 54 and Figure 55, respectively. Selectivities of DME were found around 13% for Zr-2 catalyst and 8% Zr-3 catalyst. These low DME selectivities are due to low Brönsted acidity of these catalysts.

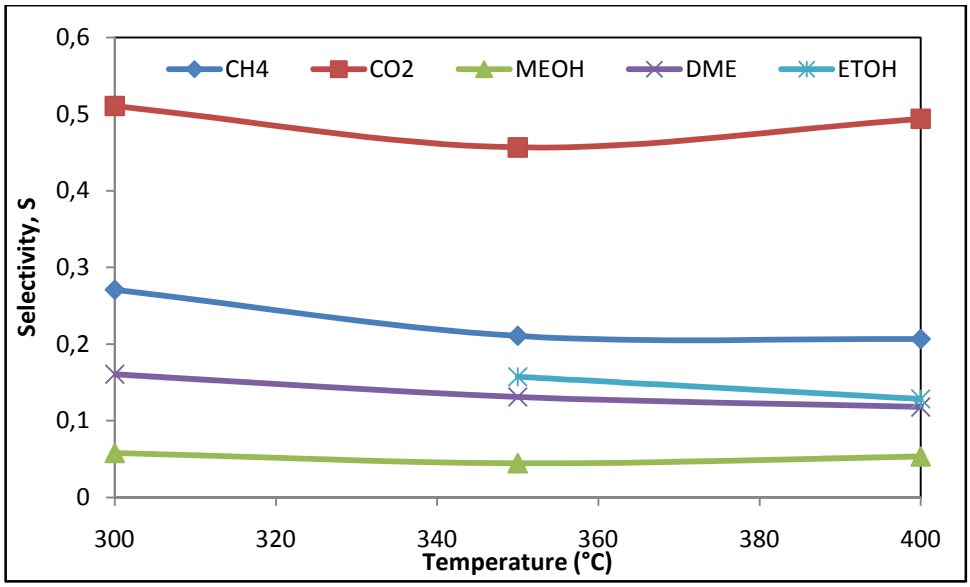

Figure 54. The variation of selectivities of products with 0.2 g of Zr-2 catalyst (Feed stream molar ratio (H_2/CO=1)

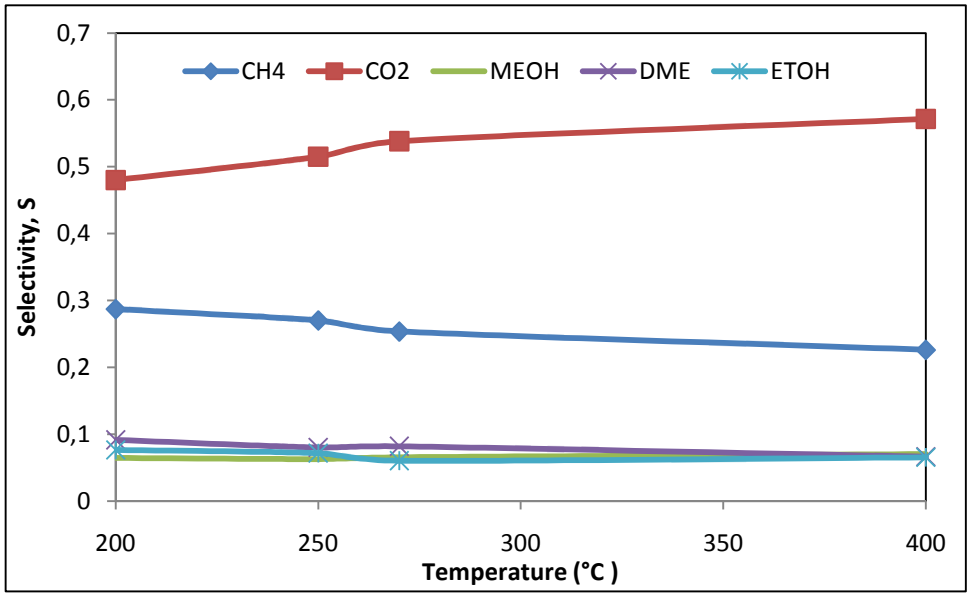

Figure 55. The variation of selectivities of products with 0.2 g of Zr-3 catalyst (Feed stream molar ratio (H_2/CO=1)

Methanol and ethanol were formed with both of these catalysts. However CO_2 and CH_4 selectivities were much higher than alcohol selectivities. Results indicated that reverse dry reforming reaction was quite significant with these catalysts. However, CO_2 selectivity values were found to be higher than the CH_4 selectivity. This might be due to the water gas shift reaction, in which the water formed in ethanol synthesis reaction could be used as the reactant. Zr-3 catalyst is quite active. However, in order to increase the DME selectivity, its Brönsted acidity should be increased. Also, formation of CO_2 and CH_4 should be decreased by inhibiting reverse dry reforming of methane. Improved results might be obtained by using CO_2 in the feed stream as the reactant.

9.2.3. Activity tests of HS4 catalyst

The HS4 catalyst was synthesized by Na_2CO_3 modified one-pot hydrothermal synthesis method. This catalyst showed activity between 300-400°C and the change in the carbon monoxide conversion is given in Figure 56. The carbon monoxide conversion values obtained in the activity test was quite low.

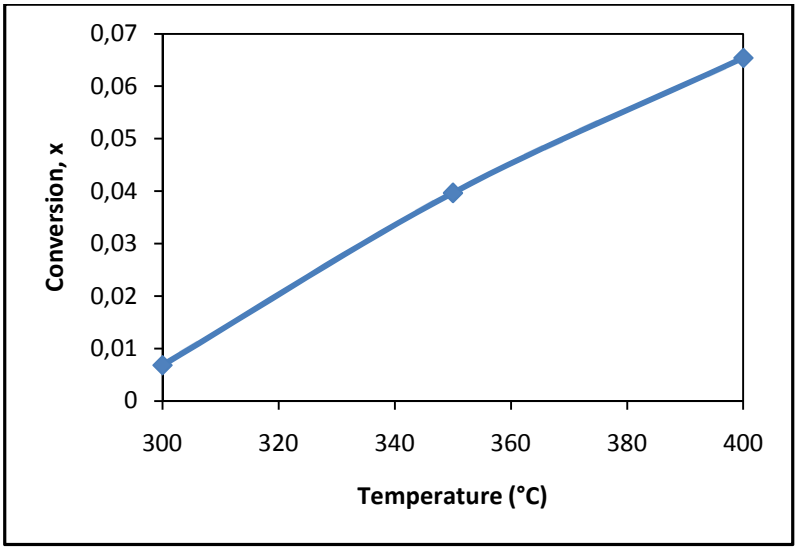

Figure 56. The variation in carbon monoxide conversion with 0.2 g of HS4 catalyst (Feed stream molar ratio (H_2/CO=1)

Carbon monoxide conversion was found around 7 % and it is due to low Al/Si ratio of the catalyst. The product selectivity results were presented in Figure 57. DME and ethanol production were started after 350°C and their selectivites were found 8% and 18%, respectively. Methanol and ethanol selectivity values were found to be around 0.15. The similar trends of the methane and carbondioxide selectivity curves showed the formation of reverse drying reforming of methane reaction. However, in this case CH_4 selectivities were higher than CO_2 selectivities.

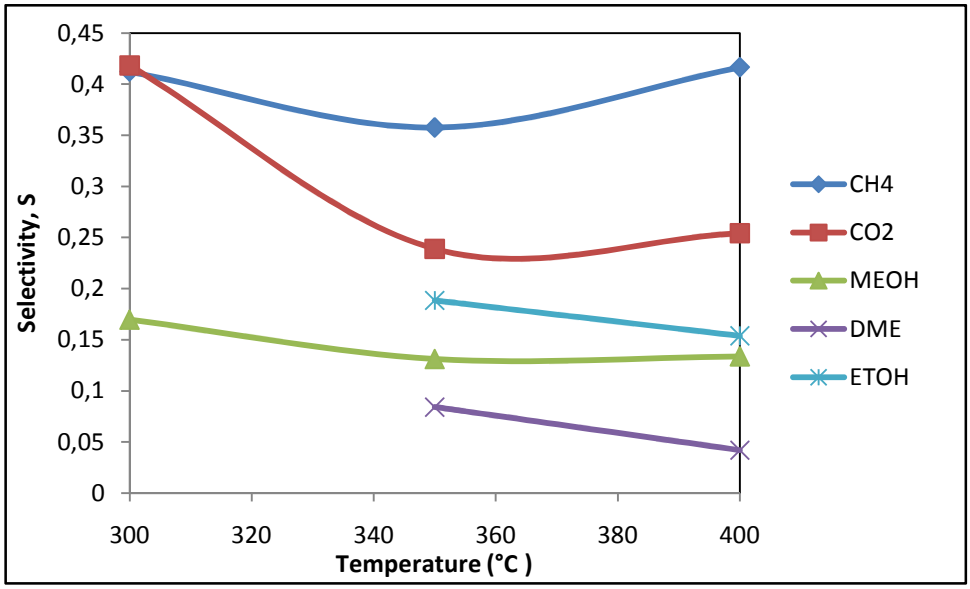

Figure 57. The variation of selectivities of products with 0.2 g of HS4 catalyst (Feed stream molar ratio (H_2/CO=1)

9.2.4. Activity tests of TRC75(L)-C catalyst

TRC75(L) is a highly effective solid acid catalyst developed in our laboratory for dehydration of alcohols [77, 87]. Recent studies of Ciftci [87] had shown that this catalyst was very active in methanol dehydration, yielding DME selectivities of about 100% in a temperature range of 200-400^{o}C, at very high methanol conversions.

In our work, this catalyst was physically mixed with a commercial methanol reforming catalyst (HiFUEL-R120, by Alfa Aesar) to test the catalytic performance

in the synthesis of DME from synthesis gas. This mixed catalyst was denoted as TRC75(L)-C. For the comparison purposes, activity tests of HiFUEL-R120 catalyst alone, were also made with the same feed stream (having equimolar quantities of hydrogen and carbon monoxide) in the same temperature range of 200-400^{o}C.

As shown in Figure 58, carbon monoxide conversion values increased with temperature using both TRC75(L)-C and HiFUEL-R120 catalysts. Activity of the mixed catalyst was considerably higher than the commercial HiFUEL-R120 catalyst.

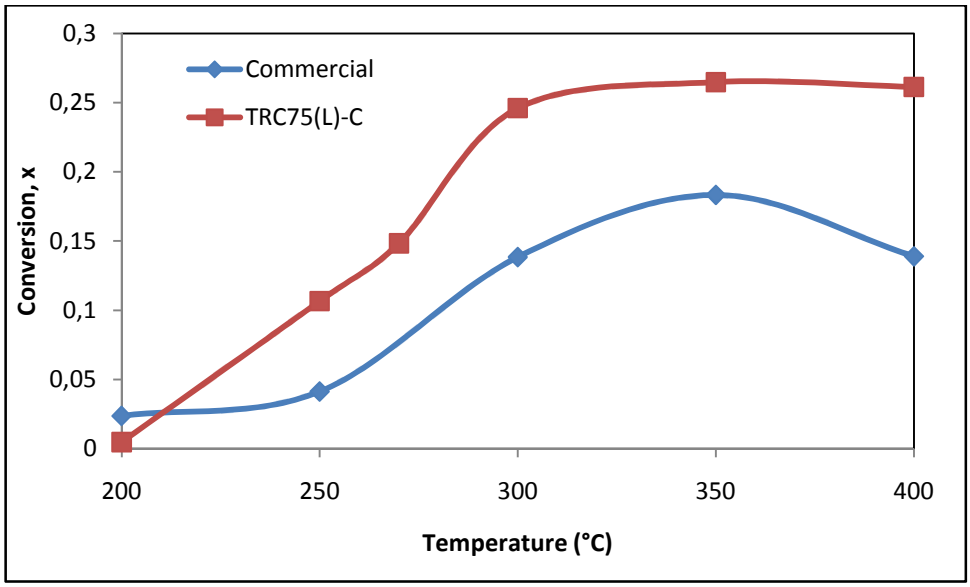

Figure 58. The variation in carbon monoxide conversion with 0.2 g of commercial methanol reforming and TRC75(L)-C catalyst (Feed stream molar ratio (H_2/CO=1)

CO conversion values reached to about 25% at temperatures 300^{o}C and higher. Looking at the product selectivity values observed with TRC-75(L)-C and HiFUEL-R120 (Figures 59 and 60), it was observed that quite high DME selectivity (about 60%) was obtained in a temperature range of 250-275^{o}C with the mixed catalyst. However, DME selectivity was much less (about 10%) with the commercial catalyst. This is more clearly seen in Figure 61.

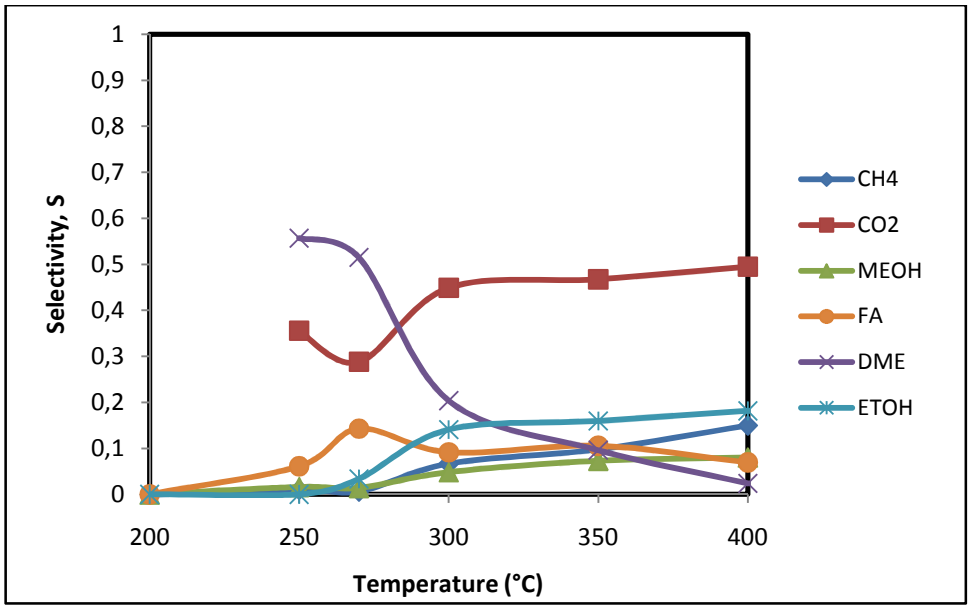

Figure 59. The variation of selectivities of products with 0.2 g of TRC75(L)-C catalyst (Feed stream molar ratio (H_2/CO=1)

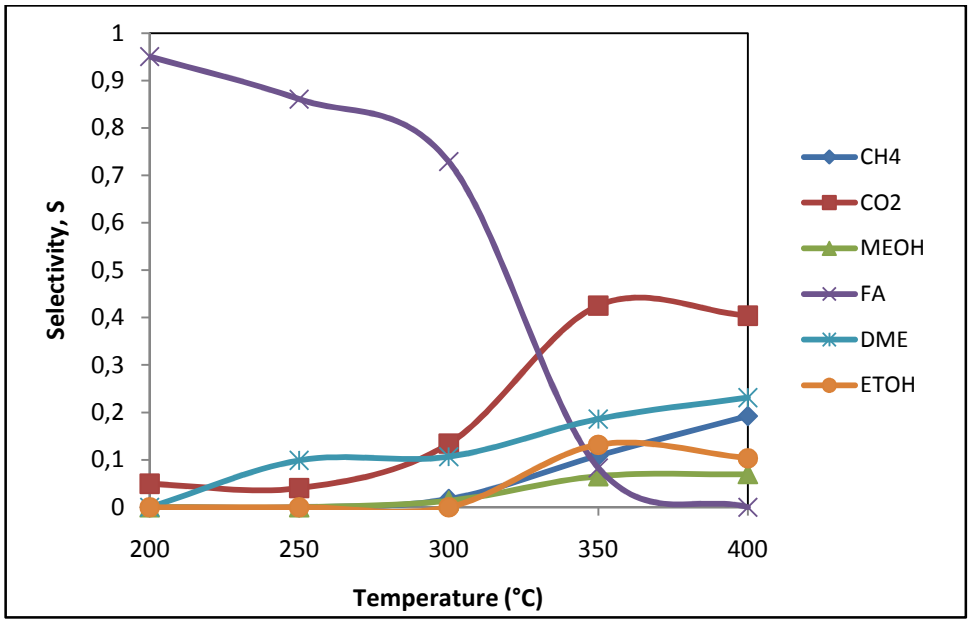

Figure 60. The variation of selectivities of products with 0.2 g of commercial catalyst (Feed stream molar ratio (H_2/CO=1)

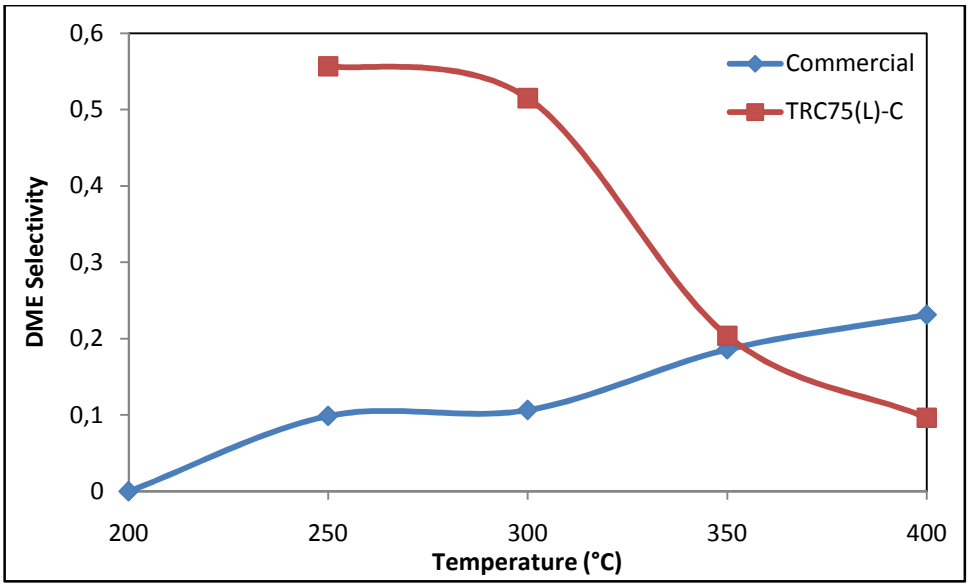

Figure 61. DME selectivities of TRC75(L)-C and commercial methanol reforming catalysts (Feed stream molar ratio (H_2/CO=1)

With the commercial methanol reforming catalyst HiFUEL-R120, formation of significant amout of formic acid was observed, especially at temperatures lower than 350^{o}C. Formation of formic acid was not observed with any of the other catalysts tested in this work.

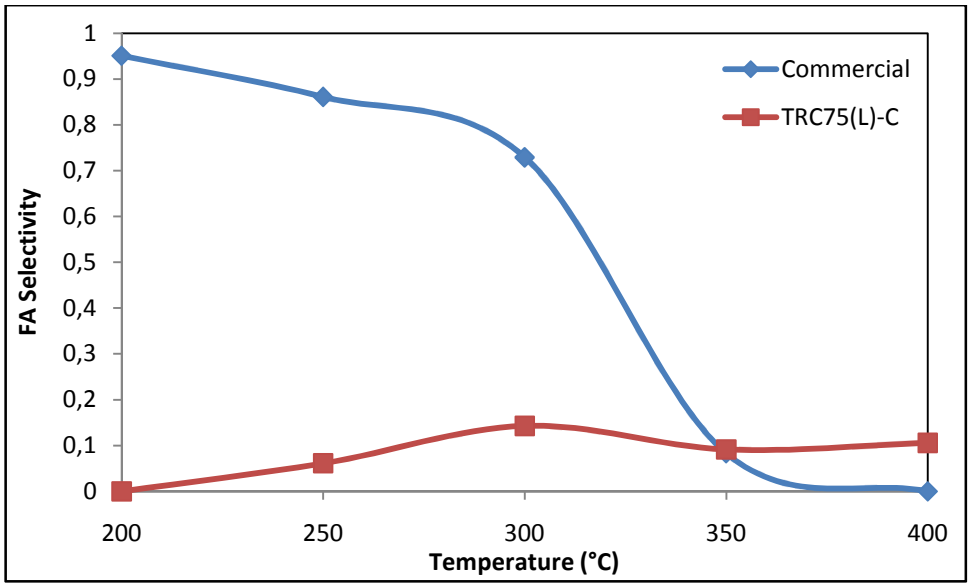

Figure 62. Formic acid selectivities of TRC75(L)-C and commercial methanol reforming catalysts (Feed stream molar ratio (H_2/CO=1)

As shown in Figure 62, formic acid mole fraction was very low in the case of mixed catalyst TRC75(L)-C. This was considered as an indication of conversion of formic acid formed over the HiFUEL-R120 catalyst to DME with the catalytic action of TRC75(L).

$$2CH_2O_2 + 4H_2 \leftrightarrow (CH_3)_2O + 3H_2O \quad (26)$$

This overall reaction may proceed by the formation methanol as an intermediate.

$$CH_2O_2 + 2H_2 \leftrightarrow CH_3OH + H_2O \quad (27)$$

$$2(CH_3OH) \leftrightarrow (CH_3)_2O + H_2O \quad (28)$$

Formation of some methanol and ethanol was also observed with these catalysts at temperatures over 250^{o}C.

$$CO + 2H_2 \leftrightarrow CH_3OH \quad (1)$$

$$2CO + 4H_2 \leftrightarrow C_2H_5OH + H_2O \quad (23)$$

Formation of methane together with CO_2 was an indication of contribution of reverse dry reforming reaction to the product distribution.

$$2CO + 2H_2 \leftrightarrow CH_4 + CO_2 \quad (24)$$

However, CO_2 concentrations were much higher than CH_4 especially with the mixed catalyst. Besides the reverse dry reforming reaction, formation of CO_2 may take place through the water gas shift reaction, through DME synthesis reaction and also through coke formation on the catalyst surface.

$$H_2O + CO \leftrightarrow H_2 + CO_2 \ (WGS) \quad (3)$$

$$3CO + 3H_2 \leftrightarrow (CH_3)_2O + CO_2 \quad (9)$$

$$2CO \rightarrow CO_2 + C \quad (29)$$

Commercial methanol reforming reaction HiFUEL-R120 was actually designed for hydrogen production from methanol.

$$CH_3OH + H_2O \leftrightarrow CO_2 + H_2 \quad (30)$$

Reverse of this reaction together with water gas shift reaction may be responsible for the synthesis of small amount of methanol in this system.

With the commercial catalyst, CO conversion values were quite low at temperatures of 250^{o}C and lower. However, the observed high selectivity of formic acid at such low temperatures indicated the occurance of the following reaction over this catalyst.

$$CO_2 + H_2 \leftrightarrow CH_2O_2 \quad (31)$$

Another possibility is the reaction of CO with H_2O.

$$CO + H_2O \leftrightarrow CH_2O_2 \quad (32)$$

In fact, formic acid was reported to decompose quite easily through the reverse of these reactions. Formation of formic acid over the commercial catalyst at low temperatures may also be due to the reaction of CO with H_2.

$$2CO + H_2 \rightarrow CH_2O_2 + C \quad (33)$$

At 200^{o}C, fractional conversion values obtained with both of the catalysts was close to zero. Consequently, the selectivity values obtained at this temperature were not included into the figures discussed in this section.

Results obtained with the mixed TRC75(L)-C and HiFUEL-R120 catalysts indicated that the performance of the mixed catalyst was quite promising for the conversion of synthesis gas to DME. 60% DME selectivity is quite high for this reaction. Results also indicated that the inclusion of CO_2 to the feed stream could enhance the formation of formic acid (and methanol) which may then be converted to DME over the TRC75(L)-C solid acid catalyst.

All these results gave very important clues related to the required catalyst composition and the feed stream composition for further studies to produce DME.

CHAPTER 10

CONCLUSIONS AND RECOMMENDATIONS

In this study, novel bifunctional DME synthesis catalytic materials were synthesized by one pot hydrothermal synthesis, impregnation and physical mixing methods. The synthesized materials were characterized by XRD, EDS, N_2 phsisorption, SEM, and DRIFTS of pyridine adsorption techniques. A high pressure fixed bed flow reactor was built in Reaction Engineering Laboratory and the activity tests of the synthesized materials were carried out between the temperature range of 200-400°C and under 50 bars pressure.

Three different catalyst synthesis procedures were used for the preparation of catalytic materials and the synthesized materials were grouped according to their similarities. In the first group of catalysts, one-pot hydrothermal synthesis and impregnation procedures were used. The effect of pH value of the synthesis solution on the catalyst physical and chemical properties was investigated by following hydrothermal synthesis procedure in basic (HS1) and acidic (HS5) routes. In addition to these catalysts, copper and zinc were impregnated on aluminum silicate and this catalyst was denoted as IMP1. The characterization results of these catalysts showed that synthesis solution pH value was highly effective on final catalyst properties. Incorporation of copper, zinc and aluminum into the catalyst mesoporous network was increased with increasing pH value of synthesis solution. Also, XRD results showed that CuO crystallites were formed in the catalyst structure with increasing pH value. Pyridine adsorbed DRIFT spectra of the catalysts showed that all catalysts had Lewis acid sites however intensities of Brönsted acid sites –which are essential for methanol dehydration reaction- are negligibly small. The highest relative intensities of Lewis acid sites were observed in IMP1 catalyst. For this reason,

among the catalysts synthesized in this group, catalytic activity tests were carried out only for IMP1 catalyst in this thesis. Due to extremely low Brönsted acidity of these catalysts, DME formation was not observed. It was concluded that these catalysts were more suitable for the synthesis of methanol and ethanol from synthesis gas, rather than production of DME. Formation of CO_2 and CH_4 suggested the occurance of reverse dry reforming reaction.

In the second group, catalysts synthesized by Na_2CO_3 modified one pot hydrothermal synthesis procedure were investigated. Characterization results showed that by addition of Na_2CO_3, metals were penetrated into the catalyst pore network successfully. However, the decrease in the surface area (207-353 m^2/g) and formation of CuO crystallites in the catalyst structure showed that formed crystallites were blocked the mesoporous of MCM-41 structure. In this group of catalyst, because of their similar properties, the catalytic activity tests were performed with the synthesized catalytic material denoted as HS4. Formation of DME and ethanol were started at the temperatures higher than 350°C. At 400°C, DME selectivity was found around 5%. This low DME selectivity was due to low acid strength of this catalyst.

In the third group of catalysts, effect of Zirconium metal loading in the direct hydrothermal synthesis procedure was investigated. The catalysts were synthesized by following acidic and neutral hydrothermal synthesis routes with different ZrO_2 weight ratios. Characterization results showed that increase in the Zr metal content enhanced the incorporation of zinc into the catalyst structure. The catalyst named as Zr-3 was synthesized by following neutral hydrothermal synthesis route. Results showed that increase of pH value of the synthesis solution promoted metal incorporation into the catalyst structure. All of the metals were successfully incorporated into the mesoporous network of MCM-41 structure at pH value of 6.0. Moreover, nitrogen physisorption analyses showed that addition of Zr metal increased the surface area of the catalysts (858-958 m^2/g).

Incorporation of zinc into the catalyst structure increased the catalytic activity of the synthesized material. On the other hand, in the catalytic activity tests of Zr-3 catalyst, 40% carbon monoxide conversion was achieved and DME selectivity was

found around 8%. It was concluded that addition of Zr considerably increased the activity of the catalyst.

Finally, catalysts were prepared by physical mixing method. In this method, silicotungstic acid incorporated methanol dehydration catalyst (TRC75(L)) was physically mixed with commercial methanol reforming catalyst with a weight ratio of one to one. Carbon monoxide conversion was found to be around 25% in the catalytic activity tests carried out with mixture of TRC75(L) and the commercial methanol reforming catalyst between the temperature range of 200-400°C. Highest DME selectivity (60%) was observed at about 275°C. Different from the other synthesized catalytic materials, in the activity tests of this catalyst, formic acid formation was observed. High DME selectivity and relatively high CO conversion values obtained with this catalyst mixture proved the significance of presence of Brönsted acid sites on DME production.

As a result, in the future synthesis of silicotungstic acid, Cu, Zn, Zr incorporated MCM-41 type catalytic materials were recommended to be synthesized and tested for DME synthesis from synthesis gas.

It was also concluded that, addition of CO_2 to the reactor feed stream might have a positive effect by reducing formation of methane from reverse dry reforming and also by enhancing methanol formation which would then be converted to DME over the Brönsted acid sites. In addition to these, synthesis of DME and alcohols starting from CO_2 is a promising solution for global warming by reducing the carbon dioxide concentration in the atmosphere.

REFERENCES

[1] Doğu, T., Varışlı, D., "Alcohols as Alternates to Petroleum for Environmentally Clean Fuels and Petrochemicals", Turkish Journal of Chemistry, 2007, 31, 551-567.

[2] Olah, G. A., Goeppert, A., Surya Prakash, G.K., "Beyond Oil and Gas: The Methanol Economy", Wiley-VCH Verlag GmbH & Co. KGaA, 1st Ed., 2006, Weinheim.

[3] Rozovskii A. Ya., Lin G. I., "Problems of Producing Motor Fuels from Alternative Raw Materials", Russian Chemical Bulletin, International Edition, 2004, 53, 2455-2466.

[4] Song C., "Global challenges and strategies for control, conversion and utilization of CO_2 for sustainable development involving energy, catalysis, adsorption and chemical processing", Catalysis today, 2006, 115, 2-32.

[5] DME Handbook, Japan DME Forum, 2007.

[6] Semelsberger T. A., Borup R. L., Greene H. L., "Dimethyl ether (DME) as an alternative fuel", Journal of power sources, 2006, 156, 497-511.

[7] Ogawa T., Inoue N., Shikada T., Ohno Y., "Direct dimethyl ether synthesis", Journal of natural gas chemistry, 2003, 12, 219-227.

[8] Shikada T., Ohno Y., Ogawa T., Ono M., Mizuguchi M., Tomura K., Fujimoto K., "Direct synthesis of dimethyl ether from synthesis gas", Studies in Surface Science and Catalysis, 1998,119, 515-520.

[9] Bollon F., Europian Association of Liquefied Petrol Gas (AEGPL) Conference, Nice, 6-8 June 2007.

[10] Fleisch T. H., Basu A., Gradassi M. J., Masin J. G., "Dimethyl ether: a fuel for 21th century", Studies in Surface Science and Catalysis, 1997, 107, 117-124.

[11] Lange J., "Methanol synthesis: a short review of technology improvements", Catalysis Today, 2001, 64, 3-8.

[12] Tijm P.J.A., Waller F.J., Brown D.M., "Methanol technology developments for the new millennium", Applied Catalysis A: General, 2001, 221, 275-282.

[13] Klier K., Beretta A., Sun Q., Feeley O. C., Herman R. G., "Catalytic synthesis of methanol, higher alcohols and ethers", Catalysis today, 1997, 36, 3-14.

[14] Ramos F.S., de Farais A.M.D., Borges L.E.P., Monteiro J.L., Fraga M.A., Sousa-Aguiar E.F., Appel L.G., "Role of dehydration catalyst acid properties on one–step DME synthesis over physical mixtures", Catalysis Today, 2005, 101, 39-44.

[15] Cheng W-H., Kung H. H., "Methanol production and use", Marcel Dekker Inc., 270 Madison Avenue, 1994, New York.

[16] Blaszkowski S. R., Santen R. A., "The mechanism of dimethyl ether formation from methanol catalyzed by zeolitic protons" J. Am. Chem. Soc. 1996, 118, 5152-5153.

[17] Royaee S. J., Falamaki C., Sohrabi M., Talesh S.S.A., "A new Langmuir–Hinshelwood mechanism for the methanol to dimethylether dehydration reaction over clinoptilolite-zeolite catalyst", Applied Catalysis A: General, 2008, 338, 114-120.

[18] Ogawa T., Inoue N., Shikada T., Inokoshi O., Ohno Y., "Direct dimethyl ether (DME) synthesis from natural gas", Studies in Surface Science and Catalysis, 2004, 147, 379-384.

[19] Adachi Y., Komoto M., Watanabe I., Ohno Y., Fujimoto K., "Effective utilization of remote coal through dimethyl ether synthesis", Fuel, 2000, 79, 229-234.

[20] Peng X. D., Wang A. W., Toseland B.A., Tijm P.J.A, "Single-step syngas-to-dimethyl ether processes for optimal productivity, minimal emissions, and natural gas-derived syngas", Ind. Eng. Chem. Res., 1999, 38, 4381-4388

[21] Ohno Y., Omiya M., "Coal conversion into dimethyl ether as an innovative clean fuel", 12th International Conference on Chemical Structures (ICCS), November-2003.

[22] Ng K.L., Chadwick D., Toseland B.A., "Kinetics and modeling of dimethyl ether synthesis from synthesis gas", Chemical Engineering Science, 1999, 54, 3587-3592.

[23] International DME Association, DME About, http://www.aboutdme.org/, 15 September 2009.

[24] Grzesik M., Skrzypek J., "Chemical equilibria in direct synthesis of dimethyl ether", Studies in Surface Science and Catalysis, 1999, 122, 407-410

[25] Herman R. G., "Advances in catalytic synthesis and utilization of higher alcohols", Catalysis Today, 2000, 55, 232-245

[26] Yang C., Ma Z., Zhao N., Wei W., Hu T. and Sun Y., "Methanol synthesis from CO_2-rich syngas over a ZrO_2 doped Cu/ZnO catalyst", Catalysis Today, 2006, 115, 222-227

[27] Zhang, Y., Fei, J., Yu, Y. and Zheng, X., "Methanol synthesis from CO_2 hydrogenation over Cu based catalyst supported on zirconia modified γ- Al_2O_3", Energy Conversion and Management, 2006, 47, 3360-3367

[28] Sloczynski, J., Grabowski, R., Olszewski, P., Kozlowska, A., Stoch, J., Lachowska, M., Skrzypek, J., "Effect of metal oxide additives on the activity and stability of Cu/ZnO/ZrO_2 catalysts in the synthesis of methanol from CO_2 and H_2", Applied Catalysis A: General, 2006, 310, 127-137.

[29] Sloczynski, J., Grabowski, R., Kozlowska, A., Lachowska, M., Skrzypek, J., "Effect of additives and a preparation method on catalytic activity of Cu/ZnO/ZrO_2 system in the carbon dioxide hydrogenation to methanol", Studies in Surface Science and Catalysis, 2004, 153, 161-164

[30] Sloczynski, J., Grabowski, R., Kozlowska, A., Olszewski, P., Lachowska, M., Skrzypek, J., Stoch, J., "Effect of Mg and Mn oxide additions on structural and adsorptive properties of Cu/ZnO/ZrO_2 catalysts for the methanol synthesis from CO_2", Applied Catalysis A: General, 2003, 249, 129-138

[31] Chen H.Y., Lin J., Tan K.L., Li J., "Comparative studies of manganese-doped copper-based catalysts: the promoter effect of Mn on methanol synthesis", Applied Surface Science 1998, 126, 323–331

[32] Huang X., Ma L., Wainwright M.S., "The influence of Cr, Zn and Co additives on the performance of skeletal copper catalysts for methanol synthesis and related reactions", Applied Catalysis A: General, 2004, 257, 235–243

[33] Melián-Cabrera I., Granados M.L., Terreros P., Fierro J.L.G., "CO_2 hydrogenation over Pd-modified methanol synthesis catalysts" Catalysis Today, 1998, 45, 251-256

[34] Kilo M., Weigel J., Wokaun A., Koeppel R.A., Stoeckli A., Baiker A., "Effect of the addition of chromium- and manganese oxides on structural and catalytic properties of copper/zirconia catalysts for the synthesis of methanol from carbon dioxide", Journal of Molecular Catalysis A: Chemical, 1997, 126, 169-184

[35] Ma H. T., Deng G.C., Guo X.Z., Chen R. T., "The effect of rare earth on the activity of methanol synthesis catalyst" Chinese Chemical Letters, 1999, 10, 691-692

[36] Kim, J.H., Park, M.J., Kim S.J., Joo, O.S., Jung, K.D., "DME synthesis from synthesis gas on the admixed catalysts of Cu/ZnO/Al_2O_3 and ZSM-5", Applied Catalysis, 2004, 264, 37-41.

[37] Vishwanathan V., Jun K.W., Kim J.W., Roh H.S., "Vapour phase dehydration of crude methanol to dimethyl ther over Na-modified H-ZSM-5 catalysts", Applied Catalysis A: General, 2004, 276, 251-255.

[38] Yaripour, F., Baghaei, F., Schmidt, I., Perregaard, J., "Synthesis of dimethyl ether from methanol over aluminum phosphate and silica–titania catalysts", Catalysis Communications, 2005, 6, 542-549.

[39] Xu, M., Lunsford, J.H., Goodman, D.W., "Synthesis of dimethyl ether (DME) from methanol over solid-acid catalysts", Applied Catalysis A: General, 1997, 149, 289-301.

[40] Kim S.M., Lee Y.J., Bae J.W., Potdar H.S., Jun K.W., "Synthesis and characterization of a highly active alumina catalyst for methanol dehydration to dimethyl ether", Applied Catalysis A: General 2008, 348, 113-120

[41] Fu Y., Hong T., Chen J., Auroux A., Shen J., "Surface acidity and the dehydration of methanol to dimethyl ether", Thermochimica Acta, 2005, 434, 22–26

[42] Raoof F., Taghizadeh M., Eliassi A., Yaripour F., "Effects of temperature and feed composition on catalytic dehydration of methanol to dimethyl ether over γ-alumina", Fuel, 2008, 87, 2967-2971

[43] Kim S.D., Baek S.C., Lee Y.J., Jun K.W., Kim M.J., Yoo I.S., "Effect of γ-alumina content on catalytic performance of modified ZSM-5 for dehydration of crude methanol to dimethyl ether", Applied Catalysis A: General, 2006, 309, 139-143

[44] Xia J., Mao D., Zhang B., Chen Q., Zhang Y., Tang Y., "Catalytic properties of fluorinated alumina for the production of dimethyl ether", Catalysis Communications, 2006, 7, 362-366

[45] Xu M., Goodman D.W., Bhattacharyya A., "Catalytic dehydration of methanol to dimethyl ether (DME) over Pd/Cab-O-Sil catalysts", Applied Catalysis A: General, 1997, 149, 303-309

[46] Naik S.P., Du H., Wan H., Bui V., Miller J.D., Zmierczak W.W., "A Comparative Study of ZnO-CuO-Al_2O_3/SiO_2-Al_2O_3 Composite and Hybrid Catalysts for Direct Synthesis of Dimethyl Ether from Syngas" Ind. Eng. Chem. Res., 2008, 47, 9791-9794

[47] Kim E.J., Park N.K., Han G.B., Ryu S.O., Lee T.J., "A reactivity test of Cu–Zn-based catalysts prepared with various precursors and precipitates for the direct synthesis of DME", Process Safety and Environmental Protection, 2006, 84(B6), 469–475

[48] Kang S.H., Bae J.W., Jun K.W., Potdar H.S., "Dimethyl ether synthesis from syngas over the composite catalysts of Cu–ZnO–Al_2O_3/Zr-modified zeolites", Catalysis Communications, 2008, 9, 2035-2039

[49] Venugopal A., Palgunadi J., Deog J.K., Joo O.S., Shin C.H., "Dimethyl ether synthesis on the admixed catalysts of Cu-Zn-Al-M (M=Ga, La, Y, Zr)and γ- Al_2O_3:

The role of modifier", Journal of Molecular Catalysis A: Chemical, 2008, doi:10.1016/j.molcata.2008.11.038
[50] Sun K., Lu W., Qiu F., Liu S., Xu X., "Direct synthesis of DME over bifunctional catalyst: surface properties and catalytic performance", Applied Catalysis A: General, 2003, 252, 243-249

[51] Moradi G.R., Nosrati S., Yaripor F., "Effect of the hybrid catalysts preparation method upon direct synthesis of dimethyl ether from synthesis gas", Catalysis Communications, 2007, 8, 598-606

[52] Takeguchi T., Yanagisawa K., Inui T., Inoue M., "Effect of the property of solid acid upon syngas-to-dimethyl ether conversion on the hybrid catalysts composed of Cu–Zn–Ga and solid acids", Applied Catalysis A: General, 2000, 192, 201-209

[53] Qing-li X., Ting-chen L., Yong-jie Y., "Effects of CaO-modified zeolite on one-step synthesis of dimethyl ether", J Fuel Chem Technol, 2008, 36(2), 176-180

[54] Mao D., Yang W., Xia J., Zhang B., Song Q., Chen Q., "Highly effective hybrid catalyst for the direct synthesis of dimethyl ether from syngas with magnesium oxide-modified HZSM-5 as a dehydration component", Journal of Catalysis, 2005, 230, 140–149

[55] Khandan N., Kazemeini M., Aghaziarati M., "Synthesis of Dimethyl Ether over Modified H-Mordenite Zeolites and Bifunctional Catalysts Composed of $Cu/ZnO/ZrO_2$ and Modified H-Mordenite Zeolite in Slurry Phase", Catal Lett, 2009, 129, 111-118

[56] Yoo K.S., Kim J.H., Park M.J., Kim S.J., Joo O.S., Jung K.D., "Influence of solid acid catalyst on DME production directly from synthesis gas over the admixed catalyst of $Cu/ZnO/Al_2O_3$ and various SAPO catalysts Applied Catalysis A: General, 2007, 330, 57-62

[57] Mao D., Yang W., Xia J., Zhang B., Lu G., "The direct synthesis of dimethyl ether from syngas over hybrid catalysts with sulfate-modified γ-alumina as methanol dehydration components", Journal of Molecular Catalysis A: Chemical, 2006, 250, 138-144

[58] Chiola V., Ritsko J.E., Vanderpool C.D., US Patent No.3 556-725, 1971

[59] Di Renzo F., Cambon H., Dutartre R., "A 28-year-old synthesis of micelle-templated mesoporous silica", Microporous Materials, 1997, 10, 283-286

[60] Kresge C.T., Leonowicz M.E., Roth W.J., Vartuli J.C., Beck J.S., "Ordered mesoporous molecular-sieves synthesized by a liquid-crystal template mechanism", Nature, 1992, 359, 710-712

[61] Beck J. S., Vartuli J.C., Roth W.J., Leonowicz M.E., Kresge C.T., Schmitt K. D., Chu C.T.W., Olson D. H., Sheppard E.W., McCullen S. B., Higgins J.B.,

Schlenker J.L., “A New Family of Mesoporous Molecular Sieves Prepared with Liquid Crystal Templates”, J. Am. Chem. Soc., 1992, 114, 10834-10843

[62] J. Xu, “Spectroscopic studies of synthesis, modification and characterization of novel mesoporous molecular sieves”, PhD Thesis, University of Houston, December 1999.

[63] Behrens P., Glaue A., Haggenmüller C., Scheshner G., “Structure directed materials syntheses: synthesis field diagrams for the preparation of mesostructured silicas”, Solid State Ionics, 1997,101, 255-260

[64] Ciesla, U., Schüth, F., “Ordered Mesoporous Materials”, Microporous and Mesoporous Materials, 1999, 27, 131-149

[65] Øye G., Sjöblom J., Stöcker M., “Synthesis, characterization and potential applications of new materials in the mesoporous range”, Adv. in Coll. and Inter. Sci., 2001, 89-90, 439-466

[66] Sayari A., Liu P., “Non-silica periodic mesostructured materials: recent progress”, Microporous Materials, 1997, 12, 149-177.

[67] Khan R.A., “Metal Incorporation in MCM-41 for Hydrodesulfurization”, MSc. Thesis, King Fahd University of Petroleum and Minerals, January 2003

[68] Vartuli, J.C., Schmitt K. D., Kresge C.T., Roth W.J., Leonowicz M.E., McCullen S.B., Hellring S.D., Beck J.S., Schlenker J.L., Olson D.H., Sheppard E.W., “Effect of surfactant/silica molar ratios on the formation of mesoporous molecular sieves: Inorganic mimicry of surfactant liquid-crystal phases and mechanistic implications”, Chem. Mater., 1994, 6, 2317-2326

[69] Taguchi A., Schüth F., “Ordered mesoporous materials in catalysis”, Microporous and Mesoporous Materials, 2005, 77, 1-45

[70] Beck J.S., Vartuli, J.C., Kennedy G.J., Kresge C.T., Roth W.J., Schramm S.E., “Molecular or supramolecular templating: Defining the role of surfactant chemistry in the formation of microporous and mesoporous molecular sieves”, Chem. Mater., 1994, 6, 1816-1821

[71] Nalbant A., “Synthesis and characterization of Cu-MCM-41 and Ni-MCM-41 type catalytic materials”, MSc. Thesis, Middle East Technical University, January 2005.

[72] Sener C., “Synthesis and characterization of Pd-MCM-type mesoporous nanocomposite materials”, MSc. Thesis, Middle East Technical University, January 2006.

[73] Roth W.J., “Synthesis of the cubic mesoporous molecular sieve MCM-48’ US Patent No:6.096.288, 2000

[74] Schumacher K., Ravikovitch P. I., Chesne A., Neimark A.V., Unger K.K., "Characterization of MCM-48 materials", Langmuir, 2000, 16, 4648-4654

[75] Yao N., "Synthesis and characterization of Pt/Sn-MCM-41 petroleum reforming catalysts", PhD Thesis, Yale University, January 2002.

[76] Sayari A., "Periodic mesoporous materials; synthesis, characterization and potential applications", Studies in Surface Science and Catalysis, 1996, 102, 1-46

[77] Varisli D., "Kinetic Studies for Dimethyl ether and Diethyl ether Production", Ph.D. Thesis, Middle East Technical University, September 2007.

[78] Franco L.N., Perez I.H., Pliego J.A., Franco A.M., "Selective hydroxylation of phenol employing Cu-MCM-41 catalysts", Catalysis Today, 2002, 75, 189-195

[79] Ozdogan E., "Steam reforming of ethanol for hydrogen production using Cu-MCM41 and Ni-MCM41 type mesoporous catalytic materials", Msc. Thesis, Middle East Technical University, August 2007.

[80] Yasyerli S., Dogu G., Ar I., Dogu T., "Dynamic Analysis of Removal and Selective Oxidation of H_2S to Elemental Sulfur over Cu-V and Cu-V-Mo mixed oxides in a fixed bed reactor", Chemical Engineering Science, 2004, 59, 4001-4009

[81] Velu S., Wang L., Okazaki M., Suzuki K., Tomurai S., "Characterization of MCM-41 mesoporous molecular sieves containing Copper and Zinc and their catalytic performance in the selective oxidation of alcohols to aldehydes", Microporous and Mesoporous Materials, 2002, 54, 113-126

[82] Schwarz J. A., "Methods for preparation of catalytic materials", Chem. Rev. 1995, 95, 477-510

[83] Perego C., Villa P., "Catalyst preparation methods", Catalysis Today, 1994, 34, 281-305

[84] White R.J., Luque R., Budarin V.L., Clark J.H., Macquarrie D.J., "Supported metal nanoparticles on porous materials. Methods and applications", Chemical Society Reviews, 2009, 38, 481-494

[85] Sandler S.I., "Chemical and Engineering Thermodynamics", 3th Ed., Wiley, New York, 1999

[86] Meyers R.A., "Handbook of Petrochemicals Production Processes", McGraw Hill, 2005

[87] Ciftci A., "Nanocomposite nafion and heteropolyacid incorporated mesoporous catalysts for dimethyl ether synthesis from methanol", Msc. Thesis, Middle East Technical University, August 2009.

[88] Wachs, I.E., Fitzpatrick, L.E., "Characterization of Catalytic Materials", Manning Publications Co., 1992, Greenwich.

[89] Ozaydin Z., “Mezogözenekli Cu-MCM-41 ile yüksek sıcaklıkta proses gazı desülfürizasyonu”, Yüksek lisans tezi, Gazi Üniversitesi, Haziran 2007

[90] Tennyson W., “X-Ray diffraction: the basics followed by a few examples of data analysis”, Nanolab/NSF NUE/Bumm

[91] Sing K.S.W., Everett D.H., Haul R.A.W., Moscou L., Pierotti R.A., Rouquerol J., Siemieniewska T., “Reporting physisorption data for gas/solid systems: with special reference to the determination of surface area and porosity”, Pure & Appl. Chem., 1985, 57, 4, 603-619

[92] Varisli, D., Dogu, T., Dogu, G., “Silicotungstic Acid Impregnated MCM-41-like Mesoporous Solid Acid Catalysts for Dehydration of Ethanol”, Ind. Eng. Chem. Res., 2008, 48, 4071.

[93] Damyanova S., Cubeiro M.L., Fierro J.L.G., “Acid-redox properties of titania-supported 12-molybdophosphates for methanol oxidation”, Journal of Molecular Catalysis A: Chemical, 1999, 142, 85-100

APPENDIX A

THERMODYNAMIC CALCULATIONS

A.1. Fugacity Coefficients of the Species

Fugacity coefficients of each species were calculated at different temperature values by using Peng-Robinson equation for the pressure values of 1 bar, 10 bar, 30 bar, 50 bar and 80 bar. The calculations were done by using MATHCAD software programme and sample calculations for DME, CO, H_2, H_2O and CO_2 at 540K and 50 bar are presented in this chapter.

A.1.1. Fugacity Coefficient of DME by Peng-Robinson Equation of State

$Tc := 400.05 \qquad T := 540 \ K$

$Pc := 53.7 \qquad P := 50 \ bar$

$R := 8.314 \cdot 10^{-5}$

$Tr := \frac{T}{Tc}$

$Tr = 1.35$

$\omega := 0.192$

$\kappa := 0.37464 + 1.54226 \cdot \omega - 0.26992 \cdot \omega^2 \qquad \kappa = 0.661$

$F := \left[1 + \kappa \cdot \left(1 - \sqrt{Tr}\right)\right]^2 \qquad F = 0.798$

$a := 0.45724 \cdot \left(\frac{R^2 \cdot Tc^2}{Pc}\right) \qquad a = 9.419 \times 10^{-6}$

$b := 0.07780 \cdot \left(\frac{R \cdot Tc}{Pc}\right) \qquad b = 4.819 \times 10^{-5}$

$A := \frac{a \cdot F \cdot P}{(R \cdot T)^2} \qquad A = 0.186$

$$B := \frac{b \cdot P}{R \cdot T} \qquad B = 0.054$$

$$\alpha := -1 + B \qquad \alpha = -0.946$$

$$\beta := A - 3 \cdot B^2 - 2 \cdot B \qquad \beta = 0.07$$

$$\gamma := -A \cdot B + B^2 + B^3 \qquad \gamma = -6.966 \times 10^{-3}$$

$$Z^3 + \alpha \cdot Z^2 + \beta \cdot Z + \gamma = 0 \text{ solve}, Z \rightarrow \begin{pmatrix} 3.5672160978729389095 \cdot 10^{-2} - 8.1788054134366916260 \cdot 10^{-2} \cdot i \\ 3.5672160978729389095 \cdot 10^{-2} + 8.1788054134366916260 \cdot 10^{-2} \cdot i \\ .87499009765768709394 \end{pmatrix}$$

$$Z := .87499009765768709394$$

$$\ln\left(\frac{f}{P}\right) = Z - 1 - \ln(Z - B) - \frac{A}{2\sqrt{2} \cdot B} \cdot \ln\left[\frac{Z + \left(1 + \sqrt{2}\right) \cdot B}{Z + \left(1 - \sqrt{2}\right) \cdot B}\right] \text{ solve}, \left(\frac{f}{P}\right) \rightarrow .87871289024236667660$$

f/P= .87871289024236667660

A.1.2. Fugacity Coefficient of H_2O by Peng-Robinson Equation of State

$$Tc := 647.3 \qquad T := 540 \text{ K}$$

$$Pc := 220.48 \qquad P := 50 \text{ bar}$$

$$R := 8.314 \cdot 10^{-5}$$

$$Tr := \frac{T}{Tc}$$

$$Tr = 0.834$$

$$\omega := 0.343$$

$$\kappa := 0.37464 + 1.54226 \cdot \omega - 0.26992 \cdot \omega^2$$

$$\kappa = 0.872$$

$$F := \left[1 + \kappa \cdot \left(1 - \sqrt{Tr}\right)\right]^2 \qquad F = 1.157$$

$$a := 0.45724 \cdot \left(\frac{R^2 \cdot Tc^2}{Pc}\right) \qquad a = 6.006 \times 10^{-6}$$

$$b := 0.07780 \cdot \left(\frac{R \cdot Tc}{Pc}\right) \qquad b = 1.899 \times 10^{-5}$$

$$A := \frac{a \cdot F \cdot P}{(R \cdot T)^2} \qquad A = 0.172$$

$$B := \frac{b \cdot P}{R \cdot T} \qquad B = 0.021$$

$$\alpha := -1 + B \qquad \alpha = -0.979$$

$$\beta := A - 3 \cdot B^2 - 2 \cdot B \qquad \beta = 0.129$$

$$\gamma := -A \cdot B + B^2 + B^3 \qquad \gamma = -3.188 \times 10^{-3}$$

$$Z^3 + \alpha \cdot Z^2 + \beta \cdot Z + \gamma = 0 \text{ solve}, Z \rightarrow \begin{pmatrix} 3.2570156846572171753 \cdot 10^{-2} \\ .11821845510942638568 \\ .82806227063014346267 \end{pmatrix}$$

$$Z := .82806227063014346267$$

$$\ln\left(\frac{f}{P}\right) = Z - 1 - \ln(Z - B) - \frac{A}{2\sqrt{2} \cdot B} \cdot \ln\left[\frac{Z + \left(1 + \sqrt{2}\right) \cdot B}{Z + \left(1 - \sqrt{2}\right) \cdot B}\right] \text{ solve}, \left(\frac{f}{P}\right) \rightarrow .85176992551735828459$$

f/P= .85176992551735828459

A.1.3. Fugacity Coefficient of CO by Peng-Robinson Equation of State

$$Tc := 132.86 \qquad T := 540 \text{ K}$$

$$Pc := 34.935 \qquad P := 50 \text{ bar}$$

$$R := 8.314 \cdot 10^{-5}$$

$$Tr := \frac{T}{Tc}$$

$$Tr = 4.064$$

$$\omega := 0.05$$

$$\kappa := 0.37464 + 1.54226 \cdot \omega - 0.26992 \cdot \omega^2 \qquad \kappa = 0.451$$

$$F := \left[1 + \kappa \cdot \left(1 - \sqrt{Tr}\right)\right]^2 \qquad F = 0.293$$

$$a := 0.45724 \cdot \left(\frac{R^2 \cdot Tc^2}{Pc}\right) \qquad a = 1.597 \times 10^{-6}$$

$$b := 0.07780 \cdot \left(\frac{R \cdot Tc}{Pc}\right) \qquad b = 2.46 \times 10^{-5}$$

$$A := \frac{a \cdot F \cdot P}{(R \cdot T)^2} \qquad A = 0.012$$

$$B := \frac{b \cdot P}{R \cdot T} \qquad B = 0.027$$

$\alpha := -1 + B$ $\alpha = -0.973$

$\beta := A - 3 \cdot B^2 - 2 \cdot B$ $\beta = -0.045$

$\gamma := -A \cdot B + B^2 + B^3$ $\gamma = 4.527 \times 10^{-4}$

$$Z^3 + \alpha \cdot Z^2 + \beta \cdot Z + \gamma = 0 \text{ solve}, Z \rightarrow \begin{pmatrix} -5.2680685973966361141 \cdot 10^{-2} \\ 8.4503260251615945449 \cdot 10^{-3} \\ 1.0168342221479152840 \end{pmatrix}$$

$Z := 1.0168342221479152840$

$$\ln\left(\frac{f}{P}\right) = Z - 1 - \ln(Z - B) - \frac{A}{2\sqrt{2} \cdot B} \cdot \ln\left[\frac{Z + \left(1 + \sqrt{2}\right) \cdot B}{Z + \left(1 - \sqrt{2}\right) \cdot B}\right] \text{ solve}, \left(\frac{f}{P}\right) \rightarrow 1.0164495674393445475$$

f/P= 1.0164495674393445475

A.1.4. Fugacity Coefficient of CO_2 by Peng-Robinson Equation of State

$Tc := 329.25$ $T := 540$ K

$Pc := 73.97$ $P := 50$ bar

$R := 8.314 \cdot 10^{-5}$

$Tr := \frac{T}{Tc}$

$Tr = 1.64$

$\omega := 0.343$

$\kappa := 0.37464 + 1.54226 \cdot \omega - 0.26992 \cdot \omega^2$ $\kappa = 0.872$

$F := \left[1 + \kappa \cdot \left(1 - \sqrt{Tr}\right)\right]^2$ $F = 0.57$

$a := 0.45724 \cdot \left(\frac{R^2 \cdot Tc^2}{Pc}\right)$ $a = 4.632 \times 10^{-6}$

$b := 0.07780 \cdot \left(\frac{R \cdot Tc}{Pc}\right)$ $b = 2.879 \times 10^{-5}$

$A := \frac{a \cdot F \cdot P}{(R \cdot T)^2}$ $A = 0.066$

$$B := \frac{b \cdot P}{R \cdot T} \qquad B = 0.032$$

$$\alpha := -1 + B \qquad \alpha = -0.968$$

$$\beta := A - 3 \cdot B^2 - 2 \cdot B \qquad \beta = -1.666 \times 10^{-3}$$

$$\gamma := -A \cdot B + B^2 + B^3 \qquad \gamma = -1.041 \times 10^{-3}$$

$$Z^3 + \alpha \cdot Z^2 + \beta \cdot Z + \gamma = 0 \text{ solve}, Z \rightarrow \begin{pmatrix} -1.4100788334895843967 \cdot 10^{-3} - 3.2711257094283702071 \cdot 10^{-2} \cdot i \\ -1.4100788334895843967 \cdot 10^{-3} + 3.2711257094283702071 \cdot 10^{-2} \cdot i \\ .97075554438531843546 \end{pmatrix}$$

$$Z := .97075554438531843546$$

$$\ln\left(\frac{f}{P}\right) = Z - 1 - \ln(Z - B) - \frac{A}{2\sqrt{2} \cdot B} \cdot \ln\left[\frac{Z + (1 + \sqrt{2}) \cdot B}{Z + (1 - \sqrt{2}) \cdot B}\right] \text{ solve}, \left(\frac{f}{P}\right) \rightarrow .96910365674701281192$$

+

f/P= .96910365674701281192

A.1.5. Fugacity Coefficient of H_2 by Peng-Robinson Equation of State

$Tc := 33.3$ $\quad T := 540$ K

$Pc := 12.97$ $\quad P := 50$ bar

$$R := 8.314 \cdot 10^{-5}$$

$$Tr := \frac{T}{Tc}$$

$$Tr = 16.216$$

$$\omega := -0.215$$

$$\kappa := 0.37464 + 1.54226 \cdot \omega - 0.26992 \cdot \omega^2 \qquad \kappa = 0.031$$

$$F := \left[1 + \kappa \cdot \left(1 - \sqrt{Tr}\right)\right]^2 \qquad F = 0.823$$

$$a := 0.45724 \cdot \left(\frac{R^2 \cdot Tc^2}{Pc}\right) \qquad a = 2.702 \times 10^{-7}$$

$$b := 0.07780 \cdot \left(\frac{R \cdot Tc}{Pc}\right) \qquad b = 1.661 \times 10^{-5}$$

$$A := \frac{a \cdot F \cdot P}{(R \cdot T)^2} \qquad A = 5.52 \times 10^{-3}$$

$$B := \frac{b \cdot P}{R \cdot T} \qquad B = 0.018$$

$$\alpha := -1 + B \qquad \alpha = -0.982$$

$$\beta := A - 3 \cdot B^2 - 2 \cdot B \qquad \beta = -0.032$$

$$\gamma := -A \cdot B + B^2 + B^3 \qquad \gamma = 2.463 \times 10^{-4}$$

$$Z^3 + \alpha \cdot Z^2 + \beta \cdot Z + \gamma = 0 \text{ solve}, Z \rightarrow \begin{pmatrix} -3.8193687258936193491 \cdot 10^{-2} \\ 6.3641756344396541828 \cdot 10^{-3} \\ 1.0133342661863058428 \end{pmatrix}$$

$$Z := 1.0133342661863058428$$

$$\ln\left(\frac{f}{P}\right) = Z - 1 - \ln(Z - B) - \frac{A}{2\sqrt{2} \cdot B} \cdot \ln\left[\frac{Z + (1 + \sqrt{2}) \cdot B}{Z + (1 - \sqrt{2}) \cdot B}\right] \text{ solve}, \left(\frac{f}{P}\right) \rightarrow 1.0132449736965203383$$

f/P= 1.0132449736965203383

The calculated fugacity coefficients at different pressure values were listed in the tables below.

Table 26. Fugacity coefficients of the species at 1 bar

T (K)	f/P (DME)	f/P (H_2O)	f/P (CO)	f/P (H_2)	f/P (CO_2)
400	0.992944766	0.992930089	1.000095354	1.000290727	0.997394232
420	0.993915608	0.993809442	1.000153342	1.000287412	0.997837587
440	0.994734198	0.994555088	1.000199062	1.000283458	0.99820572
460	0.995428923	0.995191587	1.000235082	1.000279069	0.998513242
480	0.996022025	0.995738226	1.000263381	1.000274394	0.99877152
500	0.996531107	0.996210309	1.000285494	1.000269543	0.998989483
520	0.996970228	0.99662009	1.000302625	1.000264598	0.999174215
540	0.997350717	0.996977467	1.000315724	1.00025962	0.999331379
560	0.997681771	0.997290498	1.000325547	1.000254655	0.999465541
580	0.997970913	0.997565788	1.0003327	1.000249736	0.999580409
600	0.998224338	0.997808793	1.000337671	1.000244888	0.99967901

Table 27. Fugacity coefficients of the species at 10 bar

T (K)	f/P (DME)	f/P (H_2O)	f/P (CO)	f/P (H_2)	f/P (CO_2)
400	0.93059864	0.929606561	1.001020593	1.002927782	0.974245658
420	0.940140043	0.938372278	1.00159031	1.002892274	0.978627856
440	0.948184908	0.945799392	1.002039292	1.002850762	0.982267882
460	0.955013666	0.952136248	1.002392799	1.002805192	0.985309672
480	0.960845211	0.957576885	1.002670275	1.002756999	0.987865207
500	0.96585239	0.962274698	1.00288683	1.002707246	0.990022507
520	0.970173095	0.966352217	1.003054311	1.002656719	0.991851397
540	0.973918333	0.969908227	1.003182078	1.002606002	0.993407747
560	0.977178217	0.973023042	1.003277578	1.002555528	0.994736609
580	0.980026446	0.975762462	1.003346778	1.002505612	0.995874574
600	0.982523716	0.978180774	1.003394485	1.002456485	0.996851558

Table 28. Fugacity coefficients of the species at 30 bar

T (K)	f/P (DME)	f/P (H_2O)	f/P (CO)	f/P (H_2)	f/P (CO_2)
400	0.798259936	0.079768589	1.003499758	1.009039188	0.923786151
420	0.826385653	0.141952096	1.005142725	1.008915384	0.936764106
440	0.849878531	0.236563931	1.00652785	1.008775817	0.947547869
460	0.869724307	0.372427105	1.007557412	1.008625916	0.956564358
480	0.886631316	0.557852472	1.00836382	1.008469672	0.964144379
500	0.901133073	0.799686702	1.008991342	1.008310021	0.97054743
520	0.913643325	0.899889369	1.009474715	1.008149127	0.975979231
540	0.924489429	0.910498824	1.009709506	1.007988583	0.980604374
560	0.933934258	0.919778858	1.009978203	1.007829553	0.984555641
580	0.942191375	0.927932756	1.010170605	1.007672879	0.987940952
600	0.949435945	0.934278043	1.010300675	1.007519165	0.990848614
620	0.955812812	0.941496418	1.010379733	1.007271548	0.993431289
640	0.961442592	0.947156344	1.010416998	1.007126858	0.995561934
660	0.966426359	0.952201126	1.010420011	1.00698595	0.997401725
680	0.970849292	0.956710706	1.010394969	1.00684892	0.998992087
700	0.974783543	0.960752772	1.010346977	1.006715807	1.000367841

Table 29. Fugacity coefficients of the species at 50 bar

T (K)	f/P (DME)	f/P (H_2O)	f/P (CO)	f/P (H_2)	f/P (CO_2)
400	0.66872125	0.048530719	1.006652689	1.015292264	0.876388019
420	0.718763838	0.086331067	1.009315695	1.015060346	0.897467958
440	0.757996525	0.724279441	1.011410119	1.014806129	0.914978512
460	0.790428825	0.760307422	1.013054103	1.014537897	0.929623666
480	0.817794964	0.789170157	1.014338881	1.014261704	0.941942669
500	0.841162911	0.813342653	1.015335552	1.013981983	0.95235602
520	0.861281829	0.833968604	1.016099983	1.013701975	0.961196109
540	0.87871289	0.851769926	1.016449567	1.013244973	0.969103656
560	0.893892795	0.867258717	1.017100072	1.013149881	0.975167718
580	0.907169817	0.880820945	1.017399269	1.012880714	0.980687751
600	0.918826478	0.892758306	1.017596812	1.012617386	0.985431368
620	0.929094884	0.90331238	1.017473862	1.012196292	0.989634147
640	0.938167606	0.912679964	1.017520094	1.011949599	0.993113898
660	0.946205713	0.92102346	1.017511253	1.011709774	0.996119509
680	0.953344841	0.928478268	1.017457356	1.011476905	0.998718209
700	0.959699883	0.93515822	1.017366658	1.011250995	1.000966568

Table 30. Fugacity coefficients of the species at 80 bar

T (K)	f/P (DME)	f/P (H_2O)	f/P (CO)	f/P (H_2)	f/P (CO_2)
400	0.474550115	0.030969895	1.012111933	1.025001184	0.810436944
420	0.563379594	0.055061668	1.01607782	1.02457067	0.842849536
440	0.631511795	0.091692871	1.01919207	1.024113616	0.869738019
460	0.682960608	0.144273764	1.021630596	1.023641529	0.892233446
480	0.724959409	0.216026899	1.02352963	1.023162741	0.911174902
500	0.760379146	0.309630317	1.024995593	1.022683281	0.927206695
520	0.790732089	0.426851114	1.026112272	1.022207495	0.940834552
540	0.816996908	0.568176121	1.026946113	1.021738487	0.95246157
560	0.839878182	0.732405857	1.027550158	1.021278439	0.962412791
580	0.859914381	0.810956498	1.027967004	1.020828856	0.970952765
600	0.87753218	0.827971964	1.028231048	1.020390729	0.978298485
620	0.893077677	0.847043915	1.028370208	1.019697169	0.984782462
640	0.906836187	0.861957715	1.028407245	1.019289382	0.990181344
660	0.919045702	0.875203688	1.028360795	1.018893907	0.994847122
680	0.929906544	0.887016507	1.028246171	1.018510719	0.998882923
700	0.939588548	0.897588177	1.028076002	1.018139674	1.002375676

A.2. Equilibrium Conversions

Equilibrium conversions at different temperature values in the range 400-700K were calculated by using MATHCAD software programme for reactions (9) and (10). The feed ratio (H_2/CO) of the reactants was taken one for both of the reactions. Sample calculations for equilibrium conversion at 540K and 50 bar, for both of the reactions are presented.

A.2.1. Equilibrium conversion calculation for feed ratio (H_2/CO) of 1 [considering reaction (9): $3CO+3H_2 \rightarrow CH_3OCH_3 + CO_2$]

$P := 50\ bar$

$T := 540\ K$

$$\ln\left(\frac{K}{6.2\cdot 10^{16}}\right) = \left[\frac{-\left[-246200 + (-132.427)\cdot(T - 298) + \left(23.952\cdot\frac{10^{-2}}{2}\right)\cdot\left(T^2 - 298^2\right) + \left(-11.544\cdot\frac{10^{-5}}{3}\right)\cdot\left(T^3 - 298^3\right)\right]}{8.314}\right]\cdot\left[\left(\frac{1}{T}\right) - \left(\frac{1}{298}\right)\right] \text{ solve, K } \rightarrow 2.7942579357271718234\cdot 10^{-4}$$

$K := 2.7942579357271718234\cdot 10^{-4}$

$(f/P)_{CH3OCH3} = A$ $\quad A := 0.87871289$

$(f/P)_{CO2} = B$ $\quad B := 0.968728582$

$(f/P)_{CO} = C$ $\quad C := 1.016676404$

$(f/P)_{H2} = D$ $\quad D := 1.013424039$

$$K = \left(\frac{A\cdot B}{C^3\cdot D^3}\right)\cdot\frac{\left[\left(\frac{\frac{50}{3}x}{100 - \frac{200}{3}\cdot x}\right)\cdot P\right]^2}{\left[\left[\frac{(50 - 50x)}{\left(100 - \frac{200}{3}\cdot x\right)}\right]\cdot P\right]^3\cdot\left[\left[\frac{(50 - 50x)}{\left(100 - \frac{200}{3}\cdot x\right)}\right]\cdot P\right]^3} \text{ solve, x } \rightarrow \begin{pmatrix} .8332854853961178 8935 \\ .9372676770805169 5318 - .1459697152942565 1944\cdot i \\ .9372676770805169 5318 + .1459697152942565 1944\cdot i \\ 1.0833572573019410553 - .1076055183576276 9957\cdot i \\ 1.0833572573019410553 + .1076055183576276 9957\cdot i \\ 1.1254646458389660936 \end{pmatrix}$$

$x := .83328548539611788935$

A.2.2. Equilibrium conversion calculation for feed ratio (H_2/CO) of 1 [considering reaction (10): $2CO+4H_2 \rightarrow CH_3OCH_3 + H_2O$]

$P := 50\ bar$

$T := 540\ K$

$$\ln\left(\frac{K}{6.02\cdot 10^{11}}\right) = \left[\frac{-\left[-205000 + (-123.398)\cdot(T - 298) + \left(18.536\cdot\frac{10^{-2}}{2}\right)\cdot\left(T^2 - 298^2\right) + \left(-6.853\cdot\frac{10^{-5}}{3}\right)\cdot\left(T^3 - 298^3\right)\right]}{8.314}\right]\cdot\left[\left(\frac{1}{T}\right) - \left(\frac{1}{298}\right)\right] \text{ solve, K } \rightarrow 3.7250695737779347112\cdot 10^{-6}$$

$K := 3.7250695737779347112\cdot 10^{-6}$

$(f/P)_{CH3OCH3} = A$ $\quad A := 0.87871289$

$(f/P)_{H2O} = B$ $\quad B := 0.851769926$

$(f/P)_{CO} = C$ $\quad C := 1.016676404$

$(f/P)_{H2} = D$ $\quad D := 1.013424039$

$$K = \left(\frac{A\cdot B}{C^2\cdot D^4}\right)\cdot\frac{\left[\left(\frac{\frac{x}{4}}{2-x}\right)\cdot P\right]^2}{\left[\left[\frac{(1-x)}{(2-x)}\right]\cdot P\right]^4\cdot\left[\left[\frac{\left(1-\frac{x}{2}\right)}{(2-x)}\right]\cdot P\right]^2} \text{ solve, x } \rightarrow \begin{pmatrix} 1. - .30646747648660274701\cdot i \\ 1. + .30646747648660274701\cdot i \\ .71880695591747033085 \\ 1.2811930440825296691 \end{pmatrix}$$

$x := .71880695591747033085$

The equilibrium conversion values calculated at different temperature values were listed below in Tables 31 and 32.

Table 31. Equilibrium conversion values for reaction (9) at different temperature and pressure values [feed ratio (H_2/CO) = 1]

T (K)	Xeq (1 atm)	Xeq (10atm)	Xeq (30 atm)	Xeq (50 atm)	Xeq (80 atm)
400	0.931953012	0.986256964	0.993689547	0.995691019	
420	0.866707168	0.973999589	0.988078112	0.991840773	0.994400545
440	0.747662385	0.95294658	0.978544699	0.985281404	0.989794695
460	0.548984664	0.917801488	0.962936547	0.974582214	0.98229253
480	0.299220836	0.860362964	0.93808822	0.957669957	0.970473223
500	0.116414741	0.768675825	0.899355757	0.931579399	0.952353077
520		0.629643733	0.840051316	0.892080303	0.925162088
540		0.444732442	0.751365558	0.833285485	0.885051272
560		0.256204221	0.625081843	0.747770986	0.826835539
580		0.122525752	0.463800953	0.628982939	0.744242877
600			0.295466452	0.479122296	0.632035272
620			0.162061183	0.31997951	0.491876953
640			0.08077451	0.187073764	0.341789448
660			0.038881834	0.09950425	0.210922151
680			0.018804975	0.050737503	0.118878461
700			0.009318766	0.025772404	0.063923314

Table 32. Equilibrium conversion values for reaction (10) at different temperature and pressure values [feed ratio (H_2/CO) = 1]

T (K)	Xeq (1 atm)	Xeq (10atm)	Xeq (30 atm)	Xeq (50 atm)	Xeq (80 atm)
400	0.816846783	0.982027279	0.996901769	0.998441439	0.999210619
420	0.619164518	0.96012457	0.992029495	0.995954542	0.997900699
440	0.350168842	0.91715369	0.981089882	0.98553543	0.994913936
460	0.14083895	0.83839932	0.958218146	0.970978283	0.988604578
480		0.706536435	0.913449828	0.94485468	0.976098553
500		0.517636673	0.831671132	0.900242924	0.952693386
520		0.311428289	0.709447644	0.827998282	0.911190543
540		0.154998974	0.547538778	0.718806956	0.841635324
560			0.365726653	0.570508115	0.733150918
580			0.210159612	0.400538845	0.592223502
600			0.108574148	0.246118834	0.433837087
620			0.053719135	0.136152757	0.282148212
640			0.026505316	0.071336725	0.166178126
660			0.013224135	0.036896458	0.092819522
680			0.006820778	0.019386779	0.049993674
700			0.003628432	0.010416189	0.027226891

APPENDIX B

CALIBRATION OF GAS CHROMATOGRAPH

Calibration experiments were done in order to determine the retention times and calibration factors of the reactants and products. Calibration factors and retention times of carbondioxide (CO_2), methane (CH_4), methanol (CH_3OH), ethanol (C_2H_5OH) and DME (CH_3OCH_3) were determined by using the equations given in the following parts of this section. The calibration factor of carbon monoxide was taken 1.0. Gas mixtures of these substances with different feed ratios were fed to the GC and results were obtained by using Peak327 software programme.

B.1. Calibration Factors for Carbondioxide, Methane and DME

In the calibration experiments of CO_2, CH_4 and DME, same amounts of gases were used and the same procedure was followed. In this section, sample calculations for carbondioxide were presented.

For the calibration experiments of CO_2, gas mixture containing carbon monoxide, carbondioxide and hydrogen was fed to the GC. By using the following relations, calibration factor of CO_2 was calculated.

Flow rate of CO = 25 ml/min
Flow rate of H_2 = 25 ml/min
Flow rate of CO_2 = 10 ml/min

} Total flow rate F_{total} = 60 ml/ min

The mole fraction of each gas was calculated as follow:

$$y_{CO} = \frac{F_{CO}}{F_{Total}} = \frac{25\ ml/min}{60\ ml/min} = 0.417$$

$$y_{H2} = \frac{F_{H2}}{F_{Total}} = \frac{25\ ml/min}{60\ ml/min} = 0.417$$

$$y_{CO2} = \frac{F_{CO2}}{F_{Total}} = \frac{10\ ml/min}{60\ ml/min} = 0.167$$

Calibration factor of CO_2 was calculated by using the following equations;

$$y_{CO} = \frac{A_{CO} \times \beta_{CO}}{(A_{CO} \times \beta_{CO}) + (A_{CO2} \times \beta_{CO2}) + (A_{H2} \times \beta_{H2})}$$

$$y_{CO2} = \frac{A_{CO2} \times \beta_{CO2}}{(A_{CO} \times \beta_{CO}) + (A_{CO2} \times \beta_{CO2}) + (A_{H2} \times \beta_{H2})}$$

By dividing these equations side by side, the following relation was obtained. Peak areas of CO and CO_2 were calculated by using software programme of GC. Since the calibration factor of CO was known, from the relation below calibration factor of CO_2 was calculated as 0.83.

$$\frac{y_{CO}}{y_{CO2}} = \frac{A_{CO} \times \beta_{CO}}{A_{CO2} \times \beta_{CO2}}$$

By following the same procedure, the calibration factors of CH_4 and DME were calculated and found 1.36 and 0.49, respectively.

B.2. Calibration Factors for Methanol and Ethanol

Methanol and ethanol were in the liquid phase so that they were fed to the line connected to GC by syringe pump. All the connection lines from syringe pump to GC was heated up to 150°C to vaporize methanol and ethanol before entering GC.

In addition to methanol and ethanol, mixture of carbon monoxide and hydrogen was fed in the GC from the same connection line.

By using the following relations, calibration factors of methanol and ethanol were calculated.

Firstly, gas phase densities of methanol and ethanol were calculated by following relation;

$$\rho_{gas} = \frac{P.M}{R.T}$$

$T = 298\ K\ (room\ temperature)$

$P = 1\ atm\ (atmospheric\ pressure)$

$R = 8.205746 \times 10^{-5}\ m^3.atm/mol.K$

$M_{CH3OH} = 32.04\ g/mol$

$M_{C2H5OH} = 46.07\ g/mol$

By using the given information, gas phase densities of the substances were found as;

$\rho_{CH3OH}(gas\ phase) = 1.2578 \times 10^{-3}\ g/ml$

$\rho_{C2H5OH}(gas\ phase) = 1.808 \times 10^{-3}\ g/ml$

The flow rate of the syringe pump was adjusted to 0.4 ml/ h and by using this information gas volumetric flow rates of methanol and ethanol were calculated. Alcohol mixture was prepared with equal volumes of methanol and ethanol.

$$v_{liquid\ (total)} = \frac{0.4ml}{h} \times \frac{1\ h}{60\ min} = 6.67 \times 10^{-3} ml/min$$

$$v_{liquid\ (CH3OH)} = v_{liquid\ (C2H5OH)} = \frac{6.67 \times 10^{-3} ml/min}{2} = 3.335 \times 10^{-3} ml/min$$

$$v_{liquid} \times \rho_{liquid} = v_{gas} \times \rho_{gas}$$

$$\left.\begin{array}{l} v_{gas(CH3OH)} = 2.10\ ml/min \\ v_{gas(C2H5OH)} = 1.45 ml/min \\ v_{CO} = 25\ ml/min \\ v_{H2} = 25\ ml/min \end{array}\right\} \quad v_{total} = 53.55\ ml/min$$

The mole fraction of each gas was calculated as follow:

$$y_{CO} = \frac{v_{CO}}{v_{total}} = \frac{25\ ml/min}{53.55\ ml/min} = 0.467$$

$$y_{H2} = \frac{v_{H2}}{v_{total}} = \frac{25\ ml/min}{53.55\ ml/min} = 0.467$$

$$y_{CH3OH} = \frac{v_{CH3OH}}{v_{total}} = \frac{2.10\ ml/min}{53.55\ ml/min} = 0.039$$

$$y_{C2H5OH} = \frac{v_{C2H5OH}}{v_{total}} = \frac{2.10\ ml/min}{53.55\ ml/min} = 0.027$$

Calibration factors of methanol and ethanol were calculated by using the following relations;

$$y_{CO} = \frac{A_{CO} \times \beta_{CO}}{(A_{CO} \times \beta_{CO}) + (A_{CH3OH} \times \beta_{CH3OH}) + (A_{C2H5OH} \times \beta_{C2H5OH}) + (A_{H2} \times \beta_{H2})}$$

$$y_{CH3OH} = \frac{A_{CH3OH} \times \beta_{CH3OH}}{(A_{CO} \times \beta_{CO}) + (A_{CH3OH} \times \beta_{CH3OH}) + (A_{C2H5OH} \times \beta_{C2H5OH}) + (A_{H2} \times \beta_{H2)}}$$

$$y_{C2H5OH} = \frac{A_{C2H5OH} \times \beta_{C2H5OH}}{(A_{CO} \times \beta_{CO}) + (A_{CH3OH} \times \beta_{CH3OH}) + (A_{C2H5OH} \times \beta_{C2H5OH}) + (A_{H2} \times \beta_{H2)}}$$

B.3. Calibration Factor for Formic Acid

In the calibration factor analyses experiments, a mixture was prepared with different volumes of formic acid and ethanol. A gas stream composed of carbon monoxide and hydrogen was fed to the system and at the same time 1µl of formic acid and ethanol mixture was injected directly to the column of GC. The calibration factor of formic acid (FA) was evaluated by using the following relations.

$M_{CH2O2} = 46.03\ g/mol$

$M_{C2H5OH} = 46.07\ g/mol$

$\rho_{CH2O2}(liquid\ phase) = 1.22\ g/ml$

$\rho_{C2H5OH}(liquid\ phase) = 0.788\ g/ml$

$m_{CH2O2} = V_{CH2O2} \times \rho = (5\ ml) \times (1.22\ g/ml) = 6.1\ g$

$m_{C2H5OH} = V_{C2H5OH} \times \rho = (10\ ml) \times (0.788\ g/ml) = 7.88\ g$

$$y_{CH2O2} = \frac{n_{CH2O2}}{n_{Total}} \qquad y_{C2H5OH} = \frac{n_{C2H5OH}}{n_{Total}}$$

$$y_{CH2O2} = \frac{A_{CH2O2} \times \beta_{CH2O2}}{(A_{CH2O2} \times \beta_{CH2O2}) + (A_{C2H5OH} \times \beta_{C2H5OH})}$$

$$y_{C2H5OH} = \frac{A_{C2H5OH} \times \beta_{C2H5OH}}{(A_{CH2O2} \times \beta_{CH2O2}) + (A_{C2H5OH} \times \beta_{C2H5OH})}$$

Results of the calibration experiments were listed in Table 33.

Table 33. Calibration Results

Component	Retention time (min)	Calibration factor, β
CO	1.27-1.28	1.00
CO_2	4.2-4.3	0.83
CH_4	2.4-2.6	1.36
CH_3OH	11.8-11.9	1.40
DME	23.3-23.5	0.49
C_2H_5OH	25.8-26.0	1.44
FA	11.8-12.0	1.80

B.4. Conversion of Carbon Monoxide and Selectivities of Products

Conversion of carbon monoxide and selectivities of products were calculated by using following relations.

$$n_{total,0} = n_{CO} + n_{CO2} + n_{CH4} + n_{CH3OH} + 2n_{CH3OCH3} + 2n_{C2H5OH} + n^{*}_{CH2O2}$$

*Formic acid (CH_2O_2) was added to mole balance equation only for the calculation of CO conversion and selectivities of products, for commercial methanol reforming and TRC75(L)-C catalysts.

Conversion of carbon monoxide was calculated by following equation.

$$x_{CO} = \frac{n_{total,0} - n_{CO}}{n_{total,0}}$$

Selectivities of products were calculated by using following relations.

$$S_{CO2} = \frac{n_{CO2}}{n_{total,0} - n_{CO}} \qquad S_{CH4} = \frac{n_{CH4}}{n_{total,0} - n_{CO}}$$

$$S_{CH3OH} = \frac{n_{CH3OH}}{n_{total,0} - n_{CO}} \qquad S_{CH3OCH3} = \frac{n_{CH3OCH3}}{n_{total,0} - n_{CO}}$$

$$S_{C2H5OH} = \frac{n_{C2H5OH}}{n_{total,0} - n_{CO}} \qquad S_{CH2O2} = \frac{n_{CH2O2}}{n_{total,0} - n_{CO}}$$

APPENDIX C

CRYSTALLITE THICKNESS CALCULATIONS

Thicknesses of CuO crystallites observed in the XRD pattern of synthesized catalysts were calculated by using Scherrer's formula.

$$t = \frac{k \times \lambda}{B \times \cos(\theta)}$$

t = thickness of crystallite

K = constant dependent on crystallite shape (0.89)

λ = X-ray wavelength

B = FWHM (full width at half max) or integral breadth

θ = Bragg Angle

The values of λ, B and θ were calculated with the data obtained from X-Ray diffraction pattern analyses of the catalysts. A schematic representation of the XRD pattern for HS1 catalyst is presented in Figure 63.

C.1. Crystalline thickness calculations of HS1 catalyst

$\lambda = 0.154\ nm$

$I/2 = 491.667/2 = 245.83$

$B = (2\theta\ high) - (2\theta\ low) \rightarrow B = 39.11° - 38.34° = 0.77° = 0.013\ radians$

$K = 0.89$

$2\theta = 38.68° \rightarrow \cos(\theta) = 0.94$

$$t = \frac{0.89 \times 0.154}{0.013 \times 0.94} = 11.2\text{nm} \cong 11\text{nm}$$

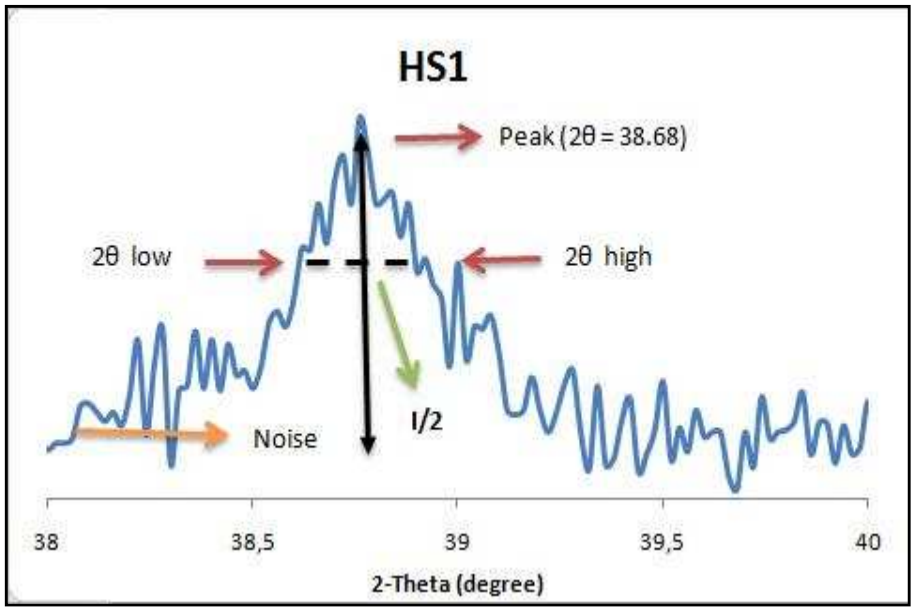

Figure 63. XRD Pattern of HS1 catalyst (2θ= 38-40°)

C.2. Crystalline thickness calculations of IMP1 catalyst

$\lambda = 0.154\ nm$

$I/2 = 933.33/2 = 466.665$

$B = 35.83° - 35.37° = 0.46° = 0.00803\ radians$

$K = 0.89$

$2\theta = 35.62° \rightarrow \cos(\theta) = 0.952$

$$\text{t} = \frac{0.89 \times 0.154}{0.952 \times 0.00803} = 17.9\text{nm} \cong 18\text{nm}$$

C.3. Crystalline thickness calculations of HS3 catalyst

$\lambda = 0.154\ nm$

$I/2 = 396.667/2 = 198.33$

$B = 39.27° - 38.16° = 1.11° = 0.0191\ radians$

$K = 0.89$

$2\theta = 38.80° \rightarrow \cos(\theta) = 0.943$

$$\text{t} = \frac{0.89 \times 0.154}{0.943 \times 0.0191} = 7.61\ \text{nm} \cong 8\ \text{nm}$$

C.4. Crystalline thickness calculations of HS4 catalyst

$\lambda = 0.154\ nm$

$I/2 = 413.333/2 = 206.7$

$B = 39.20° - 38.50° = 0.7° = 0.012\ radians$

$K = 0.89$

$2\theta = 38.78° \rightarrow \cos(\theta) = 0.943$

$$\mathrm{t} = \frac{0.89 \times 0.154}{0.012 \times 0.943} = 12.1\mathrm{nm} \cong 12\mathrm{nm}$$